Investigations on Bi2Sr2CaCu2O8+z superconductors : magnetic relaxation, vortex pinning, substitution effects and transport measurements

Investigations on $Bi_2Sr_2CaCu_2O_{8+z}$ Superconductors

Magnetic relaxation, vortex pinning,
substitution effects and transport measurements

Dian-wen Hu

Investigations on $Bi_2Sr_2CaCu_2O_{8+z}$ Superconductors

Magnetic relaxation, vortex pinning,

substitution effects and transport measurements

Proefschrift

ter verkrijging van de graad van doctor aan de Technische Universiteit Eindhoven,

op gezag van de Rector Magnificus, prof.dr. M. Rem, voor een commissie aangewezen

door het College van Dekanen in het openbaar te verdedigen op

woensdag 4 december 1996 om 16.00 uur

door

Dian-wen Hu

geboren te Gan-Xian, China

The laws of nature can be investigated and expressed; however, our expressions will not always be as valid as we would expect, therefore, they will change with time.

（道可道，非常道）

----------from "Lao Tse", Chapter. 1, by Lao Tse, Taoism, ca. 800 B.C.

Contents

Chapter I. General Introduction

1.1. Subject and outline of this thesis

After the discovery of high-T_c superconductors, soon it was found that the weak pinning and thermally activated flux motion in these materials are the main problems to limit their potential large-scale application. From a fundamental scientific point of view, it was of great interest that many new features of the vortex dynamics were found, which were not known for traditional superconductors. This thesis deals with experimental studies and modelling of the physical properties of $Bi_2Sr_2CaCu_2O_{8+z}$ (Bi-2212) high-T_c superconductors with the emphasis on vortex dynamics.

In Chapter I, a general introduction will be given. The basic knowledge introduced in this chapter will be useful in understanding the later chapters (except Chapter II) which are written more or less in the form of published papers. Some general references are indicated at the beginning of the sections of this chapter, and more specific references are given in the text. The experimental techniques used will be briefly described in Chapter II. After that, the experimental results of the magnetic relaxation and critical current density in Bi-2212 single crystals and polycrystalline samples are described in Chapter III. Those experimental results, especially the nonlogarithmic decay of the magnetization, will be analysed and discussed in Chapter IV and V. In Chapter IV, a generalised model with a non-linear current dependence of the effective pinning potential will be discussed; a different approach, i.e.: a distribution of pinning energies will be the topic of Chapter V. In Chapter VI, both experimental results and a phenomenological model for the irreversibility line of Bi-2212 superconductors will be presented. In Chapter VII, the experimental results of chemical substitutions in Bi-2212 single crystals and the effects upon the pinning behaviour are reported. In Chapter VIII, some recent results of transport measurements obtained by means of the so called flux-transformer geometry will be discussed.

1.2. Introduction to high-temperature superconductors [1, 2]

Superconductivity is the phenomenon that below a critical temperature T_c, the resistivity of some materials becomes zero. It was in 1911 that Heike Kamerling Onnes in Leiden first discovered superconductivity in mercury at liquid-helium temperature. During the long period from 1911 to 1986, superconductivity was found mainly in metals and alloys with a maximum transition temperature T_c of 23.2 K observed for the technical important alloy Nb_3Ge. Some oxide materials like $Li_{1+x}Ti_{2-x}O_4$ [3] and $BaPb_xBi_{1-x}O_3$ [4] were also known as superconductors at low temperatures ($T_c < 15$ K). In 1986, K. A. Müller and J. G. Bednorz in Switzerland found superconductivity in the oxide compound La-Ba-Cu-O with a critical temperature around 30 K [5]. It was considered as a break-through in the research of superconductivity, for which they were awarded the Nobel Prize in 1988. In 1987, Chu et al. in the United States synthesised the compound Y-Ba-Cu-O with a T_c of 92 K [6], well above the temperature of liquid-nitrogen of 77 K. Since then, many new superconductors and new physical phenomena have been discovered and studied. Up to now, the highest known T_c was found in the Hg-Ba-Ca-Cu-O system with T_c to be 135 K at ambient pressure [7] and 160 K under high pressure [8]. The historical development of the highest observed T_c is shown in Fig. 1.1, where the highest known T_c for a specific
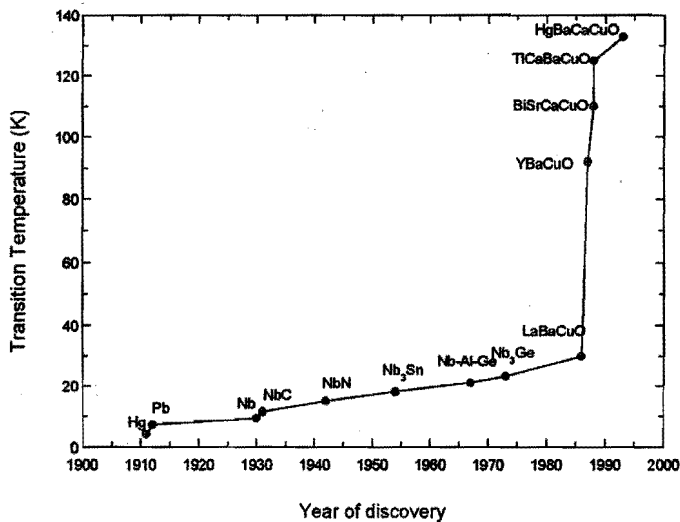
Fig. 1.1. The historical development of the highest known T_c.

material at each time period has been plotted against the year of its discovery.

This thesis is focused on one of the high-T_c superconductors, namely, the Bismuth-based cuperate oxide, $Bi_2Sr_2CaCu_2O_{8+z}$, discovered by Maeda et al. [9] . Single crystals with relatively large size can be grown for this material, which makes it very convenient for the investigation of its physical properties. This oxide, which has a T_c of about 85 K, is highly anisotropic and displays many interesting physical phenomena.

1.3. The structure of $Bi_2Sr_2CaCu_2O_{8+z}$ (Bi-2212) superconductors [2,10]
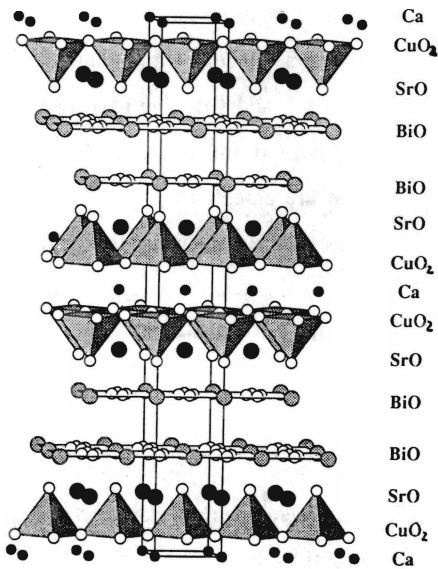
Fig. 1.2. The structure of Bi-2212 superconductor.

The structure of Bi-2212, as schematically shown in Fig. 1.2, consists of a stack of BiO, SrO, CuO_2 and Ca layers, with two Cu-O layers in one unit cell. This structure can be described by a pseudo-tetragonal unit cell with the lateral dimension a≈b=5.4 Å

and with c-axis length c=30.96 Å. It has been shown extensively that the Cu-O layers are responsible for superconductivity in high-T_c superconductors.

Since the Cu-O bond in the CuO_2 layers is the strongest in the structure, it determines the a and b lattice constant to be about 5.4 Å. However, the distance of the Bi-O bond is normally 2.0-2.5 Å, which is shorter than b/2=2.7 Å. The Bi-O layers are forced to match the structure of CuO_2 layers and consequently there are some deformations of the simplified stacking structure of Fig. 1.2. Due to the lattice mismatch, an incommensurate modulation in the b-direction occurs, which consists Bi-dilute and Bi-condensed regions with a superperiod of about 4.7b. In the Bi-dilute regions, one extra oxygen is incorporated in the BiO layers [11]. Therefore, the amount of excess oxygen per unit can be calculated to be 1/4.7=0.21.

Since other cations (except Cu) have their usual charges, i.e. Bi^{3+}, Sr^{2+} and Ca^{2+}, the excess oxygen atoms in the BiO layers introduce holes into the CuO_2 sheets. The copper charge is thus a mixture of Cu^{2+} and Cu^{3+} with an average charge of (2+p), where p represents the hole density per Cu ion. Because of this, the Bi-O layers are considered as charge reservoirs that are essential for providing carriers in the Cu-O layers. It has been found that T_c has a maximum when the hole density is about 0.2-0.3, which is about the same value as the excess oxygen density of 0.21 calculated above. This suggests that the hole doping in the Bi-2212 phase is mainly caused by the excess oxygen in the Bi-O layers.

Due to the layered structure of the Bi-2212 compound, its physical properties are highly anisotropic: the resistivity, coherence length, penetration depth, critical current density and upper critical field along the c-axis are quite different from that in the ab-plane. Since the coherence length along the c-axis, i.e. ξ_c (about 1.6 Å), is much smaller than the distance between the separated CuO_2 planes (15.5 Å), this compound is considered to be a quasi-two-dimensional (2D) superconductor with weak Josephson couplings between the Cu-O layers.

1.4. The crystal growth of Bi-2212 single crystals [12]

For the investigation of the physical properties of materials, single crystals have much more advantage than ceramic samples, because the effects of impurity phases and grain boundaries can be eliminated and the anisotropic effects can be studied. Single crystals of Bi-2212 can be grown either by the self-flux crucible method or by the travelling solvent floating zone (TSFZ) method.

As a first-step towards the crystal growth of Bi-2212, single-phase polycrystalline samples are prepared by a solid state reaction method. The procedure is as follows:

a.   mixing and milling of Bi_2O_3, $CaCO_3$, $SrCO_3$ and CuO powders;

b.   calcination at 800 ^{0}C for 16 hours with oxygen flow (1 atm.);

c.   grinding and milling;

d.   prefiring at 850 ^{0}C for 16 hours with oxygen flow (1 atm.);

e.   grinding and milling;

f.   isostatically pressing of the rods with 2.5 kbar pressure;

g.   sintering at 860 ^{0}C for 50 hours with air flow.

With this procedure, single phase Bi-2212 material was obtained in our experiments.

The Bi-2212 compound is known to melt incongruently, which means that upon heating, the compound decomposes into a liquid of a different composition and a solid phase. In order to illustrate this, a schematic partial phase diagram of a compound A_2B
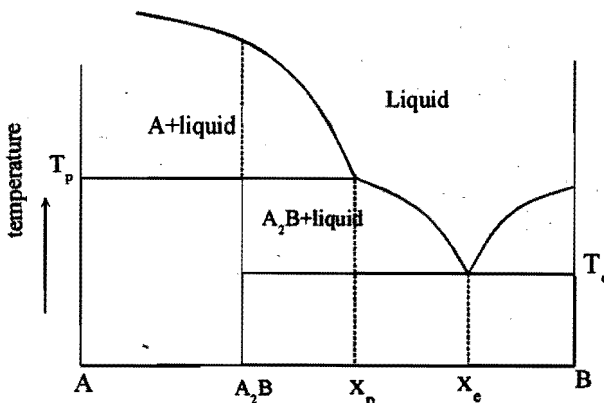
Fig.1.3. Schematic partial phase diagram of a compound A_2B that melts incongruently.

that melts incongruently is shown in Fig. 1.3. As the temperature is raised above T_p, A_2B decomposes into a solid A and a liquid of composition between A_2B and x_p. Between temperature T_e and T_p, as shown in the Figure, A_2B is in equilibrium with a liquid having a composition between x_p and x_e. In order to grow single crystals of A_2B, the composition of the melt has to be maintained between x_e and x_p. For the Bi-2212 compound, this means that the "pure" (stoichiometric) compound can only be grown from a melt which is within a certain composition range different from the Bi-2212 composition. Actually, some excess of Bi in the melt is needed, which depresses the melting temperature and acts as a chemical flux.

The two crystal growth methods will be briefly described below.

<u>1). Travelling solvent floating zone (TSFZ) method</u>

The travelling solvent floating zone method has the advantage that large single crystals with more homogeneous oxygen concentration can be obtained for Bi-2212 superconductors. In our experiments, a home-build mirror furnace (see Chapter II) was used for the crystal growth by the TSFZ method.

As shown in Fig. 1.4, a melting zone is formed when a light beam is focused between the feed and seed rods. When the light is slowly moved upwards, the feed rod is gradually dissolved into the solvent, and crystals grow on the top of the seed rod. The driving force for the crystal growth in the TSFZ method is the temperature gradient in the melted zone. Since the crystals are grown at a constant temperature, they are more homogeneous compared with crystals grown by the self-flux crucible method, in which the composition range of the crystals can change during cooling. Large crystals with dimensions of $10 \times 3 \times 0.3$ mm^3 could be obtained in our experiments. The single crystalline nature of the samples was confirmed by the X-ray diffraction and Laue transmission photographs. The as-grown single crystals have a pseudo-tetragonal structure with $c \approx 30.97$ Å, and $a \approx b = 5.4$ Å. Wet chemical analysis gave the composition of the single crystals very close to the nominal one [13].
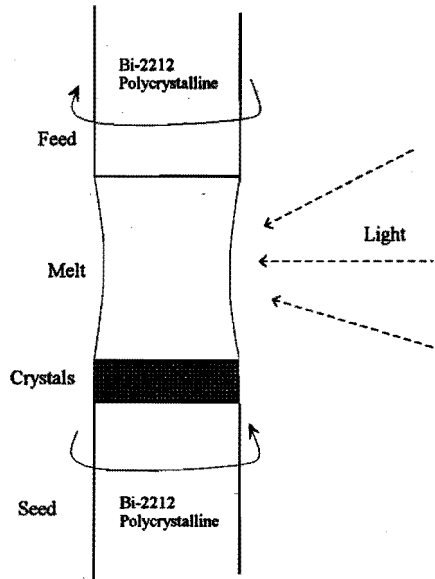
Fig. 1.4 Schematic view for the crystal growth by TSFZ method.

2) Self-flux crucible method

In this method, the off-stoichiometric (i.e. Bi-rich) Bi-2212 polycrystalline material is put in an Al_2O_3 crucible and quickly heated to 1100 ^{0}C for 3 hours. The material is melted at that temperature. It is then cooled to 900 ^{0}C at a rate of 50 ^{0}C/h, followed by a slower cooling to 800 ^{0}C at a rate of 1 ^{0}C/h. The crystal growth occurs during this slow cooling period. From 800 ^{0}C, the crucible is cooled down to room temperature at a rate of 50 ^{0}C/h. In this method, the driving force for crystal growth is the cooling. The size of crystals grown by this method is typically $2 \times 1 \times 0.05$ mm^3.

1.5. Vortices and vortex pinning in type-II superconductors [1-2,14]

High-T_c superconductors are so-called type II superconductors. This means that for small magnetic fields (H<H_{c1}), the magnetic field is expelled from the sample, but for higher fields (H_{c1}<H<H_{c2}), the magnetic field partially penetrates into the sample in the form of vortices, as shown in Fig. 1.5. The core of the vortices has a size about the same as the coherence length ξ and is in the normal state. For 3-dimensional superconductors, the vortices are also called flux lines. Flux lines are surrounded by screening supercurrents whose extension is the penetration depth λ. Each fluxoid is quantized, i.e. with a unit of Φ_0=hc/2e=2.07x10^{-15} Weber. At very high magnetic field (H>H_{c2}), the vortices overlap, and the sample loses its superconductivity and becomes entirely normal. The region between H_{c1} and H_{c2} in the H-T phase diagram is called the mixed state.
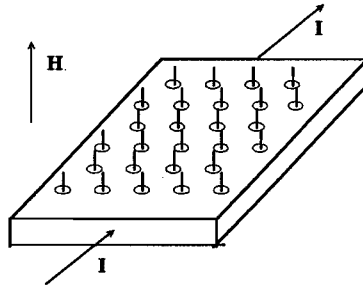
Fig. 1.5. In the mixed state the magnetic field penetrates into the superconductor in form of vortices each with a flux quantum of (hc)/(2e).

Since most of the applications deal with the mixed state of type II superconductors, it is important to consider what happens when a current density **j** is flowing in the sample. In the presence of a current, a vortex experiences a Lorentz force f_l per unit length (Note that in this thesis, the boldface-type symbols represent vector quantities):

$$f_l = j \times \Phi_0/c \, . \qquad\qquad (1.1)$$

If there is no other force, the vortices will move freely with a velocity **v** and this will induce a electric field **E** with

$$E=(B/c)\times v, \qquad\qquad (1.2)$$

where $B=n\Phi_0$ is the magnetic induction (n is the density of the vortices). This electric field will cause dissipation (which is proportional to E•j) in the sample. In such a situation, no current can be sustained in the superconductor, which means that the superconductor would be useless for applications. However, the situation changes if defects of approximately the same size as the coherence length are present, as shown in Fig. 1.6. Since it requires some energy to create the normal conducting cores of the flux lines (When the material becomes superconducting, it is in a lower energy state;
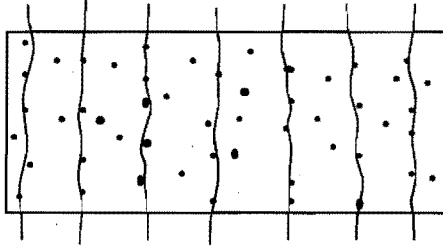
*Fig. 1.6 In the presence of defects, the vortices are pinned at
the defects due to lower free energy in these sites.*

the energy difference is called condensation energy.), a part of this energy can be conserved if the cores of the flux lines stick to these defects. The energy conserved by a point defect can be expressed as

$$U_0 \approx \frac{H_c^2}{8\pi}V_p , \qquad\qquad (1.3)$$

where H_c is the thermodynamic critical field, and V_p the volume of the defect. This energy is called the pinning energy. The pinning force of a defect acting on the flux line (per unit length) can be estimated as:

$$f_p \approx U_0/\xi \qquad\qquad (1.4)$$

where ξ is the coherence length of the vortex. Now, when a current is flowing in the superconductor, due to the pinning, the defects will provide a counter-force to the

Lorentz force and the superconductor can sustain a current. The maximum current density that a superconductor can sustain is called the critical current density J_c, and can be determined when the pinning force equals the Lorentz force, or:

$$J_c \times (B/c) = N_p U_0/\xi , \qquad\qquad (1.5)$$

where N_p is the number of defects per unit volume.

Several types of pinning centres can be distinguished:

a. Precipitates: precipitates of secondary, nonsuperconducting phase are usually very strong pinning centres which can interact with the flux lines.

b. Dislocations.

c. Oxygen vacancies: oxygen vacancies are considered to be the main pinning centers in high-T_c superconductors.

d. Twin boundaries: for YBCO superconductors, in addition to the oxygen vacancies, twin boundaries are strong pinning centers.

e. other defects like grain boundaries, voids, and radiation damages.

1.6. Thermally activated flux motion [1-2, 14]

As introduced above, due to the pinning of flux lines, type-II superconductors can sustain a current with a maximum current density of J_c. When a magnetic field is applied to a type II superconductor and then switched off, a current with a density of J_c will flow inside the sample. Ideally, this current in the superconductor can persist forever without dissipation, which is the principle of Superconducting Magnetic Energy Storage.

However, for high-T_c superconductors, a pronounced decay of the magnetisation (i.e. a decrease of the current) has been observed, unlike the traditional metallic superconductors. Fig 1.7 gives an example of our measurements for a Bi-2212 single crystals at 10 K; the remanent magnetisation reduced to 70% of its initial value in 20 minutes. This phenomenon has been attributed to the thermally activated flux motion at
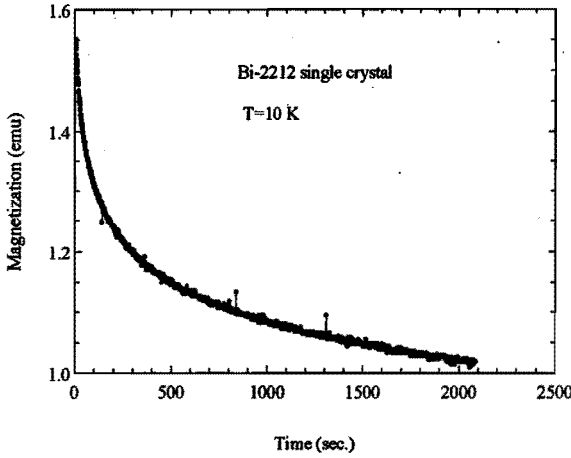
Fig. 1.7 For high-T_c superconductors the magnetization decays rapidly with time, a phenomenon known as giant flux creep.

finite temperatures: the vortices pinned by the defects can jump out of the potential wells due to thermal energy. The hopping rate r of the vortices can be expressed as:

$$r = \Omega_0 e^{-U_{eff}/kT}, \tag{1.7}$$

where Ω_0 is the hopping frequency of the vortices. In the case of thermally activated flux motion, this would be the characteristic frequency of the flux-line vibration, which is assumed to be in the range of 10^5-10^{11} s^{-1} [16]. As illustrated in Fig. 1.8, due to a distortion of the pinning potential by the Lorentz force, the effective pinning energy U_{eff} is reduced from its original depth U_0. In this case, the vortices prefer to hop forwards along the direction of the Lorentz force. The movement of the vortices will induce an electric filed, i.e. $E=(B/c)\times v$, and causes energy dissipation. For traditional low-T_c superconductors, $U_0 \gg kT$, therefore, the hopping velocity of the vortices is very slow. For high-T_c superconductors, however, U_0 is much smaller than that of the conventional superconductors due to a shorter coherence length, and in addition, the thermal energy kT can be higher because of the higher T_c. Therefore, the movement of the vortices is much faster in high-T_c superconductors than the traditional superconductors, which is often called giant flux creep for the high-T_c materials.
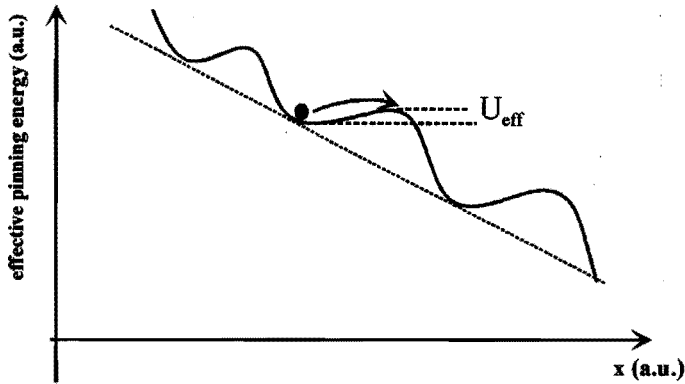
Fig. 1.8. In the presence of Lorentz force the effective pinning potential is reduced from the initial depth of the potential well, i.e. U_0, which favours the forward hopping of the vortices.

There are several important consequences because of this giant flux creep in high-T_c superconductors:

a. the magnetisation in the critical state decays much faster compared with the conventional superconductors;

b. the critical current density $j_c(T)$ is strongly temperature dependent;

c. the critical current density j_c may not be well defined but depends on the voltage criterion. Because of the thermally activated flux motion, the current-voltage characteristics of high-T_c superconductors can be schematically shown in Fig. 1.9. Unlike the traditional superconductors, the critical current density j_c is not well defined but depends on the voltage criterion, i.e. E_c.

Since the critical current density j_c is not well defined for high-T_c superconductors, a voltage criterion has to be specified for j_c. In later Chapters, when a voltage criterion can be found (usually in the experiments), j_c will be used to denote the critical current density; when no specific voltage criterion is defined (usually in the theoretical discussions), j instead of j_c will be used to denote the (critical) current density in the critical state. $J_c(T)$ defined by Eq. (1.5) will be used to denote the critical current density when flux creep is absent; and J_{c0} will be used to denote the critical current density at zero temperature.
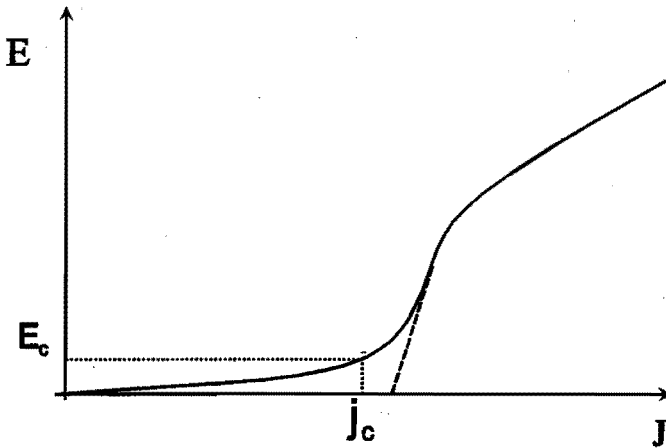
***Fig. 1.9** Scheme of the current-voltage characteristics of high-T_c superconductors (E: electric field, J: current density). The value of the critical current density j_c strongly depends on the electric field measured, as shown with the short dashed lines. For a comparison, a typical current-voltage characteristics of traditional superconductors is shown with the long dashed line.*

1.7. Determination of the critical current density j_c [1-5]

For many applications, large currents are required. Thus, the critical current density j_c is an important parameter of a superconductor. The value of j_c can be determined directly from transport measurements, i.e. the critical current density is measured when a small electric field (usually 1 mV per cm) is measured over the superconductors (This electric field is often called the voltage criterion). However, single crystals of high-T_c are quite small and j_c is usually quite large at low temperatures. For instance, for Bi-2212 single crystals, $j_c \approx 10^6$ A/cm^2 at 4.2 K. This makes it hardly possible to do transport measurements for the determination of j_c, especially at low temperatures. Usually, the j_c of high-T_c superconductors is determined from the magnetic hysteresis measurements using the Bean model [15], as described below.

As an applied field increases above H_{c1}, the magnetic field will gradually penetrate into a type-II superconductor in the form of vortices which has a density gradient in the

sample due to the vortex pinning. A current flow will be built up in the sample to
screen the applied magnetic field, according to the Maxwell equation: $\mu_0 j = \nabla \times \mathbf{B}$. When
the magnetic field is switched off, flux lines will be trapped in the material due to the
pinning. A maximum magnetic moment is reached when the current density reaches its
maximum value, i.e. the critical current density j_c, within the entire sample, which is
called the critical state. A typical magnetic hysteresis loop for type-II superconductors
is shown in Fig. 1.10.

For a rectangular-parallelepiped sample, the relationship between j_c and the maximum
value of the magnetisation can be calculated to be:

$$M_+ - M_- = \frac{j_c l_1}{2}\left(1 - \frac{l_1}{3l_2}\right), \qquad (1.6)$$

where l_1 and l_2 are the lateral dimension of the sample ($l_2 > l_1$). The voltage criterion for
the j_c in the hysteresis measurements is proportional to the sweep rate the magnetic
field, i.e. $E_c \propto dH/dt$.
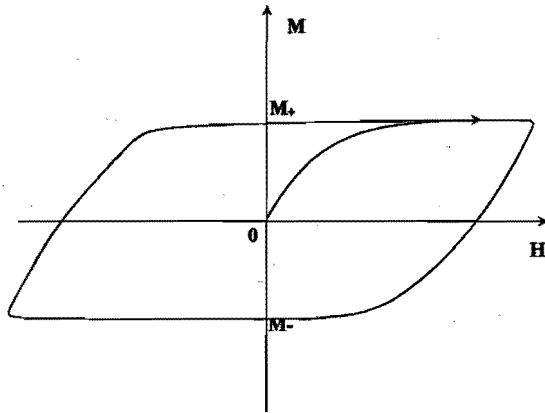
*Fig. 1.10 Magnetic hysteresis of type II superconductors. The
critical current density can be calculated from the maximum value of
the magnetization M.*

1.8. Resistivity transition in magnetic fields

In Section 1.6, the flux creep in the presence of large Lorentz was considered. For resistivity measurements, however, the Lorentz force is quite small due to the small applied current (typically 10 mA for a flowing area of about 1 mm^2). In this situation, as shown in Fig. 1.11, both forward and backward hopping of the vortices should be considered. The resulting electric field can be expressed as [16]:

$$E = (2a_0 B\Omega_0) \frac{j_a U_0}{J_c kT} \exp(-U_0/kT) \qquad (1.8)$$

where a_0 is the distance between the vortices, j_a the applied current density, J_c the critical current density in case of no thermal activation [see Eq. (1.5)], and U_0 the pinning energy defined by Eq. (1.3). This model is called thermally activated flux flow (TAFF) [17]. Under the TAFF regime, the resistive transition shows a broadening in the presence of magnetic field. An example of our measurements for a Bi-2212 single crystal is given in Fig. 1.12.
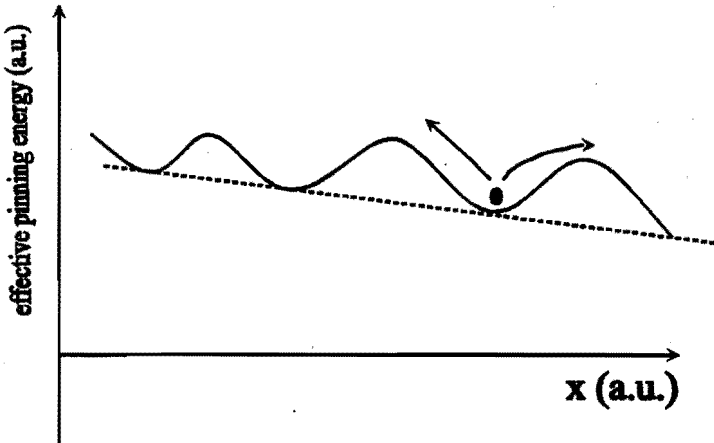
Fig. 1.11. When the Lorentz force is small, both forward and backward hopping of the vortices should be considered.
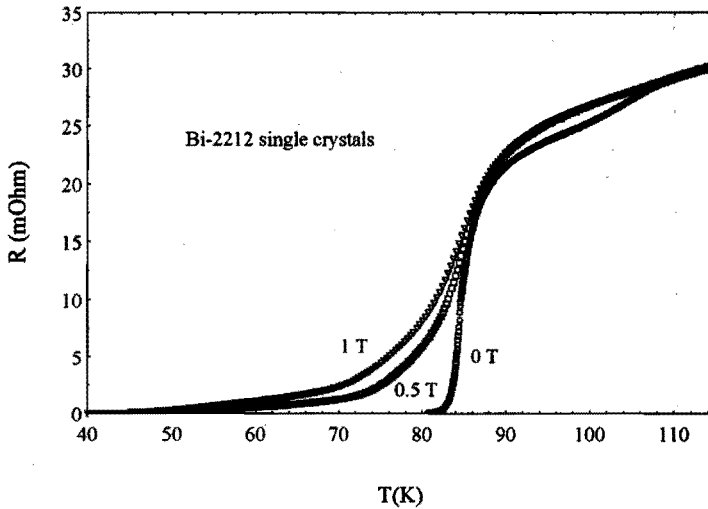
Fig. 1.12. The resistive transition of a Bi-2212 single crystal shows a broadening effect, i.e TAFF behaviour, in the presence of magnetic fields.

1.9. Introduction to the irreversibility line and the H-T phase diagram [2, 14]

In Section 1.5, H_{c1} and H_{c2} in the H-T phase diagram and the mixed state were briefly introduced. After the discovery of high-T_c superconductors, it was soon discovered that the mixed state could be further divided into two regions: in one region the critical current density $j_c=0$; and in the other, $j_c>0$, as illustrated in Fig.1.13. The line separating those two regions is called the irreversibility line. It was first discovered in the zero-field-cooled (ZFC) and field-cooled (FC) experiments by K. A. Müller et al [18]. As shown in Fig.1.14, in the FC process, a magnetic field is applied at a high temperature ($T>T_c$), then, the sample is cooled to a temperature below T_c. During the cooling process, the magnetic field is expelled from the sample, which means that a screening current is produced simultaneously (the Meissner effect). In the ZFC process, the sample is firstly cooled to a low temperature (usually 4.2 K) below T_c, then a magnetic field is applied and the sample is warmed above T_c. In the ZFC process, an electric field is applied to the sample as a result of a sudden change in the magnetic field. Due to this electric field, a large current density with a maximum value

of j_c can be established in the sample, leading to a much larger magnetization than in the FC process. But, as the temperature increases, at a certain temperature $T_{irr}(H)$, the ZFC and FC magnetisation merge, i.e. the magnetization becomes reversible. Above this irreversibility point, which depends on the applied magnetic field, the critical current density is reduced to zero. (Note: In literature, the irreversibility line is denoted either by $H_{irr}(T)$ or $H(T_r)$. In this thesis, $H(T_r)$ will be used.)
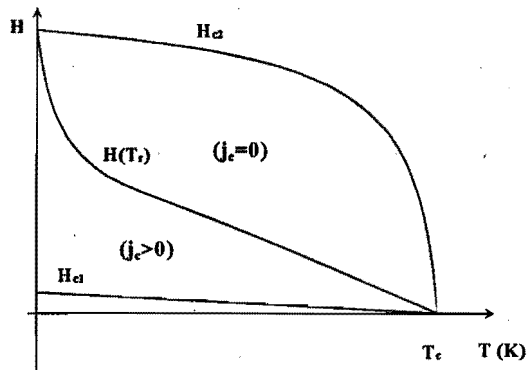
Fig. 1.13. The mixed State is separated by the irreversibility line where $j_c=0$.
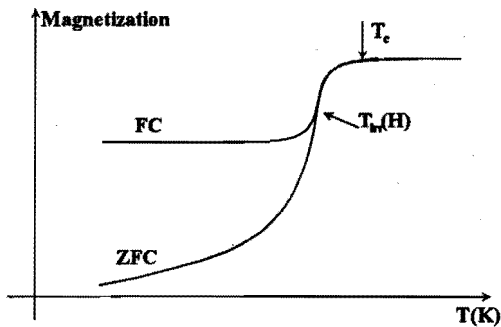
Fig.1.14 The irreversible point is determined as the FC and ZFC magnetization merge.

1.10. The resistivity measurements using the flux-transformer geometry

1). In the normal state, the resistivity of high-T_c superconductors is highly anisotropic for current parallel and perpendicular to the layers (a-b plane and c-direction) due to the layered crystal structure of the superconductors. In the standard four-contact resistivity measurements for high-T_c superconductors, a current is injected in the surface (a-b plane), and the voltage in the surface (a-b plane) is measured. However, due to the anisotropic resistivity, there is an inhomogeneous distribution of the current density in the superconductor, as illustrated in Fig. 1.15.
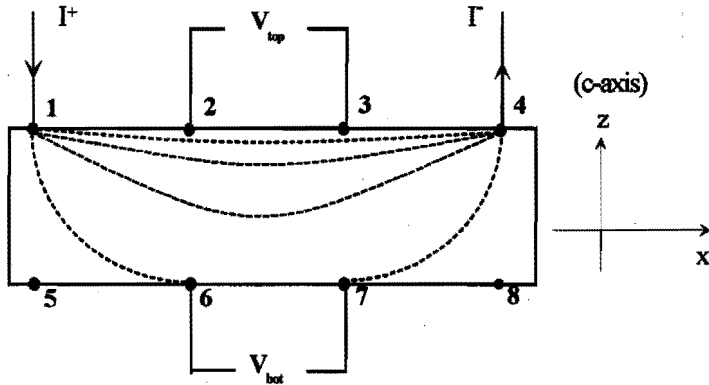
Fig. 1.15 The contact configuration in the transport measurements using the flux-transformer geometry.

By adding more contacts in the bottom of the crystal, which is called flux-transform geometry, one can measure the voltage both on the top, i.e. V_{top}, and the voltage on the bottom, i.e. V_{bot}, to monitor the distribution of the current density. From V_{top} and V_{bot}, the anisotropic resistivity ρ_{ab} and ρ_c can be calculated. In fact, for a static current, the voltage distribution $V(x,z)$ in the sample obeys the following equation [19]:

$$\text{div } j(x,z) = \frac{1}{\rho_{ab}} \frac{d^2 V(x,z)}{dx^2} + \frac{1}{\rho_c} \frac{d^2 V(x,z)}{dz^2} = 0 \ . \qquad (1.9)$$

From this equation and using the boundary conditions, one obtains [19]

$$\left[\frac{\rho_c}{\rho_{ab}}\right]^{1/2} \approx \frac{L}{\pi D} \operatorname{arccosh}\left(V_{top}\Big/V_{bot}\right) \qquad , \qquad (1.10a$$

$$\left(\rho_c \rho_{ab}\right)^{1/2} \approx \frac{V_{top}b}{2I\sin\left[\pi(x_2 - x_1)/2L\right]} \times \tanh\left[\frac{\pi D}{L}\left(\frac{\rho_c}{\rho_{ab}}\right)^{1/2}\right] \qquad , \qquad (1.10b)$$

where L is the length of the crystal along the contacts, D the thickness of the sample, b the width of the sample, x_2 and x_1 denote the coordinates of the voltage contacts, and I the applied current. The value of ρ_{ab} and ρ_c can, therefore, be calculated from (1.10a) and (1.10b) when the geometry of the contacts and the voltages on the top and bottom are known.

2). In the mixed state, the resistive dissipation is caused by the moving of the vortices, instead of the scattering of electrons in the normal state. By monitoring the voltage both on the top and bottom, i.e. V_{top} and V_{bot}, the information of the movement of the vortices across the sample and the strength of the coupling between the vortices in different layers can be obtained [20]. Two different specific situations are considered as follows:

a). The vortices are 3D flux lines across the sample

If the coupling between the superconducting layers is very strong, the vortices exists in the form of 3D flux lines. The movement of the vortices, therefore, will induce a same voltage both on the top and the bottom surface, i.e.,

$$V_{top} = V_{bot} , \qquad (1.11)$$

regardless any distribution of the current density in the sample.

b). *The vortices are 2D (pancake vortices)*

When the coupling between the superconducting layers is very weak, the vortices in each superconducting layer move independently. In this situation, due to the inhomogeneous distribution of the current, one can expect that the voltage induced by the movement of the vortices on the top surface will be larger than that on the bottom, i.e.

$$V_{top} > V_{bot} . \qquad (1.12)$$

Therefore, by comparing the voltages on the top and bottom surface in the resistivity measurement, the dimensionality of the vortices can be investigated.

References

[1] M. Tinkham, "Introduction to Superconductivity", McGraw-Hill Inc., New York (1975).

[2] "Physical Properties of High Temperature Superconductors", Vol. 1&2, Editor: D. M. Ginsberg. World Scientific, 1989.

[3] D.C. Johnston, H. Prakash, W.H. Zachariassen and R. Viswanathan, Mater. Res. Bull. 8, 777 (1973).

[4] A.W. Sleight, J.L. Gillson and F.E. Bierstedt, Solid State Commun. 17, 27 (1975).

[5] J.G. Bednorz and K.A. Müller, Z. Phys. B. 64, 189 (1986).

[6] M. K. Wu, J. R. Ashburn, C.J. Torng, P.H. Hor, R. L. Meng, L. Gao, Z. J. Huang, Y. Q. Wang and C. W. Chu, Phys. Rev. Lett. 58, 908 (1987).

[7] A. Schilling, M. Cantoni, J. D. Guo and H. R. Ott, Nature 363, 36 (1993).

[8] C.W. Chu, L. Gao, F. Chen, Z.J. Huang, R.L. Meng, Y.Y. Xue, Nature 365, 323 (1993).

[9] H. Maeda, Y. Tanaka, M. Fukutomi and T. Asano, Jpn. J. Appl. Phys. 27, L209 (1988).

[10] X. F. Zhang, Ph. D thesis, Universiteit Antwerpen (1994).

[11] S. Kambe, K. Okuyama, S. Ohshima, and T. Shimada, Physica C 250, 50 (1995).

[12] J.H.P.M. Emmen, Ph. D thesis, Eindhoven University of Technology (1992).

[13] J.H.P.M. Emmen, S. K.J. Lenczowski, J.H.J. Dalderop, V.A.M. Brabers, J. Crystal Growth 118, 477 (1992).

[14] G. Blatter, M. V. Feigel'man, V. B. Geshkenbein, A. I. Larkin, V. M. Vinokur, "Vortices in high-temperature superconductor", Rev. Mod. Phys. 66, 1125 (1994).

[15] C.P. Bean, Phys. Rev. Lett.8, 250 (1962); idem. Rev. Mod. Phys. 36, 31 (1964).

[16] D. Dew-Hughes, Cryogenics 28, 674 (1988).

[17] P. H. Kes, J. Aarts, J. van den Berg, C.J. van der Beek, and J.A. Mydosh, Supercond. Sci. Technol. 1, 242 (1989).

[18] K.A. Müller, M. Takashige, and J.G. Bednorz, Phys. Rev. Lett. 58, 1143 (1987).

[19] R. Busch, G. Ries, H. Werthner, G. Kreiselmeyer, and G. Saemann-Ischenko, Phys. Rev. Lett. 69, 522 (1992)

[20] F. de la Cruz, D. Lopez, and G. Nieva, Philos. Magz. B 70, 773 (1994).

Chapter II. Experimental Techniques

In this chapter, the experimental techniques for the crystal growth, material characterisation, magnetization measurements and transport measurements are briefly described.

2.1. The mirror furnace used for the travelling solvent floating zone (TSFZ) method
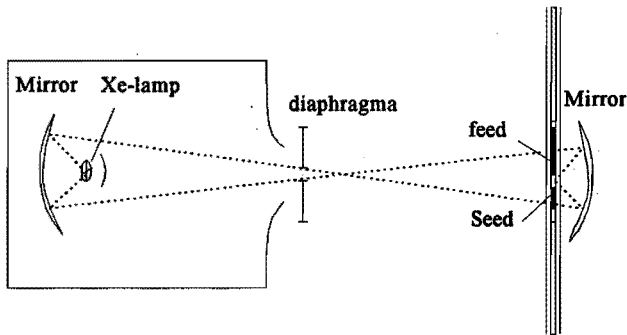
Fig. 2.1 Diagram of the mirror furnace used in our experiments for growing single crystals.

A home-built apparatus with a Xenon lamp, as shown in Fig. 2.1, was used for the TSFZ experiments. By means of two elliptical mirrors, radiation from the lamp was focused on the polycrystalline bars to form a molten zone. In order to stabilise the molten zone and make the temperature distribution of the zone more homogeneous, the feed and seed bars were rotated around the vertical axis in opposite directions (Fig. 1.4). The rotating speed of the bars was about 40 cycles/min. A first zone melting process was carried out by pulling down the seed as well as the feed bar with the same speed of 80 mm/h, by which the molten zone was travelling through the polycrystalline

feed bar. By this process, we obtained a recrystallised bar with a high density (~100% density). This is necessary in order to prevent soaking of the melt into the feed bar during the next step of crystal growth, which is performed by a zone melting process at a low pulling rate of 1 mm/h. Two different techniques were used for the crystal growth. In the TSFZ method, we added some Bi_2O_3 to the molten zone (about 20% of the weight of the molten zone), which acted as a solvent (a chemical flux) for the Bi-2212 compound. However, most of the experiments were done by the self-flux, floating zone method. This self-flux, i.e. an excess of Bi (as a solvent), was created in the fast pulling step at the end of the recrystallised bar. This recrystallised bar was then reversed as a feed bar and pulled through the hot focus at a rate of 1 mm/h. The resulting rod, with a diameter of about 7 mm and a length of about 12 cm, consisted of single-crystal platelets which extended up to several centimetres along the axis of the rod, and were 1-6 mm wide (For more details of the crystal growth process, see Ph. D. thesis of J. Emmen, Eindhoven University of Technology). All the melting experiments were performed in the flow of air at a pressure of two bar which was maintained in the surrounding silica tube. Due to the slow pulling rate, it took several days to complete the growth process.

2.2. Structure and chemical characterisation of the crystals

The platelets obtained from the crystal growth experiments were characterised by X-ray diffraction technique. From Laue transmission experiments, the single crystalline nature of the platelets with a thickness of about 0.1 mm was confirmed. The white X-rays used in the Laue transmission experiments were produced from a tungsten (W) X-ray tube. A θ–2θ scan with the incident Cu-Kα X-ray beam at an angle θ to the crystal plate was used. In Fig. 2.2, an example of such scan is shown for the Bi-2212 single crystals. Only the (00l) reflections are present on the figure, indicating that the c-axis of the crystal is perpendicular to the crystal plate. For the as-grown single crystals, the c-axis length was found to be 30.97 Å. From x-ray powder diffractograms of crushed crystals, the structure was proved to be pseudo-tetragonal with a$\approx$b$\approx$5.4 Å.
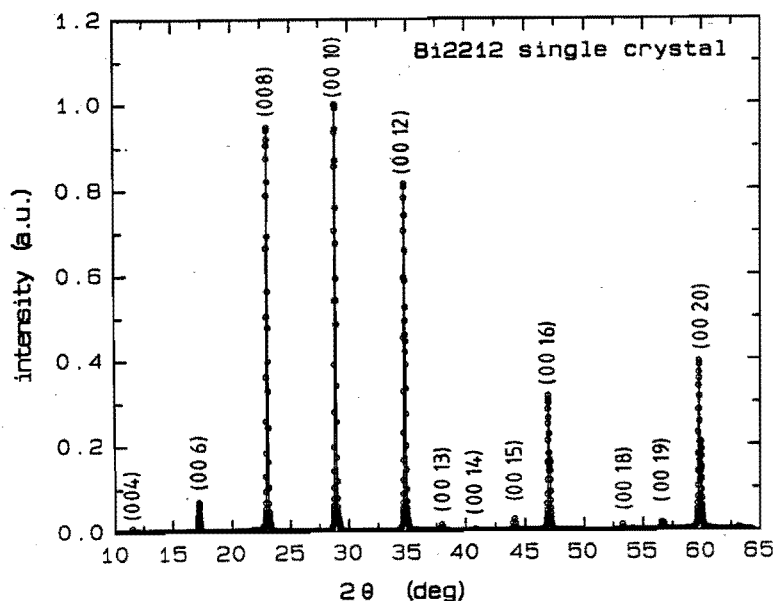
Fig.2.2 scan of a Bi-2212 single crystal. The incident Cu Ka beam has an angle θ with the Crystal plate. Only the (ool) reflections are present, indicating that the plate direction coincides with the crystallographic ab-plane.

The chemical composition of the single crystals were mostly determined by electron probe micro analysis (EPMA). The principle of this method is that each element has its characteristic atomic energy levels; the electrons of the atom are excited to higher energy levels and then emit X-rays when they return to the ground state. The spectrum and the intensity of the X-rays is measured in order to determine the elements and their relative abundance. Since EPMA only detects a small area ($1 \ \mu m^2$), several spots were examined to obtain an average value. The accuracy of EPMA, however, is within a few percent. In most cases, we used this method as a semi-quantitative analysis without standardization. To have more accurate result of the chemical composition of the pure Bi-2212 crystals, a wet chemical analysis was performed by Analytisch Laboratorian Elbach, Germany, which indicated that the composition of the as-grown crystals is $Bi_{2.02}Sr_{2.00}Ca_{0.98}Cu_{1.99}O_{8+\delta}$, which is close to the nominal composition.

2.3. AC susceptibility

The AC susceptibility is an effective method for detecting superconducting phases. As

1. DC coil (large field)
2. AC coil (small field)
3. Detect coil
4. Compensation coil
5. Sample
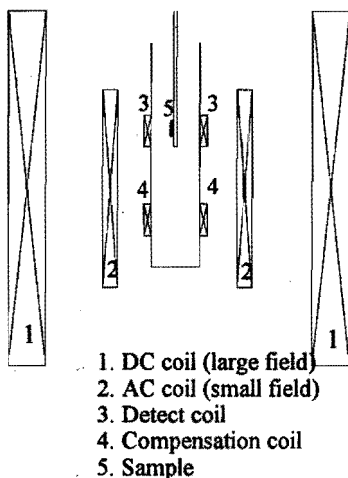
Fig. 2.3 Schematic view of the AC susceptibility equipment.

shown in Fig. 2.3, a sample is located in the centre of the detecting coil that is connected with a compensation coil. These two coil are constructed such that in the absence of a sample, the mutual inductance is equal to zero. In our experiments, an AC magnetic field of 8 gauss is generated by an AC current through a primary coil (Nr.2) with a frequency of 920 Hz. When this AC field is applied to the superconducting sample, a screening current is produced in the sample. The changing magnetization caused by this changing screening current produces a voltage in the detecting coil, which is monitored by a lock-in amplifier. The real and imaginary parts of the signal are then recorded. Additionally, a large DC magnetic field can be applied in order to study its influence on the susceptibility.

2.4. DC magnetisation measurements
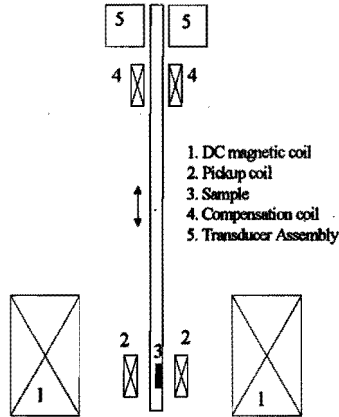
Fig. 2.4. Schematic view of the vibrating sample magnetometer (VSM)

Most of the DC magnetization of the superconductors and its decay with time were measured with a vibrating sample magnetometer (VSM). The schematic view of the VSM is shown in Fig.2.4. The transducer converts a sinusoidal AC driving signal into a sinusoidal vertical vibration of the sample rod. When a superconducting sample has a magnetic moment, the vibrating of the sample will induce a voltage which is detected by the pick-up coil. The compensation coil is constructed so that the total obtained signal is proportional only to the magnetic moment of the sample (i.e. independent of the amplitude and frequency of the vibration). By gradually increasing and decreasing the applied magnetic field, a magnetic hysteresis loop for the superconductor can be obtained (Fig. 1.7). In our experiments, the magnetic field was applied always high enough (e.g. H>0.7 T at 4.2 K) to ensure a critical state in the entire superconducting sample, i.e. the current density reaches j_c in the whole sample. The VSM insert is built in a liquid-helium dewar and the sample can be cooled to 4.2 K.

Besides a VSM magnetometer, a home-built flux-gate magnetometer, and a SQUID magnetometer (Quantum Design) were also used for some measurements of the magnetisation.

2.5. Transport measurements

For transport measurements, it is always important to make good contacts having a low contact resistance. In addition, a four-point-contact technique has to be used even for low contact resistance in order to obtain accurate results.

The contacts were made as follows. First, dots of silver with a diameter of 0.5 mm were sputtered on the Bi-2212 single crystal. To improve the contact between the silver dots and the crystal, the sample with the silver dots was annealed at 600 ^{0}C for about 2 hours in oxygen flow (1 atm.) and, subsequently it was quenched to liquid nitrogen temperature. Finally, silver paste was used to connect silver wires to the silver dots. The contact resistance at room temperature (measured by a two point method) was just a few Ohms. Linear current-voltage (I-V) characteristics at room temperature (measured by four-point method) were also measured in order to check the measurement system. In our transport measurements with the "flux transformer" geometry (Section 1.10), the four-contact technique was applied to both the top and the bottom surface. A special sample holder was designed so that the silver wires can be easily connected to the silver dots on both surfaces of the samples.

For the transport measurements, a home-built cryostat inserted with a superconducting magnet was used. Magnetic fields up to 6 T can be obtained. The applied DC current was typically 10 mA, and the voltage was detected by a Keithley-182 nanovolt-meter. For each measurement point, the direction of the current was reversed in order to eliminate the thermo-electric effect. Since it is important to have an accurate reading of the sample temperature, the temperature sensor was put close to the surface of the sample (~3 mm). To ensure a homogeneous temperature around the sample space, the sample holder is enclosed by a metallic pot which is filled with helium gas. In the cooling and heating processes, the temperature was changed with a rate of about 0.8 K/min. This rate for the cooling or heating was found to be sufficiently slow, because even at slower cooling or heating rates, identical resistance curves R(T,H) of the samples were obtained.

Chapter III. Critical current density and magnetic relaxation in Bi$_2$Sr$_2$CaCu$_2$O$_{8+z}$ superconductors: experimental results

[Part of this Chapter has been published in Physica C 200, 359 (1992).]

In this chapter, the experimental results for the critical current density and the decay of the remanent magnetization in single crystals and polycrystalline samples of Bi$_2$Sr$_2$CaCu$_2$O$_{8+z}$ (Bi-2212) will be described. It will be shown that the decay of the magnetization in these samples is non-logarithmic, and the behaviour of the magnetic relaxation is different for different types of samples.

3.1. Introduction

Since the first studies of giant flux creep [1-4] and the irreversibility line [1,5] in high-T$_C$ superconductors, the flux motion in these materials has attracted much attention. It has been shown that a model of thermally activated flux creep is appropriate to describe those phenomena in high-T$_c$ superconductors [5]. In this model, the flux lines move out of the pinning potential with an average velocity of

$$v = (\Omega_0 a_0) \exp(-U_{eff}/kT), \qquad (3.1)$$

where a$_0$ is the hopping distance of the flux lines. The first flux creep model was introduced by Anderson for conventional superconductors (Anderson-Kim model) [6,7]. Due to the thermally activated flux motion in the presence of a magnetic induction B, an electric field E will be generated, which is given by

$$E = vB/c. \qquad (3.2)$$

For large Lorentz force, the backwards hopping can be neglected (see Section 1.6), and the induced electric field can be expressed as

$$E = \frac{\Omega_0 a_0 B}{c} e^{-U_{eff}(j)/kT} . \qquad (3.3)$$

During the magnetic relaxation measurements, this electric field is proportional to the decay of magnetization M, i.e.:

$$E \propto -\frac{dM}{dt}. \qquad (3.4)$$

For the effective pinning potential, Anderson [7] assumed a linear j dependence: $U_{eff}(j)=U_0(1-j/J_c)$, where J_c is the critical current density when the flux creep is absent [For the notation of j, j_c, J_c and J_{c0} in this thesis, please refer to Section 1.6]. This linear j dependence of $U_{eff}(j)$ leads to [7]:

$$M(t,T) = M_0(T) \cdot \left[1 - \frac{kT}{U_0} \ln(1 + t/\tau_0) \right], \qquad (3.5)$$

where τ_0 is a characteristic time ranging from 10^{-6} to 10^{-10} s, and $M_0(T)$ the magnetization in the absence of flux creep (i.e. at t=0). For usual magnetic relaxation experiments, $t \gg \tau_0$, we have

$$M(t,T) \approx M_0(T) \cdot \left[1 - \frac{kT}{U_0} \ln(t/\tau_0) \right] \quad . \qquad (3.6)$$

It shows that the magnetization decays logarithmically with time, which was widely observed in conventional superconductors. For a more detailed discussion of the Anderson-Kim model for high-T_c superconductors, see Ref. [8].

However, several experiments have revealed a nonlogarithmic decay of the magnetization in high-T_C superconductors [9-14] and even in some conventional superconductors [15], which contradicts the Anderson-Kim model. The nonlogarithmic decay of magnetization was observed at high temperatures ($T>T_c/2$) even for short observation times (a time window of less than 2 decades in most cases) [9-12]. Through long term observation (a time window of more than 2.5 decades), strongly nonlogarithmic decay at temperatures down to 26 K has been reported for single crystals of Bi-2212 [14].

In order to explain the nonlogarithmic decay of the magnetization, various flux creep models have been proposed. Since the pinning sites in high-T_c superconductors are mostly point defects (oxygen vacancies), Zeldov et al. [16, 17] obtained a logarithmic current dependence of the effective pinning potential, i.e. $U_{eff}(j)=U_0\ln(J_c/j)$, by describing the pinning potential of the point defects to be a logarithmic function of the distance parameter. Such a logarithmic j dependence of $U_{eff}(j)$ will result in a power law I-V characteristic, i.e. $V \propto j^\alpha$, and a power law decay of the magnetization, i.e. $M(t) \sim t^{-\beta}$. In

the vortex-glass [18,19] and collective pinning theories [20, 21], when $j \ll J_c$, the current dependence of $U_{eff}(j)$ is found to be $U_{eff}(j)=U_0(J_c/j)^\mu$, and the magnetization will decay as $M(t)\sim[\ln(t/\tau_0)]^{-1/\mu}$. Several authors have explained their experimental results with the theory of collective pinning or vortex glass [10,13-15], although, for some relaxation curves, it is difficult to distinguish between a power law decay with $M(t)\sim t^{-\delta}$ and a decay with $M(t)\sim[\ln(t/\tau_0)]^{-1/\mu}$ due to the relative short time window of about two decades [12]. Another model yielding a nonlogarithmic decay of magnetization is a distribution of pinning energies [22-24]. Hagen and Griessen have developed a method to calculate the distribution of pinning energies from the magnetic relaxation data [22].

An interesting feature of the magnetic relaxation is the temperature dependence of the normalized initial decay rate $S(t_b,T)$, which is defined as

$$S(t_b,T) = -\frac{d\ln M(t,T)}{d\ln t}\bigg|_{t=t_b}, \qquad (3.7)$$

where t_b is the starting measurement time. It was found that $S(t_b, T)$ increases monotonically with temperature and shows a plateau with values between 0.02 and 0.035 for various YBCO-123 samples [25], including grain-aligned powders [9] and thin films [25], which was argued to be a consequence of the vortex-glass model. However, $S(t_b, T)$ exhibited a peak for some YBCO-123 ceramics [3]; and for various YBCO-123 single crystals, both a peak [4] and a plateau [25] were observed in $S(t_b,T)$. The relaxation behaviour of $S(t_b,T)$ in YBCO-123 single crystals could be complex due to the additional twin-boundary structures found in YBCO-123 crystals. For Bi-2212 single crystals, in which no twin boundaries have been observed, a strong peak in $S(t_b, T)$ has been repeatedly found for various crystals [26].

In this chapter, our experimental results, with the emphasis on the decay of magnetization, will be presented for Bi-2212 single crystals, melt-processed bulk ceramics and powdered ceramic samples. The period of observation extended over 3.5 decades of time (from 5 s to about 9 h). A nonlogarithmic decay of the magnetization was observed even at a low temperature of 10 K. It was also found that for the three different types of samples, the behaviour of the decay of magnetization and the temperature dependence of $S(t_b, T)$ is not similar.

3.2. Experimental

The experiments were performed on single crystals, bulk polycrystalline samples and polycrystalline powders of Bi-2212 superconductors. For the magnetic relaxation, most of the experiments were performed on crystals grown by the self-flux crucible method [27], and later on, additional experiments were also done on single crystals grown by the TSFZ method [28].

Single crystals grown by the self-flux crucible method have a typical size of $1.5 \times 1.5 \times 0.085$ mm^3 with a T_c of about 88 K. Single crystals grown by the TSFZ method have a typical size of $8 \times 2 \times 0.2$ mm^3 with a T_c of about 90 K. The single-phase Bi-2212 ceramic samples used in the experiments were prepared by a partial-melting method [29], which have a T_c of about 90 K. For YBCO-123 ceramic samples, weak-link behaviour of the grain boundaries were widely observed in the magnetic hysteresis measurements [30]. However, such a weak-link behaviour were not observed for these Bi-2212 ceramic samples [29]. The T_c was determined from the onset of the Meissner effect with an applied magnetic field of 20 Oe.

Magnetic hysteresis and the decay of the magnetization were measured using a vibrating sample magnetometer (VSM). For single crystals, in case of no specific description, the applied magnetic field was always parallel to the c-direction. The critical current density j_c (in the a-b-plane) was deduced from the maximum magnetization in the hysteresis curves using the Bean model, as described in Section 1.7. For Bi-2212 bulk ceramics, a ring-shaped sample (3.2 mm outer diameter, 1.6 mm inner diameter and 0.5 mm height) was used. The critical current density j_c was evaluated from the hysteresis loops using a method described in Ref. [29] which is based on the Bean model.

The magnetic relaxation experiments were performed as follows: after zero-field cooling (ZFC), a magnetic field was applied and then maintained for 30 s for the stability of the field; then the magnetic field was switched off, which took about one second. The decay of the remanent magnetization was supposed to start (t=0) after the magnetic field was reduced to zero. The applied magnetic field was chosen to be large enough (H >0.7 T

at 4.2 K) in order to reach the critical state within the entire sample. The remanent magnetization was recorded automatically every 3 seconds starting at the beginning of the switching off. Since the recorded point at t=2 s was affected by some uncertainty of the time involved with the switching off the field (1±0.4 s), the magnetization at t=5 s was taken as the first measurement point (t_b=5 s). The observation time for the magnetic relaxation was up to 9 h. While the magnetic relaxation was being measured, the temperature was controlled with an accuracy of about 0.2%. During the magnetic relaxation, an electric field was induced, i.e. E∝-dM/dt, which was calculated to be between 10^{-1} and 10^{-5} μV/cm in our experiments.

3.3. Experimental results

First, it is needed to compare the results obtained on crystals grown by different methods. It is found that the critical current density j_c differs considerably. For crystals grown by the TSFZ method, j_c(T=4.2 K)≈2.5×10^6 A/cm²; and for crystals grown by the self-flux crucible method, j_c(T=4.2 K)≈3×10^5 A/cm². One possible cause for this difference could be due to the fact that crystals grown by TSFZ methods are more mechanically sound, i.e. there are much less microcracks and voids in the crystals grown by TSFZ method than that grown by the self-flux crucible method. Another possible cause could be a difference in the oxygen content in these samples, since the critical current density depends also on the penetration depth [31] which varies with the hole density in the Cu-O layers introduced by the excess oxygen content. However, the temperature dependence of the critical current density j_c(T) and the behaviour of the magnetic relaxation were found to be similar for all the crystals. In Fig. 3.1, a comparison of the normalized critical current density j_c(T)/j_c(4.2K) is shown for single crystals grown by the two methods. The temperature dependence of j_c(T) is similar for those crystals; especially, a "kink" appears in both curves when j_c/j_c(4.2K)≈10^{-2}. Since most of the experiments were performed on the Bi-2212 crystals grown by the self-flux crucible method and there is no fundamental difference between different single crystals, the results obtained on crystals grown by the self-flux crucible method will be presented below.
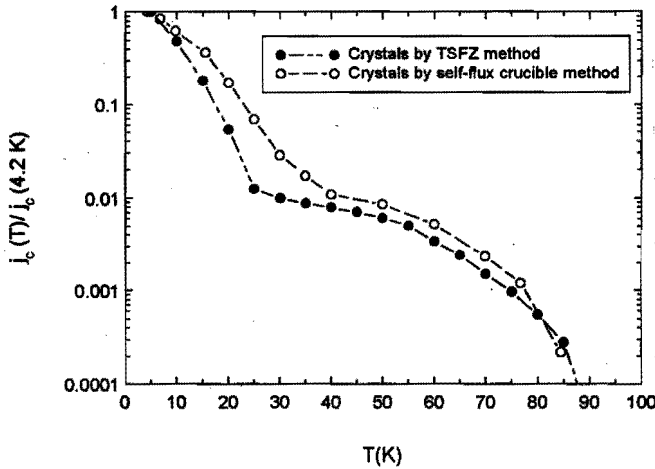
Fig.3.1 *The temperature dependence of the normalized critical current density $j_c(T)$ of the Bi-2212 single crystals grown by different method.*

3.3.1. Bi-2212 single crystals

Figure 3.2 shows the temperature dependence of the critical current density $j_c(T)$ obtained from the magnetic hysteresis loops for a Bi-2212 single crystal and a melt-processed ceramic sample. For the single crystal, a "kink" occurs in the $j_c(T)$ curve at about 25 K: j_c decreases rapidly with the temperature in the low temperature region (T<25 K), followed by a region of slower decline above 30 K. For the ceramic sample, however, j_c decreases almost exponentially from 4.2 K to about 60 K. At 4.2 K, j_c is about 2.5×10^5 A/cm^2 for the single crystal and 5.5×10^4 A/cm^2 for the ceramic sample. At 77 K, j_c is to about 300 A/cm^2 for the single crystal, while it is about 800 A/cm^2 for the ceramic sample. As discussed in Section 1.6, for a certain value of the critical current density j_c, the corresponding electric field has to be given for the high-T_c superconductors. During our measurements of the magnetic hysteresis loops, an electric field of the order of 0.1 μV/cm was induced during the sweeping of the magnetic field, which could be considered as the electric field criterion for the obtained critical current density j_c.
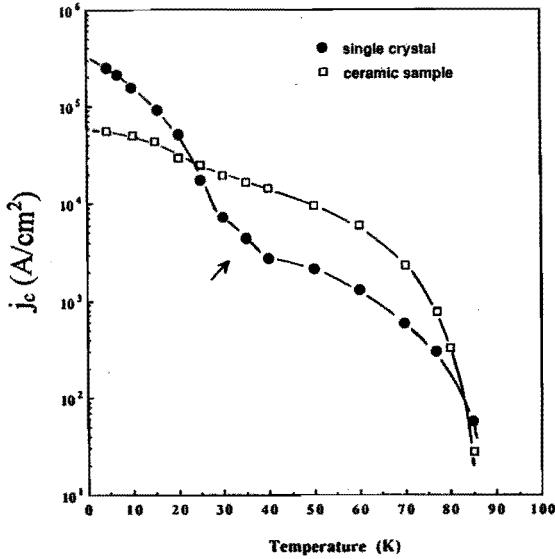
Fig.3.2. The temperature dependence of the critical current density of a Bi-2212 single crystal and a bulk polycrystalline sample in a semi-logarithmic plot.

The magnetic relaxation curves for the single crystal are shown in Fig. 3.3. The decay curve at 4.2 K is almost logarithmic over 3.5 orders of time. At 10 K, a more pronounced nonlogarithmic decay of magnetization was observed. At 21 K, the magnetic moment decayed so fast that 80% of its initial value was lost in approximately 10 min. A sharp curvature occurred in the relaxation curve at temperatures between 20-27 K, whereas the decay became much slower at T=35 K. For T>30 K, due to a much smaller signal and relative large noise level, the relaxation curves were measured only over a short time interval. The relaxation curves below 25 K can be approximately described by a power law with $M(t) \sim t^{-\beta}$. Zavaritsky et al. [26] found a kink in the $j_c(T)$ curve at about 17 K for their Bi-2212 single crystals, and around this temperature (15-18 K) the magnetic relaxation curves were also strongly nonlogarithmic, which is similar to what we observed but at a lower temperature.
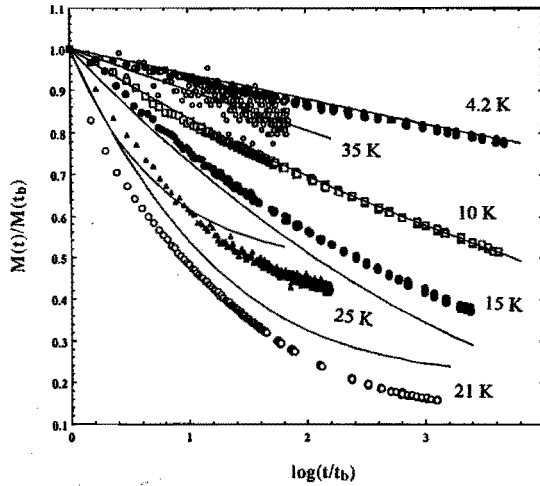
*Fig. 3.3 Magnetic relaxation curves for the Bi-2212 single
crystal, which are normalized with the first measured point of
each curve. The solid lines are fits obtained from the pinning
distribution model (Chapter V).*

The normalized initial magnetization $M(t_b,T)$ ($t_b=5$ s) of the relaxation curves is given in
Fig. 3.4(a) for the single crystal. The data are normalized to magnetization at zero
temperature, i.e. M_0 (T=0 K), which was obtained by extrapolating $M(t_b,T)$ to T=0 K. In
the critical-state model (Bean model), $M(t_b,T)$ is proportional to the critical current
density. So it is not surprising to find that the temperature dependence of $M(t_b,T)$ is
similar to that of $j_c(T)$ as shown in Fig. 3.2. In Fig. 3.4(b), the normalized initial decay
rate $S(t_b,T)$ of the relaxation curves at various temperatures is shown. $S(t_b, T)$ first
increases with temperature and then drops rapidly around 25 K, forming a peak with a
maximum of 0.35. In order to confirm that this peak was not due to the different
remanent magnetic fields at different temperatures, the decay of magnetization in a
constant applied field of 1.5 kOe was also measured, which also exhibited a peak around
23 K in $S(t_b, T)$. In addition, the relaxation of remanent magnetization was also studied
on other Bi-2212 single crystals prepared by both self-flux and TSFZ method and similar
results were obtained. Zavaritsky et al. [26] found also a peak in $S(t_b, T)$ at about 17 K,

which is at the same temperature of the kink in $j_c(T)$ for their Bi-2212 single crystals. It should be noted that a detailed analysis of the data of Shi et al. [14] for $H \parallel c$ revealed also a peak in $S(t_b, T)$ at about 30 K.

Fig. 3.4 The temperature dependence of (a) normalized initial magnetization $m(t_b, T)$, and (b) normalized initial decay rate $S(t_b, T)$ of the Bi-2212 single crystal. The error bars in (b) are due to some uncertainty in taking the initial slopes. The solid lines are the fits from the pinning distribution model (Chap. V). The dashed lines are the fits when high pinning energies above 60 meV are omitted.

In the Anderson-Kim model [Eq. (3.6)], the pinning potential is related to the normalized initial decay rate by

$$U_0 = \frac{kT}{S(t_b, T)} + kT\ln(t_b / \tau_0), \qquad (3.8)$$

which is obtained from Eqs. (3.6) and (3.7). Using this formula, the pinning energy U_0 in the Bi-2212 single crystals is estimated to be about 15 meV at low temperatures (T<25 K) and about 80 meV at high temperatures (T>25 K). The results suggest that there are two different pinning regimes for the single crystals: at T<25 K, the small pinning centres with a high density dominate the flux creep process, leading to a rapid decrease of j_c with temperature and a fast decay of magnetization; at T>25 K, however, the small pinning centres can no longer effectively pin the vortices because of thermal activation, so the larger effective pinning potentials with low density dominate the flux pinning, which lead to a slow decrease of $j_c(T)$ with temperature and slow decay of magnetization with time. Later in this chapter, a more detailed analysis will be given for the identification of different pinning regimes.

Finally, it should be mentioned that, when the magnetic field was applied perpendicular to the c-axis instead of parallel to the c-axis, the behaviour of the magnetic relaxation was found to be similar [32].

3.3.2. Bi-2212 bulk ceramic sample

The magnetic relaxation curves at various temperatures for a Bi-2212 ceramic sample are shown in Fig. 3.5. At low temperatures (T<30 K), the magnetization decayed slowly and the relaxation curves are nearly logarithmic over three decades of time. Below 30 K, the decay of the magnetization of the Bi-2212 bulk ceramic sample is much slower than that in the Bi-2212 single crystals. As the temperature increases and especially above $T_c/2$, the decay of the magnetization of the Bi-2212 bulk ceramic sample becomes faster and the relaxation curves become more nonlogarithmic over the observation time.
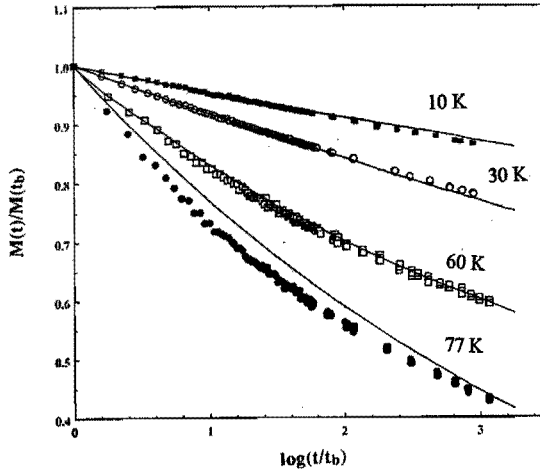
Fig.3.5 Magnetic relaxation curves for a Bi-2212 bulk ceramic sample. The solid lines are fits obtained from the pinning distribution model (Chapter V).

The normalized initial magnetization $M(t_b,T)$ and the normalized initial decay rate $S(t_b,T)$ are shown in Figs. (3.6a) and (3.6b) for the ceramic sample. The temperature dependence of $M(t_b,T)$ is similar to $j_c(T)$ in Fig.3.2 for the ceramic sample, which is expected in the Bean model. The initial decay rate $S(t_b, T)$ shown in Fig. 3.6 (b) increases monotonically with temperature. It was discussed in Ref. [25] that for some YBCO-123 samples, the normalized initial decay rate $S(t_b,T)$ is constant over a large temperature interval, suggesting a universal behaviour. However, such a behaviour has not been observed in our experiments for Bi-2212 superconductors, contradicting the proposed universal behaviour.
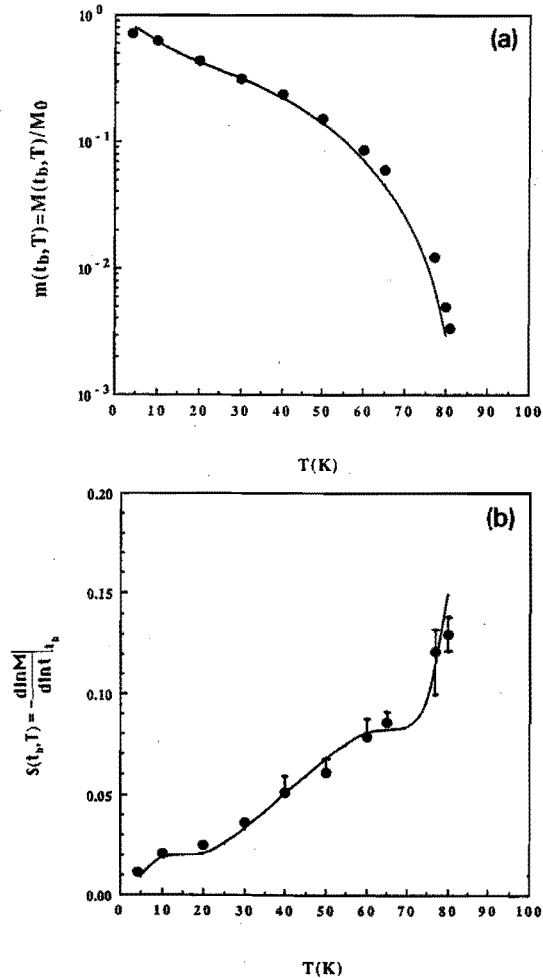
Fig. 3.6 *The temperature dependence of (a) normalized initial magnetization and (b) initial decay rate. The error bars in (b) are due to some uncertainty in taking the initial slopes. The solid lines are fits from the pinning distribution model (Chapter V).*

3.3.3. Bi-2212 ceramic powder

So far the experimental results reported in the preceding sections have shown a different decay behaviour for Bi-2212 single crystals and bulk ceramic samples, indicating that the pinning mechanism is different for the two types of samples. Since ceramic samples

consist of randomly oriented plate-like grains with a average size of about $100 \times 100 \times 2$ μm^3 (which are small crystals), the pinning centres (mostly point defects) that exist in the single crystals should also exist in the ceramic samples. Besides these pinning centres, there are many grain boundaries in the bulk ceramic samples, which could also act as pinning centres. Therefore, the pinning situation seems to be more complex in the bulk ceramic samples than in single crystals. Crushing the bulk ceramic sample into powders could reduce the numbers of grain boundaries, while preserve the nature of random orientation of the grains as in the bulk samples. If the grain boundaries are strong pinning centres in the bulk ceramic samples, it is expected that the pinning strength in the grains of powders should be less than in the bulk samples. To explore this, the bulk ceramic sample was crushed into powders with an average size of about 50 μm and the magnetic relaxation of the loosely packed powders was measured.
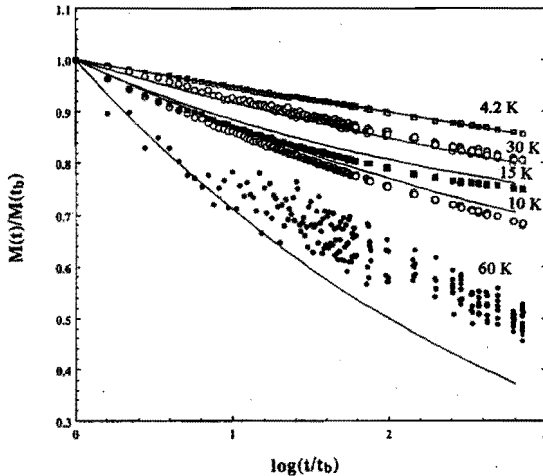
Fig.3.7 Magnetic relaxation curves for the Bi-2212 powered sample. The solid lines are fits from the pinning distribution model (Chap. V).

The magnetic relaxation curves of the powders shown in Fig 3.7 are quite different from those of the bulk sample. Around 15 K (10-17 K), the decay curves are strongly

nonlogarithmic. However, the decay became much slower at T~30 K than at lower temperatures. Between 30 and 60 K, the magnetization decayed gradually faster as the temperature increases. Except at temperatures around 15 K (10-17 K), only a weak nonlogarithmic decay could be observed in the relaxation curves below 60 K over about 3 decades of observation time.

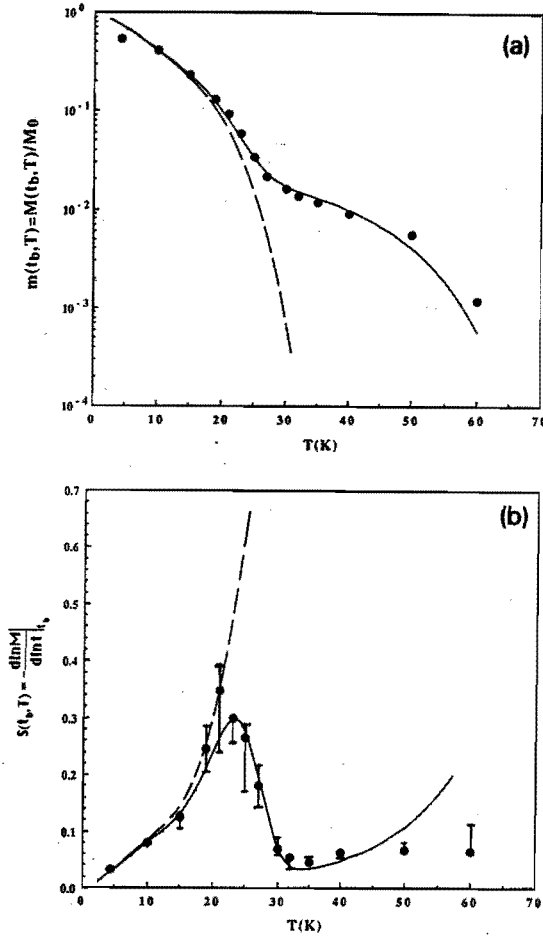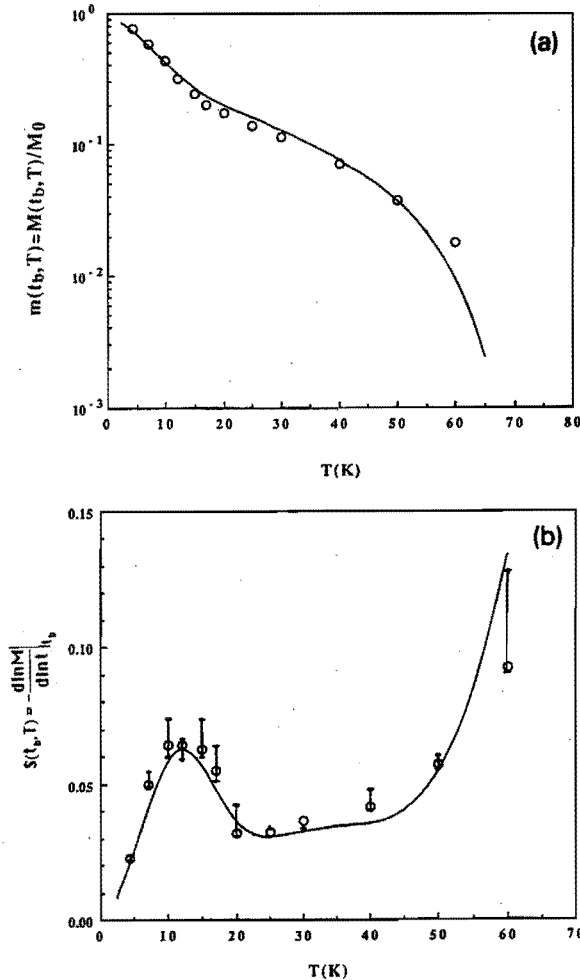*Fig. 3.8. The temperature dependence of (a) the normalized initial magnetization and (b) normalized initial decay rate of Bi-2212 powdered sample. The error bars in (b) are due to some uncertainty in taking the initial slopes. The solid lines are fits from the pinning distribution model (Chap. V).*

In Figs. 3.8 (a) and (b), the normalized initial magnetization $M(t_b,T)/M_0$ and initial decay rate $S(t_b,T)$ of the relaxation curves are shown for the powdered sample. Compared with the original bulk sample, a large difference in the relaxation behaviour of the powders can be observed: a weak "kink" appeared at 15 K in $M(t_b,T)$; and especially, a peak with a maximum of about 0.06 existed at 12 K in the curve of $S(t_b,T)$.

An explanation for the appearance of the small peak in $S(t_b,T)$ after crushing the Bi-2212 bulk sample into powders will be given here. In the bulk ceramic sample, the total magnetic moment originates from both intragrain critical current density j_c^{intra} (i.e. the critical current density in the single crystals) and intergrain critical current density j_c^{inter}. Using the Bean model, the ratio of the total magnetic moment due to the intergrain and intragrain current can be estimated to be:

$$\frac{M_{inter}}{M_{intra}} \approx \frac{j_c^{inter} R\, V}{j_c^{intra} r(N_g V_g)} \approx \frac{j_c^{inter} R}{j_c^{intra} r} \quad ,$$

where R is the macroscopic size of the bulk sample (~1cm), V the volume of the bulk sample, r the typical microscopic size of the grains (~ 100 x 100 x 2 μm^3) in the bulk sample, N_g the number of grains and V_g the (average) volume of one grain. For the Bi-2212 superconductors, if j_c^{inter} is taken as the critical current density of the bulk ceramic samples and j_c^{intra} is taken to be the critical current density of the single crystals, the difference between the value of j_c^{inter} and j_c^{intra} is within one order of magnitude (see Fig. 3.2). For the bulk ceramic samples, $R \geq 10^2 \cdot r$, so the magnetic moment produced by the intergrain current is much larger than the magnetic moment produced by the intragrain current, i.e. $M_{inter} \gg M_{intra}$. When the bulk ceramic sample was crushed into powders, however, R became the size of the powder particles, which is comparable to the size of the grains; so, both M_{inter} and M_{intra} became important for the magnetization behaviour. Since the magnetization in the powdered sample is composed of M_{inter} and M_{intra}, a small peak in $S(t_b,T)$ could be produced.

3.4 Summary of the experimental results

In summary, with an observation time of more than 3 decades, a nonlogarithmic decay
of magnetization was observed in Bi-2212 superconductors at temperatures down to 10
K, which is in contradiction to the traditional Anderson-Kim model. The behaviour of
the magnetic relaxation was found to be different for Bi-2212 single crystalline and
polycrystalline samples. The temperature dependence of the normalized initial decay rate
$S(t_b, T)$ shows a strong peak at about 25 K for Bi-2212 single crystals, while $S(t_b, T)$
increases monotonically with temperature for Bi-2212 bulk ceramic samples. By
crushing the bulk ceramic samples into powders, a small peak in $S(t_b, T)$ at about 20 K
was found. In the next two chapters, the experimental results presented in this chapter,
especially the nonlogarithmic decay of the magnetization, will be analysed and discussed
in terms of a non-linear current dependence of the pinning potential or a distribution of
pinning energies.

It has to be mentioned that besides the strong peak found in $S(t_b, T)$ at low temperature
(~25 K) for Bi-2212 single crystals, a second broad peak in $S(t_b, T)$ with a lower
maximum value at about 60 K was reported by several other groups [26, 33, 34]. Such a
peak at high temperatures was not measured in our experiments due to a lower
sensitivity and a relative higher noise level of the VSM equipment at high temperatures.

3.5. The different pinning regimes in Bi-2212 single crystals: recent developments

As discussed in the previous section, for the Bi-2212 single crystals, the observation of
both a "kink" in the $j_c(T)$ and a strong peak in $S(t_b, T)$ at about 25 K suggests that, below
and above 25 K, the mechanisms of the flux pinning are different.

Pradhan et al [33] suggested that, below 25 K, the flux pinning and inter-layer coupling
are strong, resulting 3D flux line pinning; but above 25 K, the vortices between the
layers are decoupled, resulting into 2D pancakes vortices.
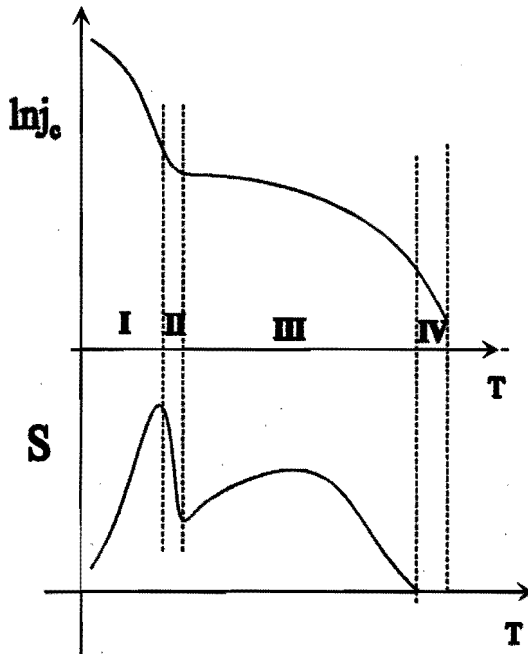
Fig. 3.9. Identification for the different pinning regimes by Metlushko et al [34], where j_c is the critical current density, and S the initial decay rate of the relaxation curves.

Here, the dimensionality of the vortices in the Bi-2212 single crystals in our magnetic relaxation experiments has to be clarified. In our remanent magnetic relaxation experiments, the self-field induced by the current density in the sample at 4.2 K is about 3-4 kG for our samples, so the vortices are three dimensional (3 D); at about 25 K, where the "kink" is present, the self-field is about 50 G, which is too weak to break the flux lines into 2 D pancakes. So the vortices in our relaxation experiments should be always 3 D. Similar argument can also be found in Ref. [34] for the magnetic relaxation experiments on their Bi-2212 single crystals.

Recently, Metlushko et al. [34] gave a detailed analysis for the relaxation behaviour of Bi-2212 single crystals and proposed that the sharp kink in the $j_c(T)$ curve corresponds to a transition from individual flux line pinning at low temperatures to the large-flux-

bundle pinning regime at high temperatures. According to the behaviours of $S(t_b, T)$ and $j_c(T)$, as shown in Fig. 3.9, four different pinning regimes were proposed in Ref. [34]. In the regime I, i.e. below the temperature of the maximum $S(t_b, T)$, the pinning of individual flux lines takes place with a characteristic energy $U_0 = H_c^2 \xi^3 (\xi/L_c)$, where L_c is the correlation length of a single vortex line pinned collectively by many nearby point defects. The pinning regime II, which is defined by the temperature interval between the Maximum $S(t_b, T)$ and the kink in $j_c(T)$, corresponds to the collective pinning of small flux bundles. Below a certain value of the critical current density current j_{cr} and for $S(t_b, T) > 0$, a regime III with large flux bundles occurs. Finally, in the temperature region between the zero value of $S(t_b, T)$ and zero value of $j_c(T)$, a pinning regime IV is found, which corresponds to molten flux lattice with a reversible behaviour of the vortex fluid. The value of j_{cr}, at which the kink occurs in $j_c(T)$, was calculated to be [34]:

$$j_{cr} = j_0/\kappa^2,$$

where j_0 is the depairing current, i.e. $j_0 = \phi_0 c/(12\pi^2\sqrt{3}\lambda_{ab}^2\xi_{ab})$, and κ the Ginsberg-Landau parameter. Using the parameters of Bi-2212, j_{cr} is estimated to be 10^4-10^5 A/cm². For our crystals prepared by the TSFZ method, j_{cr} is found indeed in this range; for the crystals prepared by the flux method, j_{cr} is a little bit smaller, which could be due to a different value of the penetration depth caused by different oxygen content [31].

However, a remark has to be made here for their identification of the pinning regime II. As it will become clear in Chapter V, within the framework of thermally activated flux creep, the peak in $S(t_b, T)$ at low temperature is directly related to the kink in $j_c(T)$. In such a case, the position (temperature) of the peak in $S(t_b, T)$ should be a little lower than the position (temperature) of the kink in $j_c(T)$. Therefore, the identification of the regime II in Ref. [34], which is because of a temperature difference between the position of the peak in $S(t_b, T)$ and the kink in $j_c(T)$, seems to be artificial.

References

[1] K.A. Müller, M. Takashige and J.G. Bednorz, Phys. Rev. Lett.58 (1987) 114.

[2]A.C. Mota. A. Pollini, P. Visani. K.A. Müller and J.G. Bednorz, Phys. Rev. B 36 (1987) 401.

[3] M. Tuominen, A.M. Goldman and M.L. Mecanney, Phys. Rev. B 37 (1988) S48.

[4] M. Tuominen, A.M. Goldman and M.L. Mecanney, Physica C 153-155 (1988) 324.

[5]Y. Yeshurun and A.P. Malozemoff, Phys. Rev. Lett. 60 (1988) 2202.

[6] Y.B. Kim, C.F. Hempstead and A.R. Strnad, Phys. Rev. Lett. 9 (1962) 306.

[7] P.W. Anderson, Phys. Rev. Lett. 9 (1962) 309.

[8] D. Dew-Hughes, Cryogenics 28 (1988) 674.

[9] Youwen Xu, M. Suenaga, A.R. Moodenbaugh and D.O. Welch, Phys. Rev. B 40 (1989) 10882.

[l0]Youwen Xu, M. Suenaga, Y. Gao. J.E. Crow and N.D. Spencer, Phys. Rev. B 42 (1990) 8756.

[11] S.W. Hsu, Y.C. Chen, K. Chen and W.H. Lee, Solid State Commun. 77 (1991) 843.

[12] Z.J. Huang. Y.Y. Xue, P.H. Hor and C.W. Chu, Physica C 176 (1991) 195.

[13] P. Svedlindh, C. Rossel, K. Niskanen, P. Norling, P. Nordblad, L. Lundgren and G.V. Chandrashekhar, Physica C 176 (1991) 336.

[14] Donglu Shi and Ming Xu, Phys. Rev. B 44 (1991) 4548.

[15] P. Svedlindh, K. Niskanen, P. Norling, P. Nordblad, L. Lundgren, C. Rossel, M. Sergent, R. Chevrel and M. Potel. Phys. Rev. B 43 (1991) 2735.

[16] E. Zeldov, N.M. Amer, G. Koren, A. Gupta, M.W. McElfresh and R.J. Gambino, Appl. Phys. Lett.56 (1990) 680.

[17] E. Zeldov. N.M. Amer, G. Koren and A. Gupta, Appl. Phys. Lett. 56 (1990) 1770.

[18] R.H. Koch, V. Foglietti, W.J. Gallagher, G. Koren, A. Gupta and M.P.A. Fisher, Phys. Rev. Lett. 63 (1989) 1151.

[19] M.P.A. Fisher, Phys. Rev. Lett. 62 (1989) 1415.

[20] M. V. Feigel'man, V B. Geshkenbein, A.I. Larkin and V.M. Vinokur, Phys. Rev Lett. 63 (1989) 2303.

[21] M.V. Feigel'man. VB. Geshkenbein an.d V.M. Vinokur, Phys. Rev. B 43 (1991) 6263.

[22] C.W. Hagen and R. Griessen, Phys. Rev. Lett. 62 (1989) 2857.

[23] R.Griessen, Physica C 175 (1991) 315.

[24] R. Griessen, Phys. Rev. Lett. 64 (1990) 1674.

[25] A.P. Malozemoff and M.P.A. Fisher, Phys. Rev. B 42 (1991) 6784.

[26] V. N. Zavaritsky and N.V. Zavaritsky, JETP Lett. 54 (1991) 22.

[27] Y. F. Fan, C.Z. Li, J.H. Wang, Q.S. Yang, Y.C. Chang, Q.S. Yang, D.S. Hou, X. Chu, Z.H. Mai, H.Y. Chang, D.N. Zeng, Y.M. Ni, S.L. Jia, D.H. Shen, and Z.X. Zhao, Mod. Phys. Lett. B2 (1988) 571.

[28] J. H. P. M. Emmen, S. K. J. Lenczowski, J. H. J. Dalderop, V. A. M. Brabers, J. Crystal Growth 118 (1992) 477.

[29] W. Paul and Th. Baumann, Physica C 175 (1991) 102.

[30] H. Dersch and G. Blatter, Phys. Rev. 38, 11391 (1988).

[31] T.W. Li, A.A. Menovsky, J.J.M. Franse, and P. H. Kes, Physica C 257, 179 (1996).

[32] M. Mittag, M. Rosenberg, D. Peligrad, R. Wernhardt, V. Brabers, J. H. P. M. Emmen, and D. Hu, Supercond. Sci. Technol. 7 (1994) 214.

[33] A. K. Pradhan, S. B. Roy, P. Chaddah, C. Chen, and B. M. Wanklyn, Phys. Rev. B 49 (1994) 12984.

[34] V.V. Meltlushko, G. Güntherodt, V.V. Moshchalkov, and Y. Bruynseraede, Europhys. Lett. 26 (1994) 371.

Chapter IV The current dependence of the pinning potential:

a generalised model

[Part of this chapter has been published in Physica C 205, 123(1993).]

Many things in this world have their common origin, just like that several children have one mother. Reveal the mother, and you understand the children better. Understand the children, and you should return to the mother. In this way, you cannot fail.

-------*Lao Tse, Chap. 52, ca. 800 B.C.*

In this chapter, the decay of the magnetization presented in Chapter III will be analysed with a general (non-linear) current dependence of the effective pinning potential $U_{eff}(j)$, in contrast to the linear current dependence of $U_{eff}(j)$ used in the Anderson-Kim model. It will be shown that the magnetic relaxation data measured at different temperatures can be combined into one single curve, from which the current dependence of $U_{eff}(j)$ can be obtained.

4.1. Introduction

The observation of the nonlogarithmic decay of the magnetization in high-T_c superconductors, which is not predicted by the traditional Anderson-Kim model, has attracted much attention both in the experimental [1-5] and theoretical [6-9] studies. Current theories attribute the nonlogarithmic decay either to a non-linear current dependence of the effective pinning potential $U_{eff}(j)$ [6-8] or a distribution of pinning energies [5,9]. The distribution of pinning energies can be derived from the magnetic relaxation data, which will be discussed in detail in the next chapter. For the current dependence of $U_{eff}(j)$, however, different forms has been proposed in different models, as will be described below.

1). In the Anderson-Kim model, as has been discussed in Chapter III, a linear j dependence of $U_{eff}(j)$ was proposed, i.e.

$$U_{eff}(j)=U_0(1-j/J_c),\qquad\qquad(4.1a)$$

where Jc is the critical curent density in the absence of flux creep [For the notation of j, j_c, J_c and J_{c0} in this cahpter, please refer to Section 1.6]. This leads to a logarithmic decay of the current density in the critical state during the magnetic relaxation experiments:

$$j(t,T)=J_c\left[1-kT\ln(t/\tau_0)/U_0\right].\qquad\qquad(4.1b)$$

Such a logarithmic decay was observed in most of the traditional superconductors. However, as discussed in Chapter III, a nonlogarithmic decay has been widely observed for the high-T_c superconductors, in contradiction to this model.

2). By considering that the pinning potential of point defects could have a logarithmic function with the distance parameter, Zeldov et al. [8] postulated a logarithmic current dependence of $U_{eff}(j)$, i.e.,

$$U_{eff}(j)=U_0\ln(J_c/j),\qquad\qquad(4.2a)$$

which leads to a power law decay of the current density in the magnetic relaxation experiments:

$$j(t,T)=J_c(t/\tau_0)^{-kT/U_0}\equiv J_c\exp\left[-kT\ln(t/\tau_0)/U_0\right].\qquad\qquad(4.2b)$$

3). In the vortex-glass [6] and the collective-pinning theory [7], the current dependence of $U_{eff}(j)$ was found to be:

$$U_{eff}(j)=\frac{U_0}{\mu}\left[\left(\frac{J_c}{j}\right)^{\mu}-1\right].\qquad\qquad(4.3a)$$

The time dependence of the current density during the magnetic relaxation is predicted to follow the law:

$$j(t,T)=J_c\left(1+\mu kT\ln(t/\tau_0)/U_0\right)^{-1/\mu},\qquad\qquad(4.3b)$$

where the exponent μ could be different in different pinning regimes [10-11].

Experimentally, these different relaxation laws have been extensively used to fit the relaxation curves in order to study which model is applicable. However, due to different samples, different magnetic fields, and different observation times, each of these

relaxation laws has been found to be applicable for some situations but not for all the situations. Therefore, no definite conclusion could be drawn in this way up to now.

From the discussion above, it can be seen that the controversies between different theories come directly from the different j dependence of $U_{eff}(j)$. *Is it possible to analyse the relaxation data without any specific assumption of the current dependence of the pinning potential $U_{eff}(j)$? Furthermore, could we obtain the current dependence of $U_{eff}(j)$ from the experimental relaxation data, rather than from theoretical considerations?*

The answer is positive. Maley et al. [12] proposed a method that used the decay curves at different temperatures to obtain the current dependence of $U_{eff}(j)$ for $YBa_2Cu_3O_{7-\delta}$ (YBCO-123) powdered samples. Here, this method is described briefly. In the flux-creep regime, for the magnetic relaxation, we have:

$$\frac{dM(t,T)}{dt} = -\frac{B\Omega_0 a_0}{\pi d} e^{-U_{eff}(j)/kT} , \qquad (4.4a)$$

which can be rewritten as:

$$U_{eff}(j) = kT\left[-\ln|dM/dt| + \ln(B\Omega_0 a_0 / \pi d)\right], \qquad (4.4b)$$

where M is the magnetization, d the average size of the powder particles. Since the current density j can be calculated from M using the Bean model, the relationship of U_{eff} vs. j can be obtained from (4.4b) as follows: firstly take the time derivative of the magnetization M(t,T) from the relaxation curves at various temperatures, and then use the "try and error" method to obtain the value of the constant term $\ln(B\Omega_0 a_0/\pi d)$ in order to make the relaxation data collapse into one single curve, i.e. $U_{eff}(j)$ verus j. However, in this method, the temperature dependence of the pinning potential $U_0(T)$ and the critical current density $J_c(T)$ is not considered. If this method is directly extended for high-temperature data, the relaxation data will not collapse into one curve [11].

In the next section, we will describe another method to answer the questions proposed early in this section. With this method, the relaxation curves at different temperatures can be combined together and the current dependence of $U_{eff}(j)$ can be obtained from the relaxation data. In contrast with Maley's method, the temperature dependence of $U_0(T)$ and $J_c(T)$ will also be included.

4.2. The model

After examining the different relaxation laws expressed in Eqs. (4.1b), (4.2b) and (4.3b), it can be seen that, although the j dependence of $U_{eff}(j)$ is different in different models, $j(t,T)$ is always a function of $kT\ln(t/\tau_0)$ in these cases.

The question is : is this universal for any j dependence of $U_{eff}(j)$? The answer is positive. Let us start from the flux-creep equation for the magnetic relaxation experiments:

$$\frac{dj(t,T)}{dt} = -\frac{B\Omega_0 a_0}{\pi g} e^{-U_{eff}(j)/kT} , \qquad (4.4c)$$

where g is the geometric factor coming from the Bean model (in this model, $j \propto M$). Assuming that at t=0, the sample is in its initial critical state, i.e. $j=J_c$ and $U_{eff}(j=J_c)=0$, after rearranging the terms in Eq.(4.4c), and taking an integral, we have

$$\int_0^{U_{eff}} e^{U_{eff}(j)/kT} \left(\frac{dU_{eff}}{dj}\right)^{-1} dU_{eff}(j) = \int_0^t \gamma dt,$$

where $\gamma = -(B\Omega_0 a_0)/(\pi g)$. On the left side of the equation, compared with the exponential term $\exp[U_{eff}(j)/kT]$, the term dU_{eff}/dj can be treated as a constant in a first approximation. Evaluating the integral [13], the following is obtained:

$$U_{eff}(j) = kT\ln(t/\tau_0 + 1)$$
$$\approx kT\ln(t/\tau_0) \quad (t \gg \tau_0) \qquad (4.5)$$

where $\tau_0 \approx kT/(\gamma\, dU_{eff}/dj)$. In Eq. (4.5), compared with T, $\ln(t/\tau_0)$ can be considered to be temperature independent, since τ_0 is contained inside the logarithmic term. The relation of Eq.(4.5) was obtained firstly by Geshkenbein and Larkin [14]. When the temperature dependence of $U_0(T)$ and $J_c(T)$ is not considered (i.e. for $T \ll T_c$), Eq. (4.5) implies that $j(t,T)$ is only a function of $kT\ln(t/\tau_0)$, or

$$j(t,T)=U_{eff}^{-1}[kT\ln(t/\tau_0)], \qquad (4.6)$$

which is valid for any j dependence of $U_{eff}(j)$. So, the postulation of the universality mentioned at the beginning of this section is solid (for $T \ll T_c$).

Now we will consider the temperature dependence of the pinning potential $U_0(T)$ and the critical current density $J_c(T)$ in order to generalise Eq. (4.5). First we define that

$$J_c(T)=J_{c0}c(T), \qquad (4.7a)$$

and

$$U_0(T)=U_{0t}b(T), \qquad\qquad (4.7b)$$

where the functions b(T) and c(T) describe the temperature dependence of $U_0(T)$ and $J_c(T)$, respectively; J_{c0} and U_{0t} are the critical current density and the pinning potential at T=0 K. Then, we assume that the two temperature factors in $U_{eff}(T,j/J_c)$ can be separated, i.e.:

$$U_{eff}[T, j/J_c(T)]=b(T)\; U_{eff,0}[j/(J_{c0}\; c(T))], \qquad (4.7c)$$

where $U_{eff,0}[j/J_c]$ is the effective pinning potential dominated by its current dependence. Eq. (4.7c) implicates that the current dependence of the function $U_{eff}(T,j/J_c)$ does not change its shape with temperature, and is only scaled by the temperature-dependent factors b(T) and c(T), which has been widely used or implied in the literature. Combining Eqs. (4.5) and (4.7c), we have

$$U_{eff,0}\left(\frac{j(t,T)}{J_{c0}c(T)}\right)=\frac{kT}{b(T)}\ln(t/\tau_0) \qquad . \qquad (4.8)$$

Equation (4.8) indicates that j/J_c is only a function of $kT\ln(t/\tau_0)/b(T)$, which could be expressed as

$$j(t,T)=J_{c0}\cdot c(T)\cdot F\left(\frac{kT\ln(t/\tau_0)}{b(T)}\right), \qquad (4.9)$$

where F is a general function.

4.3. Combining the magnetic relaxation curves and obtaining the j dependence of $U_{eff}(j)$

Equation (4.9) has some very interesting consequences. It indicates that *all the relaxation curves measured at different temperatures should collapse on one single curve by expressing them in terms of the common variable kTln(t/τ₀)/b(T), i.e. j(t,T)/c(T) vs. kTln(t/τ₀)/b(T)*. Now the problem is how to determine b(T), c(T), and the value of $\ln(1/\tau_0)$.

Taking the temperature and ln(t) derivatives of Eq. (4.9), respectively, gives:

$$\left(\frac{\partial j(t,T)}{\partial nt}\right)_T \bigg/ \left(\frac{\partial (j(t,T)/c(T))}{\partial T}\right)_t = \frac{T}{\ln(t/\tau_0)}\left[\frac{c(T)}{b(T)} \bigg/ \frac{d[T/b(T)]}{dT}\right]. \quad (4.10a)$$

Note that the unknown function F and the value of J_{c0} do not appear in the above equation. Denoting the started measurement time of the magnetic relaxation as $t=t_b$, the above equation can be written as:

$$\ln(t_b/\tau_0) = -\frac{T\left[\dfrac{d\ln j(t_b,T)}{dT} + c(T)\dfrac{dc(T)}{dT}\right]}{S(t_b,T)\left(1-\dfrac{d\ln b(T)}{d\ln T}\right)}, \quad (4.10b)$$

where

$$S(t_b,T) = -\left(\frac{d\ln j}{d\ln t}\right)_{t=t_b} \quad (4.11)$$

is the normalized initial decay rate. The definition of $S(t_b,T)$ in Eq. (4.11) is identical to Eq. (3.7), since in the Bean model, $j \propto M$.

At low temperatures, $b(T) \approx 1$ and $c(T) \approx 1$, Eq.(4.10b) reduces to to be [15]

$$S(t_b,T) = \frac{T}{\ln(t_b/\tau_0)}\left(-\frac{d\ln j(t_b,T)}{dT}\right). \quad (4.10c)$$

Using this relation, the connection between the peak on $S(t_b, T)$ and the "kink" on $j(T)$ observed in the Bi-2212 single crystals (Chapter III) can be explained. More details will be given in the next chapter (Section 5.5).

As discussed in Ref. [9], $b(T)$ or $c(T)$ should be proportional to $H_c^2(T)\xi^n(T)$, where the value of n depends on the nature of the flux bundles and could be different for $c(T)$ and $b(T)$. For $b(T)$, $0 \le n \le 3$; and for $c(T)$, $-1 \le n \le 3$. if we define $\theta = T/T_c$, and use $H_c(T) \propto (1-\theta^2)$ and $\lambda(T) \propto (1-\theta^4)^{-1/2}$ [9], $b(T)$ and $c(T)$ have the following general form:

$$(1-\theta^2)^2\,[(1+\theta^2)/(1-\theta^2)]^{n/2}\,.$$

Using this general form, the functions $c(T)$ and $b(T)$ can be determined (i.e. the exponent n can be chosen) such that $\ln(t_b/\tau_0)$ is temperature independent in Eq.(4.10b); by doing this, the value of $\ln(t_b/\tau_0)$ can be obtained too.

Now this method will be applied to the magnetic relaxation curves measured for the $Bi_2Sr_2CaCu_2O_{8+z}$ (Bi-2212) single crystals and Bi-2212 ceramic samples presented in Chapter III. Using Eq.(4.10b), we obtained that, for the single crystal, $b(T)=c(T)=(1-\theta^2)^2$ (i.e. $n=0$), and $\ln(t_b/\tau_0) \approx 13$; while for the ceramic sample, $b(T)=c(T)=1-\theta^4$ (i.e. $n=2$), and $\ln(t_b/\tau_0) \approx 23$. The relaxation data obtained at various temperatures can now be plotted in
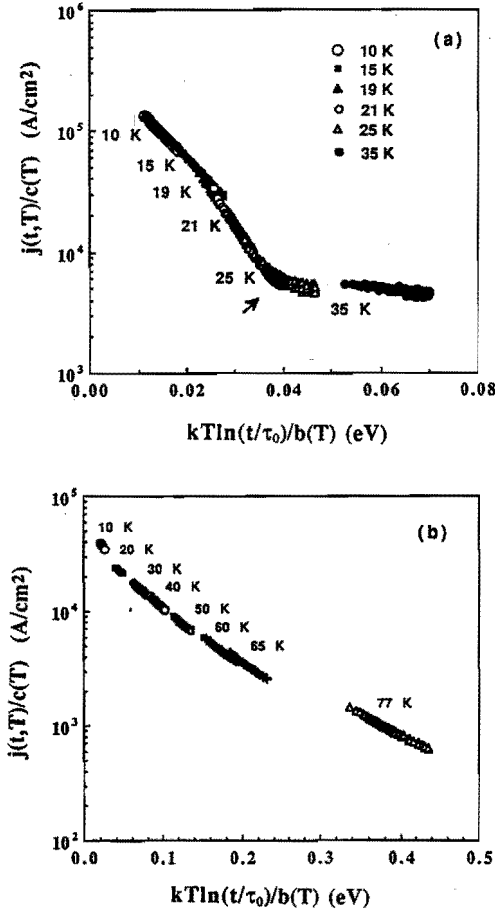
Fig.4.1. The relaxation curves at various temperatures can be combined by plotting log[j(t,T)/c(T)] vs. kTln(t/τ₀)/b(T) (see text) (a) for Bi-2212 single crystal, (b) for Bi-2212 bulk ceramic sample.

one graph, i.e. by plotting $j(t,T)/c(T)$ versus $kT\ln(t/\tau_0)/b(T)$. The results are shown in Fig. 4.1 for both types of samples. The relaxation curves measured at different temperatures indeed collapse into one single curve. Only small discrepancies are observed, probably due

to some variation of $\ln(t_b/\tau_0)$ with the temperature. Since $U_{eff,0}(j/J_c) = kT\ln(t/\tau_0)/b(T)$ [Eq. (4.8)], Fig. 4.1 actually gives the current dependence of the effective pinning potential $U_{eff,0}(j/J_{c0})$ for both samples, which shows that the j dependence of $U_{eff}(j)$ is non-linear, and more complex than what can be expected from the existing models. In the single crystal, $U_{eff,0}(j/J_c)$ increases abruptly at $j(t,T)\approx J_{c0}/70$, or when $kT\ln(t/\tau_0)/b(T)\approx 37$ meV. This is due to a transition between two different pinning mechanisms, as discussed in Chapter III.
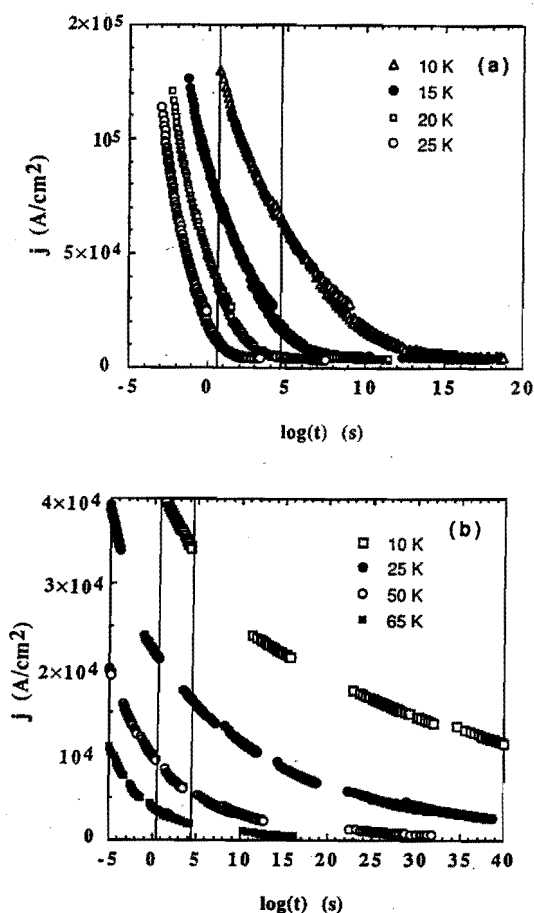
Fig. 4.2. The time dependence of current density at various temperatures obtained from the data in Fig. 4.1, (a) for the single crystal and (b) for the ceramic sample. The two vertical lines indicate the time periods used in the experiments.

Another interesting consequence of this method is that the data in Fig. 4.1 can be used to obtain the time dependence of the current density j, after evaluating the temperature factors b(T) and c(T) at any given temperature. Since Fig. 4.1 contains more data than the experimentally obtained original relaxation data at each temperature, the time dependence of the current density j obtained by this theoretical method will have a much larger time window. In order to clarify this point, the time dependence of the current density j is shown in Fig. 4.2 for several temperatures, which is directly obtained from Fig. 4.1. The original time period (i.e. about 3 decades of time, see Figs. 3.3 and 3.5) used for the experiments is indicated by two vertical lines. Fig. 4.2 shows that, firstly, the decay of the magnetization should be always nonlogarithmic when the observation time is sufficiently long; secondly, the relaxation curves obtained at different temperatures are actually parts of one single curve (the relation of U_{eff} vs j). Of course, caution is needed when interpreting the extended data in Fig. 4.2 at very long times (.i.e. the original data at high temperatures), since the method is based on the assumption for the temperature dependence of $U_{eff}[T, j/J_c(T)]$ [see Eq.(4.7c)]. This method cannot be used for very short times either, since an assumption that $t \gg \tau_0$ was made.

4.4. A method for combining current-voltage (I-V) characteristics

A similar method can be applied to electrical transport I-V curves, provided these I-V curves are measured in the flux creep regime. In the flux creep model, the electric field E induced by the movement of the vortices can be expressed as:

$$E = E_0 e^{-U_{eff}/kT}, \qquad (4.12)$$

where $E_0 = B\Omega_0 a_0$. Assuming the same temperature dependence of $U_{eff}(T, j/J_c)$ as in Eq. (4.7c), we obtain directly from Eq.(4.12) that

$$U_{eff,0}\left(\frac{j(E,T)}{J_{c0}c(T)}\right) = \frac{kT}{b(T)}\ln(E_0/E) . \qquad (4.13)$$

The above result means that $j/c(T)$ is simply a function of $kT\ln(E_0/E)/b(T)$, i.e.:

$$j(E,T) = J_{c0} \cdot c(T) \cdot F\left(\frac{kT\ln(E_0/E)}{b(T)}\right), \qquad (4.14)$$

where F is a general function. Taking the ln(E) and temperature derivatives in Eq. (4.14), to be similar to (4.10b), we obtain:

$$\ln(E_0 / E_c) = -\frac{T\left[\dfrac{d\ln j(E_c,T)}{dT} + c(T)\dfrac{dc(T)}{dT}\right]}{P(E_c,T)\left(1 - \dfrac{d\ln b(T)}{d\ln T}\right)} \qquad (4.15)$$

where $j(E_c,T)$ is the current density corresponding to a electric-field of E_c at temperature T, and $P(E_c,T)$ is defined as

$$P(E_c,T) = \left(\frac{d\ln j}{d\ln E}\right)_{E_c} , \qquad (4.16)$$

which is the slope at E_c in the logarithmic plot of j against E.

Eq. (4.14) indicates that *the I-V curves can be combined by expressing them in terms of the common variable $kTln(E_0/E)/b(T)$, which is actually $U_{eff,0}(j/J_c)$ [Eq. (4.13)]*. The value
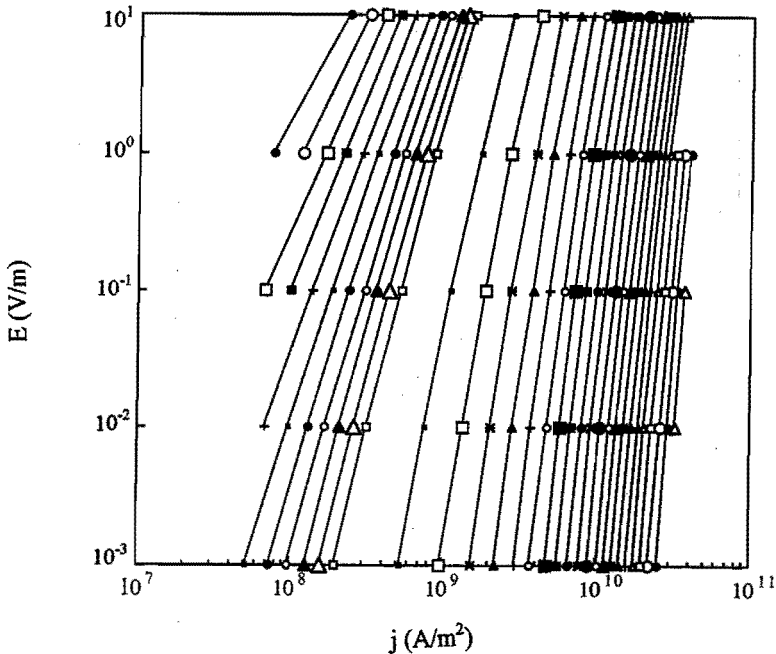
Fig. 4.3 *The E-j data extracted from Ref. [10] for a YBCO-123 film at a magnetic field of 1 T. The data are for temperatures from 18.5 K (right) to 86.5 K (left) with a temperature interval of 3 K for T<81.5 K and of 0.5 K for T>81.5 K.*

of $\ln(E_0)$ and the functions $b(T)$ and $c(T)$ can be determined from Eq. (4.15) in the same way used in above section for the magnetic relaxation curves.

Since we did not measure the transport I-V curves at low temperatures, the published data of Dekker et al. [10] was used for the application of this method. The j-E data shown in Fig. 4.3 were extracted from Ref. [10] [Fig.(1a) in that paper] for a YBCO-123 film ($\sim150\times3\times0.3$ μm^3) with a T_c of 90 K. The j-E curves were obtained at temperatures from 18.5 K to 86.5 K with an interval of 3 K below 81.5 K and of 0.5 K above 81.5 K in the presence of a magnetic field of 1 T. We use a electric field of $E_c=0.1$ V/m for obtaining the value of $j(E_c,T)$ and $P(E_c,T)$ in Eq. (4.15). In order to keep $\ln(E_0/E_c)$ in Eq. (4.15) to be temperature indepedent, the best choice for $b(T)$, $c(T)$ was found to be: $b(T)=(1-\theta^2)(1-\theta^4)^{1/2}$, and $c(T)=1$ [16]. The value of $\ln(E_0)$ was obtained to be 7.2 (from which $\Omega_0\approx2.7\times10^{10}$ Hz can be deduced). The j-E curves at various temperatures in Fig. 4.3 can now be replotted, i.e. by plotting $j(t,T)/c(T)$ versus $kT\ln(E_0/E)/b(T)$. The result is is shown in Fig. 4.4. All the data collapse into one single curve, demonstrating that the thermally activated flux creep is the fundamental mechanism of the dissipation in the YBCO-123 films in the measured regime. From Eq. (4.13), Fig. 4.4 also gives the nonlinear current dependence of the effective pinning potential $U_{eff,0}(j/J_c)$.
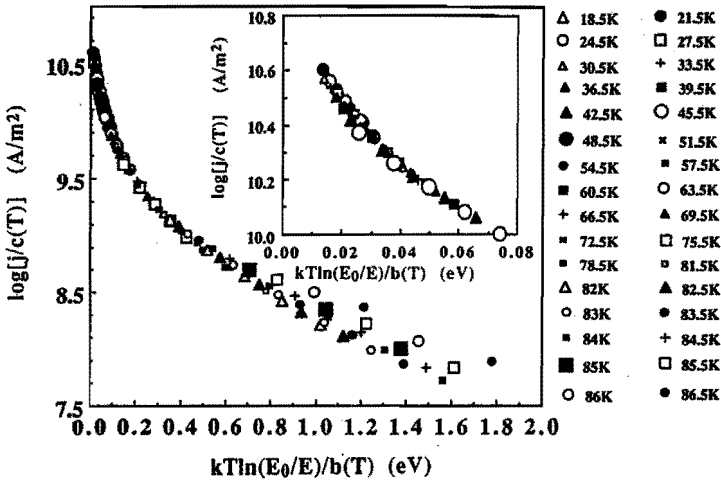
Fig. 4.4 Log[j(E,T)/c(T)] vs. kTln(E₀/E) for the E-J data in Fig. 4.3. The data collapse into one single curve. The high-current data (i.e. for T<48 K) are especially shown in the insert for clarity.

4.5. A brief discussion of other relevant models

1). Lairson et al.[4] expressed j(t,T) as an expansion of $\ln(t/\tau_0)$:

$$j(t,T) = j_0 - \frac{1}{\alpha} kT\ln(t/\tau_0) + \frac{\beta}{2\alpha^3}(kT)^2 \ln^2(t/\tau_0).$$

Here α and β are parameters, which can be determined by fitting the relaxation curves. It can be seen that this expression of j(t,T) is a special case of Eq. (4.9).

2). In the pinning distribution model [9], j(t,T) is expressed as

$$j(t,T) = j_0 c(T) \int_{U_0^*}^{\infty} N(u) \left[1 - \frac{kT}{ub(T)} \ln(t/\tau_0) \right] du .$$

where $U_0^* = kT\ln(t/\tau_0)/b(T)$. This expression is also in agreement with the universality of j(t, T) given by Eq.(4.9).

3). Schnack et al. [17] proposed a generalised inversion scheme (GIS) for obtaining the current dependence of $U_{eff}(j)$ from dynamic relaxation experiments, which are applicable over the whole superconducting temperature range. Their basic idea is also similar to Maley's method. Compared with our method, they found a relation between the temperature dependence of the pinning energies and critical current density, therefore, no assumption for the specific form of these temperature dependence [i.e. b(T) and c(T)] is needed. From this point of view, their method has less restriction and is more general. However, our approach, starting from the universality in different relaxation laws of Eqs. (4.1b), (4.2 b) and (4.3b), seems to be more straightforward in practice.

References

[1] Youwen Xu, M. Suenaga, Y. Gao, J. E. Crow and N. D. Spencer, Phys. Rev. B 42, 8756 (1990).

[2] Z. J. Huang, Y. Y. Xue, P. H. Hor and C. W. Chu, Physica C 176, 195 (1991).

[3] Donglu Shi and Ming Xu, Phys. Rev. B 44, 4548 (1991).

[4] B. M. Lairson, J. Z. Sun, T. H. Geballe, M. R. Beasley and J. C. Bravman, Phys. Rev. B 43, 10405 (1991).

[5] D. Hu, W. Paul and J. Rhyner, Physica C 200, 359 (1992).

[6] M. P. A. Fisher, Phys. Rev. Lett. 62, 1415 (1989); D. S. Fisher, M. P. A. Fisher and D. A. Huse, Phys. Rev. B 43, 130 (1991).

[7] M. V. Feigel'man, V. B. Geshkenbein, A. I. Larkin and V. M. Vinokur, Phys. Rev. Lett. 63, 2303 (1989); M. V. Feigel'man, V. B. Geshkenbein and V. M. Vinokur, Phys. Rev. B 43, 6263 (1991).

[8] E. Zeldov, N. M. Amer, G. Koren, A. Gupta, M. W. McElfresh and R. J. Gambino, Appl. Phys. Lett. 56, 680 (1990); E. Zeldov, N. M. Amer, G. Koren and A. Gupta, Appl. Phys. Lett. 56, 1770 (1990).

[9] C. W. Hagen and R. Griessen, Phys. Rev. Lett. 62, 2857 (1989).

[10] C. Dekker, W. Eidelloth and R. H. Koch, Phys. Rev. Lett. 68, 3347 (1992)

[11] C. J. Van der Beek, P. H. Kes, M. P. Maley, M. J. V. Menken and A. A. Menovsky, Physica C 195, 307 (1992).

[12] M. P. Maley, J. O. Willis, H. Lessure and M. E. McHenry, Phys. Rev. B 42, 2639 (1990).

[13] Note: In this solution, some approximation is made. This approximation can be checked by comparing the results of several cases in which an exact solution can be obtained [e.g. for $U_{eff}(j)=U_0(1-j/J_c)$]. It is then found that the expressions of the exact solution are in the same form as Eq. (4.5), but the value of τ_0 is different, namely, in the exact solution, $\tau_0=kT/[\gamma(dU_{eff}/dj)|_{j=J_{co}}]$, instead of $\tau_0 \approx kT/[\gamma(dU_{eff}/dj)]$ in Eq. (4.5).

[14] V. B. Geshkenbein and A. I. Larkin, JETP 68, 639 (1989).

[15] Note that although at $T<<T_c$, $b(T) \approx 1$ and $c(T) \approx 1$, it is not quite clear why the derivative of $b(T)$ and $c(T)$ can be approximated to be zero in order to obtain Eq.(4.10c). For this our results has been checked: for the single crystals, we obtained

$b(T)=c(T)=(1-\theta^2)^2$, the first derivative of $b(T)$ and $c(T)$ can be approximated to be zero for $T\ll T_c$; for the polycrystalline sample, $b(T)=c(T)=1-\theta^4$, it is found that for $\ln(t_b/\tau_0)>10$ and $S(t_b,T)>0.02$, the first derivative of $b(T)$ and $c(T)$ can be approximated to be zero for $T<T_c/4$.

[16] Another possible choice of $b(T)$ and $c(T)$ is that $b(T)=c(T)=1-\theta^2$, although they are not in the proposed general form. The value of $\ln E_0$ is then about 5. In this case, the data can also collapse into one single curve using our method, which is only slightly different from the one in Fig. 4.4.

[17] H. G. Schnack, R. Griessen, J. G. Lensink, and Wen Hai-Hu, Phys. Rev. B 48, 13178 (1993).

Chapter V   Distribution of Pinning Energies: Model and Application

[Part of this chapter has been published in Physica C 200, 359 (1992).]

In Chapter IV, the non-linear current dependence of the effective pinning potential $U_{eff}(j)$ was discussed, which provides an explanation for the nonlogarithmic decay of the magnetization. Another possibility leading to a nonlogarithmic decay of magnetization is the existence of more than one type of pinning center. In this chapter, firstly, the model for a distribution of pinning energies will be introduced; then, using a particular class of functions for describing the distribution of pinning energies, an analytical solution for the temperature and time dependence of the magnetization $M(t,T)$ will be obtained. The model will be applied to our experimental results on Bi-2212 superconductors. It will be shown that the high-energy tail in the distribution of pinning energies, which was not emphasized in the previous work [1-2], is essential for fitting the magnetic relaxation data. Those high pinning energies can hardly be associated with the mechanism of single-vortex pinning in Bi-2212 single crystals and should be interpreted in terms of the collective pinning theory instead.

5.1 The model for a distribution of pinning energies

In this section, the model for a distribution of pinning energies proposed by Hagen and Griessen [1, 2] will be briefly described. In this model, there is a distribution $N(u)$ of a pinning energy u, and the flux lines in the place of different pinning potentials will independently move due to thermal activation. For each pinning potential u, it is assumed that the Anderson-Kim model is applicable. Since at a certain temperature T and time t, the defects with small pinning energies cannot effectively pin the vortices, so only the pinning energies larger than a certain value U^* are effective. This value of U^* is obtained when

$$1 - \frac{kT\ln(t/\tau_0)}{U * b(T)} = 0 ,$$

which leads to $U*(t, T)=kT\ln(t/\tau_0)/b(T)$. Therefore, in the magnetic relaxation experiments, the magnetization $M(t,T)$ at temperature T and time t is represented by

$$M(t,T) = M_0 c(T) \int_{U^*(t,T)}^{\infty} N(u) \times \left[1 - \frac{kT}{ub(T)} \ln(t/\tau_0)\right] du , \qquad (5.1)$$

where M_0 is the magnetization at zero temperature, $c(T)$ and $b(T)$ describe the temperature dependence of $M_0(T)$ and $u(T)$ respectively, which are the same as defined in Eqs. (4.7a) and (4.7a). The distribution function $N(u)$ should satisfy the following normalization condition:

$$\int_0^{\infty} N(u)du = 1 \qquad (5.2)$$

It was found [1,2] that the value of the distribution function at $u=U*(t,T)$, i.e. $N(U*)$, can be calculated from the magnetic relaxation data by

$$N(U^*) = -T \frac{d}{dT}\left(\frac{m(t_b,T)}{c(T)} \frac{S(t_b,T)}{kT}\right) \Big/ \left(\frac{d}{dT}\left(\frac{T}{b(T)}\right)\right), \qquad (5.3)$$

where t_b is the time of the first measurement of the magnetic relaxation, $m(t_b, T)$ the normalized magnetization, i.e. $m(t_b, T)=M(t_b, T)/M_0$, and $S(t_b,T)$ is defined as

$$S(t_b,T) = \left[-d\ln M(t,T)/d\ln t\right]_{t=t_b},$$

which is the normalized initial decay rate. Similar to (4.10), we have:

$$\ln(t_b/\tau_0) = -\frac{T\left[\dfrac{d\ln M(t_b,T)}{dT} + c(T)\dfrac{dc(T)}{dT}\right]}{S(t_b,T)\left(1 - \dfrac{d\ln b(T)}{d\ln T}\right)}. \qquad (5.4)$$

As discussed in the Chap. IV, $b(T)$ and $c(T)$ have the following general form

$$(1-\theta^2)^2[(1+\theta^2)/(1-\theta^2)]^{n/2}$$

where $\theta=T/T_c$, and the exponent n could be different for $b(T)$ and $c(T)$. The functions $c(T)$ and $b(T)$, and the value of $\ln(t_b/\tau_0)$ can be obtained from Eq. (5.4) using the same method as indicated in Section 4.3.

5.2. The functions for a distribution of pinning energies

In Ref. [1], the model of pinning distribution was applied to the relaxation data obtained on a single crystal and a polycrystalline sample of YBCO-123, and a broad distribution of the pinning energies with a maximum at about 60 meV was found. Hagen and Griessen [1] used a log-normal function, i.e. $N(u) \sim \exp[-\gamma(\ln(u/u_0))^2]$, to fit the distribution of pinning energies. In a further study [2,3], it was shown by numerical calculations that a combination of flux creep, viscous flux flow and a log-normal pinning distribution could lead to power law I-V characteristics, i.e. $V \propto j^{\alpha}$. Such power law I-V characteristics was studied in electrical transport measurements on high-T_c superconductors [4-5] and proposed to be caused by nonlinear current dependence of the pinning potentials [6-7] in contrast to the model of pinning distribution.

However, the log-normal distribution obtained for the YBCO-123 samples [1] contains no high-energy part (when $u_0 \approx 60$ meV and $\gamma=4-6$, $N(u) \approx 0$ for $u \geq 200$ meV). If the calculation process is reversed, i.e. if the log-normal distribution is used to calculate the decay of magnetization, the omission of the high-energy tail will lead to serious discrepancies between the fits and the relaxation data at high temperatures ($T>T_c/2$), especially, no peak in $S(t_b, T)$ can be reproduced, in contrary to the experimental data on the YBCO-123 polycrystalline sample used in Ref. [1]. This problem will be clarified in more detail when applying this model to our experimental data on Bi-2212 superconductors in the next section.

Firstly, we will show that within the pinning distribution model, a power-law I-V characteristics can be obtained analytically from a particular distribution function $N_a(u)$ in the form of:

$$N_a(u) = \frac{1}{U_a} \frac{u}{U_a} \exp(-u/U_a) , \qquad (5.5)$$

where U_a is a parameter of the pinning energy at which $N_a(u)$ has a maximum value. Inserting the function $N_a(u)$ into Eq. (5.1) and evaluating the integral, a power law decay of the magnetization is obtained:

$$M(t, T) = M_0 c(T) \left(\frac{t}{\tau_0} \right)^{-kT/[U_a b(T)]} \qquad , \qquad (5.6)$$

Since, during the magnetic relaxation, the current density is proportional to the magnetization M, i.e. $j \propto M$, and the voltage V is proportional to the change of the magnetization, i.e. $V \propto dM/dt$, the above power law decay of magnetization can be transformed into a power law I-V characteristics: $V \propto j^\alpha$ with $\alpha = [U_a b(T)/kT] + 1$. In Ref. [2], the exponent α in the power-law I-V characteristics obtained by numerical calculations varies with $1/T$ at low temperatures, which is in accordance with this analytical result of $\alpha = [U_a b(T)/kT] + 1$, since at low temperatures, $b(T) \approx 1$ and $U_a/kT \gg 1$.

Compared with the log-normal function, the function $N_a(u)$ has an advantage for its analytical solution for the Eq. (5.1). However, since $N_a(u)$ has only one parameter U_a, a disadvantage of the function $N_a(u)$ for describing a distribution of pinning energies is that the width of the distribution is fixed when its mean value is known, which means that the two quantities cannot be chosen independently. Because for a general distribution of the pinning energies, its mean value and width could vary independently, it is necessary to extend $N_a(u)$ to the following class of functions:

$$N(n, U_p; u) = \frac{1}{n!} \frac{1}{U_p} \left(\frac{u}{U_p} \right)^n \exp(-u/U_p) \quad , \qquad (5.7)$$

where U_p and n are two parameters, and the coefficient of the function is determined by the normalization condition (5.2) [The function $N(n, U_p; u)$ of Eq. (5.7) belongs to the *Poisson* distribution]. $N(n, U_p; u)$ has a maximum at $U_m = n U_p$ and a width of $(n^{1/2}) U_p = U_m/n^{1/2}$. As an illustration, several functions of $N(n, U_p; u)$ with different parameters are shown in Fig. 5.1. In this work, the parameter n is taken to be an integer. This is not absolutely necessary, but it simplifies the calculations and is found to be sufficient for fitting our experimental results.

Inserting the function $N(n, U_p; u)$ of Eq. (5.7) as the distribution function into Eq. (5.1) and evaluating the integral, we obtain

$$M(t,T) = M_0 c(T)(t/\tau_0)^{\frac{-kT}{U_p b(T)}} \times \left[1 + \sum_{q=1}^{n-1} \frac{(1-q/n)}{q!} \left(\frac{kT\ln(t/\tau_0)}{U_p b(T)} \right)^q \right]. \quad (5.8)$$

When $n \gg 1$, the sums in Eq. (5.8) can be evaluated, and the well-known Anderson-Kim result, i.e. the logarithmic decay of the magnetization, is obtained:

$$M(t,T) = M_0 c(T) \left(1 - \frac{kT\ln(t/\tau_0)}{U_m b(T)} \right)$$

This is because when $n \gg 1$, $N(n, U_p; u)$ is like a δ-function corresponding to a single type of pinning barrier with the value of the pinning energy to be U_m. Another special case for $N(n, U_p; u)$ is when $n=1$, which is $N_a(u)$ defined in Eq. (5.5). When n is slightly larger than one, the time dependence of the magnetization is a power-law with logarithmic corrections, as can be seen from Eq. (5.8).
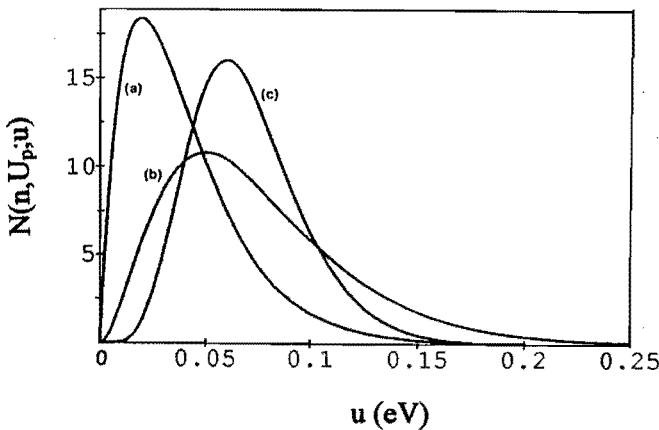
Fig.5.1 Some examples of the distribution function
N(n, U_p; u) (see text) for (a) n=1, U_p=0.02 eV; (b) n=2,
U_p=0.025 eV; (c) n=6, U_p=0.01 eV.

Because of the analytical result obtained in Eq. (5.8), the function $N(n, U_p; u)$ will be used for describing the distribution of pinning energies. Generally, a distribution of pinning energies can be represented as a linear combination of the functions $N(n, U_p; u)$:

$$N(u) = \sum_{i=1}^{k} C_i N_i\left(n_i, U_{pi}; u\right), \qquad (5.9)$$

in which C_i is a normalized coefficient. Using the result of Eq.(5.8), the magnetization due to the above pinning distribution can be obtained:

$$M(t,T) = M_0 c(T) \sum_{i=1}^{k} C_i (t/\tau_0)^{\frac{-kT}{U_{pi} b(T)}} \times \left[1 + \sum_{q=1}^{n_i-1} \frac{(1-q/n_i)}{q!} \left(\frac{kT\ln(t/\tau_0)}{U_{pi} b(T)} \right)^q \right], \qquad (5.10)$$

The parameters C_i, n_i and U_{pi} can be determined by fitting the magnetic relaxation data, as explained in detail below.

5.3. Application of the pinning distribution model to our experimental results

Using the same method discussed in Section 4.3, the temperature factors $b(T)$ and $c(T)$, and the value of $\ln(t_b/\tau_0)$ are firstly determined by Eq. (5.4). For the single crystal and the powdered sample, the best choice is found to be: $c(T)=b(T)=(1-\theta^2)^2$. The value of $\ln(t_b/\tau_0)$ is 13 for the single crystal and 15 for the powdered sample corresponding to $\tau_0=10^{-5}$ s and 1.5×10^{-6} s, respectively. For the bulk ceramic sample, $c(T)=b(T)=(1-\theta^4)$; and the value of $\ln(t_b/\tau_0)$ is about 23 corresponding to $\tau_0=10^{-10}$ s.

After the determination of $c(T)$, $b(T)$ and $\ln(t_b/\tau_0)$, the pinning distribution can be calculated from Eq. (5.3). Using the relaxation data of $m(t_b,T)$ and $S(t_b,T)$ directly for the calculations, the data for the distribution were obtained, which are shown in Figs. 5.2(a)-(c) with dotted points for the single crystal, the ceramic sample and the powdered sample, respectively. Due to some uncertainty in obtaining the initial decay rate $S(t_b, T)$ and the temperature derivatives of $m(t_b,T)$ and $S(t_b,T)$, the obtained data (i.e. the dotted points) in Fig. 5.2 were used as a first estimation for the parameters C_i, n_i and U_{pi} in Eq. (5.9). When these parameters were given, the time dependence of the magnetization at certain

temperature was obtained from Eq. (5.10). These parameters in the equation were then adjusted to obtain the best fit for the relaxation curves. The fits for the magnetic relaxation curves of $M(t)/M(t_b)$ at various temperatures, as well as $S(t_b, T)$ and $m(t_b,T)$, are presented in Figs. 3.3-3.8 (Chap. III) with solid lines, which show a satisfactory agreement with the experimental results. The corresponding distributions of the pinning energies are shown in Fig. 5.2 with solid lines for the three types of samples. The parameters of C_i, n_i and U_{pi} are given in Table 5.1.

Table 5.1 *Parameters of the functions $N(n,U_p; u)$ used for the distribution of pinning energies (see Fig.5.2).*

Functions	Parameters	Single crystal	Bulk ceramic	Powder
1	n_1	6	8	6
	U_{p1} (meV)	2.1	3.1	2.65
	centre (meV)	12.6	24.8	15.9
	width (meV)	5.144	8.77	6.49
	C_1	48.5%	35.7%	69%
2	n_2	25	4	4
	U_{p2} (meV)	1.17	25	12
	centre(meV)	29.25	100	48
	width (meV)	5.85	50	24
	C_2	48.5%	53.6%	13.8%
3	n_3	3	4	3
	U_{p3} (meV)	45	75	75
	centre(meV)	135	300	225
	width (meV)	77.94	150	129.9
	C_3	3%	10.7%	17.2%
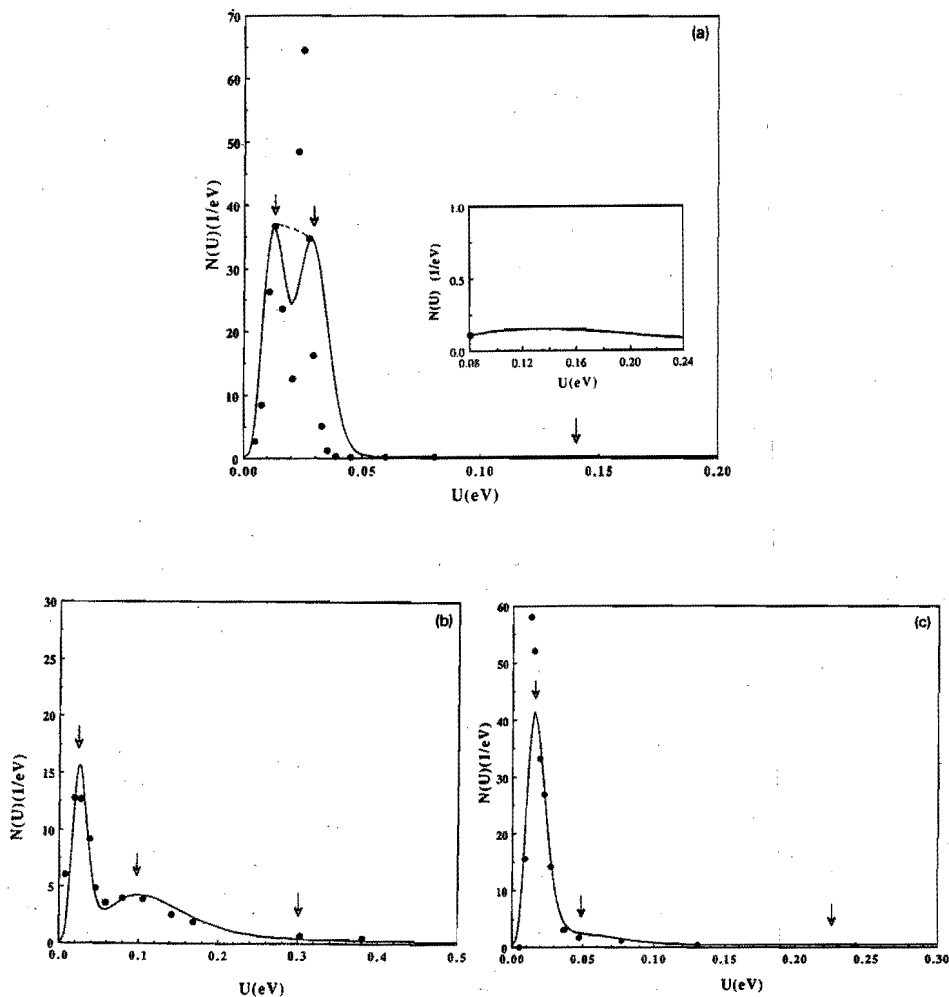
Fig. 5.2 The distribution of pinning energy for (a) a Bi-2212 single crystal; the high energy tail above 80 meV is shown in the insert; (b) a Bi-2212 bulk polycrystalline sample, (c) a Bi-2212 powdered sample. The data shown with dots (•) were calculated using the Hagen-Griessen pinning distribution model; the solid lines are final results using our approach that yields good fits for the relaxation curves (the parameters are given in Table 5.1). The arrows indicate the position of the functions. Note that for the Bi-2212 single crystals, the broad peak around 25 meV is fitted technically by two functions which are close to each other, but it does not necessarily mean that there are two different types of pinning centers around 25 meV.

Compared Fig. (5.2b) with Fig. (5.2c), it is noted that in comparison with the peak at about 0.025 eV, the relative height of the peak at 0.1 eV in the bulk sample becomes much smaller in the powered sample. This peak at 0.1 eV might be due to the pinning at grain boundaries in the bulk Bi-2212 samples, since the grain boundaries are largely reduced during the crushing of the bulk sample. However, for the Bi-2212 single crystals, in which there are no grain boundaries, a very small high-energy peak at 0.14 eV still exists, as indicated in the insert of Fig. (5.2a). In order to understand the pinning mechanisms in Bi-2212 single crystals, we consider the pinning energy U_0 due to disk-like pinning centers with a defect volume of $(\pi\xi_{ab}^2 L_c)$:

$$U_0 = \frac{H_c^2}{8\pi}(\pi\xi_{ab}^2 L_c), \qquad (5.11)$$

where L_c is the effective correlation length in the c-direction. Due to the highly anisotropic structure of Bi-2212 single crystals, the flux lines are essentially pancake vortices loosely connected by Josephson and magnetic coupling [8]. The broad peak in the distribution of pinning energies around 25 meV in the single crystals [Fig. 5.2 (a)] is likely to be due to the oxygen vacancies in the Cu-O planes. For the calculation of the pinning energy of these defects, L_c can be taken as the coherence length ξ_c. Taking the values of $H_c \approx 1$ T, $\xi_{ab} \approx 31$ Å, and $\xi_c \approx 4$ Å [9], the pinning energy U_0 is found to be 30 meV, which is close to the peak position at 25 meV in Fig. (5.2a) for the single crystals. The maximum pinning energy of the pancake vortices in Bi-2212 single crystals is obtained when the correlation length L_c equals the distance between the superconducting layers d [10]. Taking $d \approx 12$ Å, the maximum pinning energy U_{max} is about 90 meV. So, within this model, it seems to be difficult to understand the mechanism for the high pinning energies around 140 meV obtained for the Bi-2212 single crystals. It is possibly due to the fact that when the pancake vortices move in bundles [11], the effective activation energy can be greatly enhanced, as demonstrated in the theory of collective flux creep [12,13]. This point will be discussed in more detail in the next section.

5.4. The relation with the collective-pinning model

In the preceding section, it was found that for Bi-2212 single crystals, the high pinning energies around 140 meV in the distribution function N(u) are difficult to be explained by single-vortex pinning mechanism, since the maximum pinning energy of the defects is about 90 meV for such mechanism. It was suggested that the high-energy tail may be due to collective pinning effects.

One of the basic results of the collective pinning theory [12,13] is that the effective pinning potential show a strong current dependence: $U_{eff}(j)=U_0(J_c/j)^\mu$ when $j \ll J_c$, where the exponent μ could have different values for different pinning regimes. During the magnetic relaxation, the current density decays with time, so the effective pinning potential $U_{eff}(j)$ is time-dependent, i.e. $U_{eff}(t) \sim [J_c/j(t)]^\mu$ (More precisely, it was shown by Geshkenbein and Larkin [14] that $U_{eff}[j(t)] \approx kT\ln(t/\tau_0)$, also see Section 4.2 of Chap. IV). Thus, the effective pinning energy grows as a function of time, which seems to be equivalent to a "scanning" from low pinning energies to high pinning energies in the pinning distribution.

This picture suggests a reinterpretation for the high pinning energies in the distribution N(u). In the Hagen-Griessen model, it is assumed that N(u) stems from a *spatial* variation of pinning potentials, i.e., it is determined by the structure of the material. In contrast, from the point of view of the collective creep theory, the high pinning energies in the distribution function N(u) are generated dynamically at different times by the interplay between the pinning centers and elastic properties of the vortices. This leads to a natural explanation for the high-energy tail in the distribution N(u) obtained in the Hagen-Griessen model, i.e. the high pinning energies might actually arise from the current dependent effective pinning potential (the effective pinning potential grows when the current density decreases). This relation can be clarified by an interesting connection between the Hagen-Griessen model and the collective creep theory. The latter model predicts a relaxation law [13]:

$$M(t,T) = M_0 c(T) \left(1 + \mu \frac{kT\ln(t/\tau_0)}{U_0 b(T)} \right)^{-1/\mu} . \qquad (5.12)$$

This relaxation law can be obtained within the framework of the Hagen-Griessen model from the following distribution function:

$$N_c(\mu, U_0; u) = \frac{(1+\mu)u}{U_0^2} \left(1 + \mu \frac{u}{U_0} \right)^{-(2+(1/\mu))} , \qquad (5.13)$$

by inserting Eq. (5.13) into Eq. (5.1) and evaluating the integral. For $\mu \ll 1$, $N_c(u)$ becomes the distribution of $N_a(u)$ given in Eq. (5.5), which yields a power-law decay of the magnetization. When μ is slightly smaller than 1, $N_c(u)$ has a long high-energy tail. Due to the same reasons discussed above, such a long tail cannot be explained with the single-vortex pinning mechanism, but only within the collective pinning theory.

5.5. The connection between the peak in $S(t_b,T)$ and the kink in $M(t_b, T)$

The "kink" in the temperature dependence of $M(t_b,T)$ [or $j_c(T)$] and the peak in the temperature dependence of $S(t_b,T)$ at about 30 K found in Bi-2212 single crystal have indicated a transition from one pinning regime to another (see Chap. III).
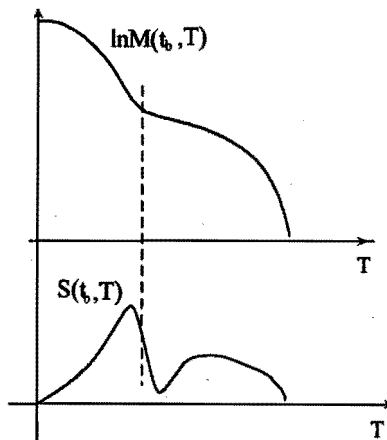
Fig. 5.3 Diagram to explain the connection between the "kink" on lnM(t_b, T) and the peak in the normalized initial decay rate S(t_b, T) at low temperature according to Eq. (5.14).

Here, we will point out that the peak in $S(t_b, T)$ at low temperature is directly related to the "kink" in a log-linear plot of $M(t_b, T)$. For both models discussed in Chap. IV and V, a relation between $\ln(t_b, T)$, $S(t_b, T)$ and $M(t_b, T)$ is obtained, i.e. Eq. (4.10) or Eq. (5.4). At low temperatures, this relation is simplified to [see Eq. (4.10c)]:

$$S(t_b, T) = \frac{T}{\ln(t_b / \tau_0)} \left(-\frac{d\ln M(t_b, T)}{dT} \right), \qquad (5.14)$$

where $\ln(t_b/\tau_0)$ can be considered to be temperature independent comparing to the factor T. Eq. (5.14) indicates a direct connection between $S(t_b, T)$ and $M(t_b, T)$. Due to the factor T in the right side of Eq. (5.14), $S(t_b, T)$ starts to increase from zero as the temperature increases from zero (Here the quantum creep is not considered). If at a certain temperature, $M(t_b, T)$ has a "kink" in a logarithmic plot, as shown in Fig. 5.3, there will be a maximum in the absolute value of its temperature derivative $|d\ln M/dT|$. Since $S(t_b, T)$ is proportional to $|d\ln M/d\ln t|$, consequently a peak will occur in $S(t_b, T)$. This connection has been actually observed in Bi-2212 single crystals and powdered samples (see Figs. 3.4 and 3.8 in Chap. III).

Since the "kink" in $M(t_b, T)$ is usually smooth (i.e. no sudden "jump" in the value of $|d\ln M/dT|$), it can be shown that the temperature position of the peak in $S(t_b, T)$ will be a little bit lower than the position of the "kink" in $M(t_b, T)$. Actually, the position of the "kink" in $M(t_b, T)$ is in the middle between the temperature of the maximum and the "dip" in $S(t_b, T)$, as indicated by a dashed line in Fig. 5.3. Such a temperature difference was used by Metlushko et al. [15] to define a new pinning regime (also see Section 3.5), which seems to be not necessary due to the reasons discussed above.

5.6. Summary of the results

Using a particular class of distribution functions $N(n, U_p; u)$, an analytical solution for the decay of the magnetization has been obtained. The parameters of the distribution were obtained by firstly using the Hagen-Griessen model and then directly fitting the relaxation curves. It has been demonstrated that the peak in the normalized initial decay rate $S(t_b, T)$

at low temperature is directly connected to the kink in $M(t_b, T)$ or $j_c(T)$, which is caused by a transition between two distinct pinning regimes. The magnetic relaxation curves of Bi-2112 single crystals, bulk ceramic samples and powdered samples are well fitted in terms of a distribution of pinning energies. It is found that it is important to include the high-pinning-energy tail in the distribution in order to fit the relaxation data. Without the high-energy tail, no kink in $j_c(T)$ and no peak in $S(t_b, T)$ could be reproduced for the Bi-2212 single crystals. However, defects with such high pinning energy around 140 meV can hardly exist in the highly anisotropic Bi-2212 single crystals, in which the maximum pinning energy of the defects is expected to be about 90 meV. It was argued that those high pinning energies in the distribution $N(u)$ can be explained by reinterpreting $N(u)$ in the framework of the collective pinning theory, namely, the high pinning energies are produced dynamically by the interaction between the vortices.

5.7. The model for a distribution of pinning energies versus the model for a non-linear current dependence of the effective pinning potential

In Chapter IV, the nonlogarithmic decay of magnetization was interpreted to be originated from a nonlinear current dependence of the pinning potential $U_{eff}(j)$; in Chapter V, however, a combination of a distribution of pinning energies and a linear current dependence of pinning potential was used to fit the nonlogarithmic decay of magnetization. A question arises naturally: which model reflects the reality better or what are the real mechanisms of the vortex dynamics?

As discussed early in this Chapter, the high-energy tail found in the pinning distribution $N(u)$ should be reinterpreted in terms of the collective pinning theory. Besides this point, there are other problems in the Hagen-Griessen model:

(1). The Hagen-Griessen model, like the Anderson-Kim model, assumes a linear current dependence of $U_{eff}(j)$ for each pinning potential. However, even if the collective pinning effects are ignored, a linear current dependence of the pinning potential is only valid for

saw-tooth-shaped pinning potentials [16]. When the pinning potential has other shapes, the current dependence of $U_{eff}(j)$ becomes nonlinear. For example, for sinus-shaped potential, we have $U_{eff}(j) \propto (1-j/J_c)^{3/2}$ [17]; and for logarithmic-shaped potentials, the current dependence of $U_{eff}(j)$ will be: $U_{eff}(j) \propto \ln(j/J_c)$ [4,6].

(2). In the Hagen-Griessen model, the vortices are treated as independent particles and the elastic properties of the flux lines are ignored. The collective pinning effects are also not considered.

Despite these problems, there are some points supporting the idea for a distribution of pinning energy:

1). Experimentally, different types of pinning centers have been identified, such as oxygen vacancies, twin boundaries, and damages caused by ion irradiation. Using the model of pinning distribution, these different types of pinning potentials can be studied. For example, in Ref. [18], the Hagen-Griessen model was used successfully to study the influence of the ion irradiation on the pinning effects in Bi-2212 single crystals.

2). As pointed out in Ref. [19], even for the model of non-linear current dependence of $U_{eff}(j)$, a non-uniform spatial distribution of the current density $j(r)$ in the sample, which can often occur in the experiments, will lead to a spatial distribution of the effective pinning energy $U_{eff}[j(r)]$.

3). The consequence of nonlinear current dependence of $U_{eff}(j)$, i.e. the nonlogarithmic decay of magnetization, can be reproduced mathematically from certain distribution of pinning energies within the model for a distribution of pinning energies.

Therefore, the conclusion is that when the model of pinning distribution is applied, a reinterpretation of the distribution of the pinning energies might be needed, which means that some pinning energies in the distribution may not correspond to certain types of

defects, but may be produced dynamically due to the interplay among vortices or may be due to a spatial distribution of the current density in the sample.

References

[1] C.W. Hagen and R. Griessen, Phys. Rev. Lett. 62 (1989) 2857.

[2] R.Griessen, Physica C 175 (1991) 315.

[3] R. Griessen, Phys. Rev. Lett. 64 (1990) 1674.

[4] E. Zeldov, N.M. Amer, G. Koren, A. Gupta, M.W. McElfresh and R.J. Gambino, Appl. Phys. Lett.56 (1990) 680.

[5] R.H. Koch, V. Foglietti, W.J. Gallagher, G. Koren, A. Gupta and M.P.A. Fisher, Phys. Rev. Lett. 63 (1989) 1151.

[6] E. Zeldov. N.M. Amer, G. Koren and A. Gupta, Appl. Phys. Lett. 56 (1990) 1770.

[7] M.P.A. Fisher, Phys. Rev. Lett.62 (1989) 1415.

[8] J.R.Clem, Phys. Rev. B43 (1991) 7837.

[9] B. Batlogg. T.T.M. Palstra, L.F. Schneemeyer, R.B. Van Dover and R.J. Cava, Physica C 153- 155 (1988) 1062.

[10] E.H. Brandt, Europhys. Lett.18 (1992) 635.

[11] C.J. Van der Beek. P.H. Kes. M.P. Maley, M.l.V. Menken and A.A. Menovsky, Physica C 195 (1992) 307.

[12] M. V. Feigel'man, V B. Geshkenbein, A.l. Larkin and V.M. Vinokur, Phys. Rev Lett. 63 (1989) 2303.

[13] M.V. Feigel'man, V.B. Geshkenbein and V.M. Vinokur, Phys. Rev. B 43 (1991) 6263.

[14] V.B. Geshkenbein and A.I. Larkin, JEPT 68 (1989) 639.

[15] V.V. Meltlushko, G. Güntherodt, V.V. Moshchalkov, and Y. Bruynseraede, Euro. phys. lett. 26 (1994) 371.

[16] H.G. Schnack, R. Griessen, L.G. Lensink, C.J. van der Beek, and P.H. Kes, Physica C 197 (1992) 337.

[17] M. R. Beasley, R. Labusch and W. W. Webb, Phys. Rev. B 181 (1969) 682.

[18] V. Hardy, A. Ruyter, J. Provost, D. Groult, and Ch. Simon, Physica C 224 (1994) 143.

[19] H. Theuss, and H. Kronmüller, Physica C 229 (1994) 17.

Chapter VI. The irreversibility line of $Bi_2Sr_2CaCu_2O_{8+x}$ superconductors

[The contents of this chapter has been published in Physica C 216, 315 (1993).]

In this chapter, the irreversibility line of Bi-2212 superconductors will be discussed. First, the experimental results will be presented. After that, a flux depinning model for the irreversibility line will be developed and applied to our experimental results.

6.1. Introduction

One of the interesting phenomena of high-T_c superconductors is the existence of a new boundary line between H_{c1} and H_{c2} in the H-T phase diagram, which is called the irreversibility line. The irreversibility line separates the reversible magnetic behaviour at higher magnetic field from the irreversible behaviour at lower magnetic fields, as has been introduced in Section 1.9. The existence of the irreversibility line was firstly reported by Müller et al. [1] from the field-cooled (FC) and zero-field-cooled (ZFC) magnetization measurements for La-Ba-Cu-O superconductors. They found that the irreversibility line $H(T_r)$ obeyed the following scaling law:

$$H(T_r)=H_0(1-T_r/T_c)^n , \qquad (6.1)$$

where T_r denotes the irreversibility temperature for a magnetic field of H. For their La-Ba-Cu-O samples, the exponent n was found to be 1.5. Soon after that, various mechanisms have been proposed for the irreversibility line (see, for instance, Ref. [2].). Below, the most important models are introduced.

(1). Yeshurun and Malozemoff [3,4] proposed that the irreversibility line is a depinning line due to thermally activated flux creep in the high-T_c superconductors. When the magnetic field increases to the irreversibility point, the distance between the flux lines $a_0=1.075(\Phi_0/B)^{1/2}$ becomes significantly smaller than the penetration depth λ. Therefore, they assumed that at the irreversibility line, a_0 scales with the coherence length ξ_{ab} in the ab-plane,

i.e. $a_0 = f\xi_{ab}$, where f is a characteristic number in the order of 10. So, the pinning energy U_0 at the irreversibility line can be expressed as:

$$U_0 = \frac{H_c^2}{8\pi}\left(\frac{a_0}{f}\right)^2 \xi_c \; . \qquad (6.2)$$

For magnetic fields at the irreversibility line, the Ginsberg-Landau theory was used to obtain the temperature dependence of $H_c(T)$ and $\xi_c(T)$ [2], i.e. $H_c(T) \propto (1-T/T_c)$, and $\xi_c(T) \propto (1-T/T_c)^{-1/2}$. Using these expressions for Eq. (6.2), the temperature and field dependence of the pinning energy $U_0(T,H)$ at the irreversibility line is derived to be:

$$U_0(T,H) \propto (1-T/T_c)^{1.5}/B \; . \qquad (6.3)$$

In the traditional Anderson-Kim flux creep model, the current density $j(t,T)$ is expressed as:

$$j(t,T) = J_c[1-kT\ln(E/E_0)/U_0], \qquad (6.4)$$

where $E_0 = Ba_0\Omega_0$. At the irreversibility line, $j(t,T)=0$, therefore, for T close to T_c, a combination of (6.3) and (6.4) leads to

$$H(T_r) = H_0(1-T_r/T_c)^{1.5} \; , \qquad (6.5)$$

which explains the scaling law (6.1) with n=1.5 (For T close to T_c, B is proportional to H i.e. B∝H).

This flux depinning model was employed by several groups to study their experimental results [5-7]. In particular, the variation of oxygen vacancies [8] or the ion irradiation on the samples [9-12] changes the pinning force and shifts the irreversibility line of the superconductors, which can be viewed as strong evidence for the depinning model. The frequency dependence of the irreversibility line [4,13-14] was also a consequence of the flux depinning by the thermally activated flux motion.

(2). It has been also proposed that the irreversibility line is a transition line from a vortex-liquid to a vortex-glass state [15, 16]. A universal scaling of the relevant physical parameters near the transition line is predicted. The same scaling law (6.1) near T_c is also obtained but with a different exponent of n=4/3. This theory was supported by some experimental results of I-V characteristics [17-20] and magnetization measurements [21].

(3). Another approach assumes that the irreversibility line is caused by a transition from a flux lattice into a flux liquid [22,23], i.e. the melting of flux lattice. This theory was argued to

be supported by the experimental results of the acoustic attenuation in Ref. [24], although their experimental results could also be interpreted by the flux depinning model [6]. Neutron scattering experiments on the field-cooled Bi-2212 single crystals reported by Cubitt et al. [25] gave strong evidence for the picture of flux lattice melting. The enhance of the irreversibility line after ion irradiation [11, 12] were also viewed as evidence for the flux-lattice-melting theory [26]. This theory also predicts a scaling law (6.1) near T_c, but with a exponent of n=2.

Since these different theories predict a different exponent n of the scaling law Eq. (6.1) (n could be 1.5, 4/3 or 2), early experimental work was focused on the scaling law (6.1) near T_c in order to study which theory is applicable (see, for instance, Ref. [5]). It was found that, when Eq. (6.1) was used to fit the irreversibility lines, the exponent n ranged from 1.2 to 2.3 for different types of samples [5,8 11]. So, it seems that from the fitting of the irreversibility lines with the scaling law (6.1) for various samples, no conclusive evidence can be given for any of the models discussed above.

The irreversibility line of YBCO-123 superconductors were usually measured at high temperatures $(T>T_c/2)$, because for a magnetic field as high as 6 T, which is usually used in the experiments, it is not enough to measure the irreversibility line at low temperatures. For other types of samples, for instance, Bi-2212 single crystals, the irreversibility line at low temperatures can be determined with a magnetic field of 6 T. Because of this, it was observed that the temperature dependence of the irreversibility line deviates from the scaling law (6.1) at low temperatures [11, 27-33]. The irreversibility line at low temperatures could be fitted with $H(T_r) \sim T_r^{-m}$ [11,28] or with $H(T_r) \sim \exp(-T_r/T_0)$ [27]. The validity of the scaling law (6.1) was found to hold for a wider temperature range for YBCO-123 superconductors than for the Bi-based superconductors [5, 27, 29, 31]. Another interesting feature of the Bi-2212 single crystals is that a "kink" (or a "strong upturn") appeared at about 30 K in the irreversibility line [30,32,34,35]. In Ref. [30, 34], the kink was suggested to be due to a transition between two different pinning regimes. However, in Ref. [32], 3D vortex melting was used to explain the irreversibility line at high temperatures (T>30 K) and 2D vortex melting was used to fit the irreversibility line at low temperatures (T<30 K). In contrast, a bulk pinning regime at low temperatures (T<30 K) and a surface pinning regime at high

temperatures (T>30 K) were proposed by Zeldov et al. [35] to explain their experimental results.

In this chapter, our experimental results on the irreversibility line of Bi-2212 single crystals and Bi-2212 bulk ceramic samples will be described. The irreversibility transition was determined down to 15 K, which made it possible to investigate the temperature dependence of the irreversibility line over a large temperature range. Within the framework of thermally activated flux creep, a model will be proposed for the irreversibility line. In comparison with the previous work in Ref. [3], which assumed a linear j dependence of the effective pinning potential $U_{eff}(j)$, our approach is valid for any j dependence of $U_{eff}(j)$; and the temperature dependence of the irreversibility line at low temperatures will be also discussed.

6.2. Experimental

Most of the Bi-2212 single crystals used in the experiments, which have a typical size of $2 \times 2 \times 0.1$ mm^3, were grown by a self-flux crucible method. Additional measurements for the irreversibility line were also performed on some Bi-2212 single crystals grown by the TSFZ method [36], and consistent results were found. The Bi-2212 bulk ceramic samples were prepared by a partial-melting process [37]. The same samples were also used for the magnetization and magnetic relaxation measurements, as described in Chapter III. The transition temperature T_c was typically 89 K for the single crystals and 90 K for the ceramic samples.

The zero-field cooled (ZFC) and field-cooled (FC) magnetization (see Section 1.9) were measured with a vibrating sample magnetometer (VSM). The applied magnetic field ranged from 20 Oe up to 80 kOe (8 T). For all the FC and ZFC curves, a heating rate of about 2 K/min. was used.

6.3. Experimental Results

As shown in Fig.6.1, the irreversibility point is determined from the ZFC and FC magnetization curves, i.e. the lowest temperature where the difference between these magnetizations becomes zero, i.e.:

$$\delta M \equiv M_{ZFC} - M_{FC} \approx 0. \qquad\qquad (6.6)$$

In order to have a same criterion δM in determining the irreversibility point at different magnetic fields, we always plotted the ZFC and FC curves around the irreversible point with a total scale of about 2×10^{-6} Am^2 for determining the merging point of the FC and ZFC curves, which means a criterion of $\delta M \leq 0.5 \times 10^{-7}$ Am^2.
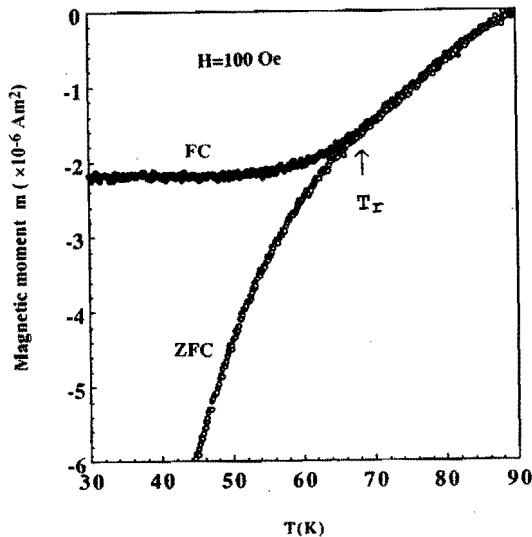
Fig. 6.1 The ZFC and FC magnetic moment (H=100 Oe) of the Bi-2212 single crystal and the determination of the irreversibility temperature T_r.

In Fig.6.2, a double logarithmic plot of the irreversibility field $H(T_r)$ versus $(1- T_r/T_c)$ is shown in order to check the scaling-law (6.1) near T_c. As shown in the figure with the dashed lines, the scaling law is only valid for T_r above about $0.65T_c$ for the ceramic samples and above about $0.8T_c$ for the single crystals. It seems that the scaling law holds for a wider temperature region for the ceramic samples than the single crystals. From the scaling law fit near T_c, the exponent n is found to be about 2.2 for the ceramic samples and about 1.2 for the single crystals. At low temperatures, however, the scaling law (6.1) does not apply to either the irreversibility line of the single crystal or the ceramic sample. In Fig.6.3, $H(T_r)$ is plotted against T_r for both the single crystal and the ceramic sample. The irreversibility line of the single crystal exhibits a "kink" at about 30 K, suggesting two different regions. A similar kink in the irreversibility line of Bi-2212 single crystals was also reported in Refs. [30,32,35].

Compared the temperature dependence of the irreversibility line in Fig. 6.3 with that of critical current density $j_c(T)$ in Fig 3.2 (Chap. III), some similarity can be observed, particularly the presence of the "kink" for the Bi-2212 single crystals. This suggests that there could be a correlation between the driving physical mechanisms underlying these two quantities. In the literature, some correlation between the two quantities $j_c(T)$ and $H(T_r)$ was also reported: for a series of YBCO-123 samples, it was found [5] that a higher value of the irreversibility field $H(T_r)$ corresponded to a higher value of $j_c(T)$; and in the ion irradiation experiments, it was found that both $j_c(T)$ and $H(T_r)$ were enhanced after the irradiation [10,11]. Such a correlation indicates that there might be a common origin for both $j_c(T)$ and $H(T_r)$. Since, in the high-T_c superconductors, the temperature dependence of $j_c(T)$ is dominated by the thermally activated flux creep (see, for instance, Ref. [4, 38-40], this favours the hypothesis that the irreversibility line is a depinning line.

Fig. 6.2 *The irreversibility line of the Bi-2212 superconductors plotted with H(T$_r$) vs. (1-T$_r$/T$_c$) in double logarithmic scales. The dashed lines are the fits of the scaling law (6.1).*

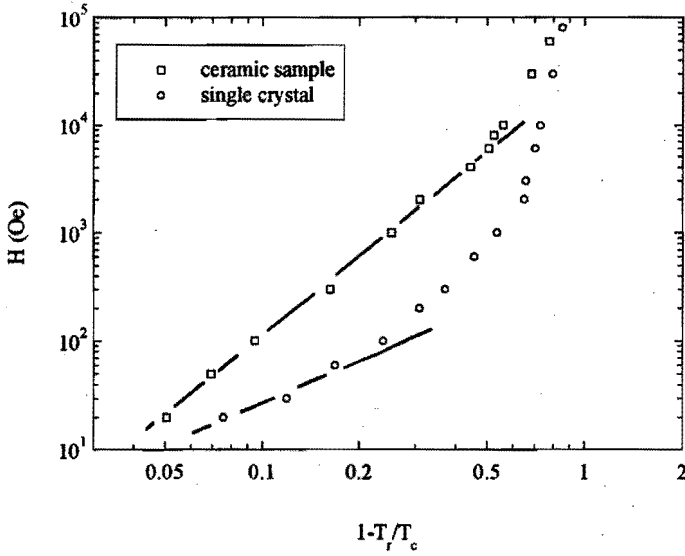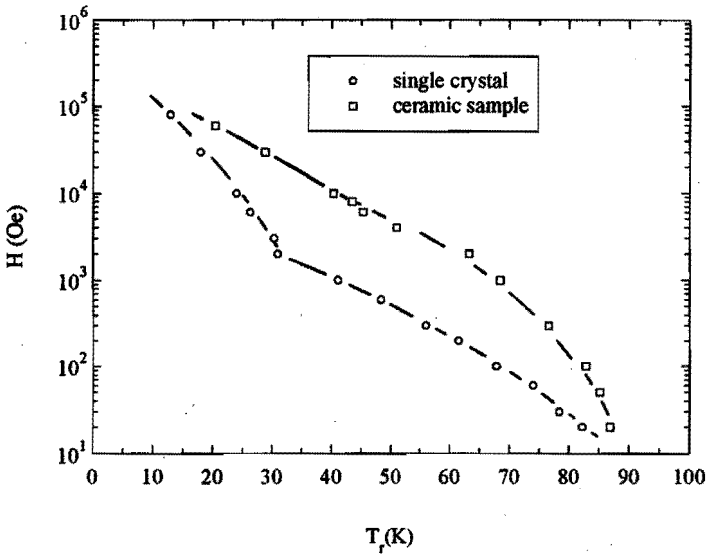**Fig. 6.3.** *The irreversibility field H as a function of the temperature T$_r$ for Bi-2212 superconductors. Note the kink around 30 K in the irreversibility line of the Bi-2212 single crystal.*

6.4. Thermally activated flux depinning model

As mentioned in the introduction of this chapter, various models have been proposed for the irreversibility line. Here, we will focus our attention on the flux depinning model, which was firstly proposed by Yeshurun and Malozemoff [3]. There are several reasons why it is necessary to improve their approach. Firstly, in Ref. [3], the Anderson-Kim model was used to discuss the irreversibility line, which assumes a linear j dependence of the effective pinning potential $U_{eff}(j/J_c)$. However, as discussed in Chapter IV, the j dependence of $U_{eff}(j/J_c)$ has been found to be generally nonlinear. Actually, the linear j dependence of $U_{eff}(j/J_c)$ is only valid for $j \approx J_c$. Therefore, the Anderson-Kim model cannot be used for modelling the irreversibility line that occurs at $j \approx 0$. Further, as discussed in the introduction, several experiments have revealed a quite different behaviour at low temperatures, in contrast to the scaling law (6.1), therefore, the irreversibility line at low temperatures has to be considered in more detail. Finally, it was postulated in Ref. [3] that the field dependence of the pinning potential can be expressed as $U_0(H) \propto H^{-1}$ [see Eq. (6.3)], but many experiments showed that $U_0(H) \propto H^{-1/m}$ with m ranging from 1 to 4 for different types of samples [8, 41-47]. In the following approach, we will take these three problems into consideration, namely, within the framework of the flux creep, the irreversibility line $H(T_r)$ in the whole superconducting temperature range will be obtained without any specific assumption of the j dependence of $U_{eff}(j)$.

6.4.1 The model

We start from the flux-creep equation which gives the dissipative electric field to be [48]:

$$E = E_0 e^{-U_{eff}(T,H,j)/kT} \qquad (6.7)$$

where $E_0 = Ba_0\Omega_0$, and $U_{eff}(T,H,j)$ is the effective pinning potential which depends on the temperature, magnetic field and the current density. In Eq. (6.7), only the forward hopping is considered and the backward hopping of the vortices is neglected in the critical state (see also Figs. 1.8 and 1.11). This neglect of the backward hopping in the our approach has to be justified. In the flux depinning model, the irreversibility line separates the flux creep regime (where only forward hopping is considered) from the thermally activated flux flow (TAFF)

regime (where both forward and backward hopping) are considered. Strictly speaking, the flux creep regime is valid [38] when

$$\frac{U_0}{kT}\frac{j}{J_c} >> 1 \quad ; \tag{6.8a}$$

and the TAFF regime is valid when [38]

$$\frac{U_0}{kT}\frac{j}{J_c} << 1 \quad . \tag{6.8b}$$

Therefore, the irreversibility line should be in the region where

$$\frac{U_0}{kT}\frac{j}{J_c} \approx 1. \tag{6.8c}$$

It can be shown that although the backward hopping is neglected in Eq. (6.7), it is still a good approximation even when Eq. (6.8c) is fulfilled. Therefore, for the simplicity of the calculations, Eq. (6.7) will be used for the discussion of the irreversibility line in this work.

Similar to the procedure for obtaining Eq. (4.7c) in Chap. IV, we assume that

$$U_{eff}(T,H,j/J_c)=b(T/T_c)\ g(H/H_0)\ U_{eff,0}(j/J_c)\ , \tag{6.9}$$

where $b(T/T_c)$ and $g(H/H_0)$ describe the temperature and field dependence of the pinning potential $U_0(T,H)$, respectively, and J_c is the critical current density in absence of flux creep. $U_{eff,0}(j/J_c)$ can be considered as mainly current dependent effective pinning potential, although J_c could be also temperature and field dependent. Such an assumption, i.e. the separation of temperature T, field H and current density j dominated factors, has been actually used or implied in the literature (For example, Ref. [3, 49]). A combination of Eqs.(6.7) and (6.9) gives

$$U_{eff,0}(j/J_c)=\frac{kT\ln(E/E_0)}{b(T/T_c)\cdot g(H/H_0)} \quad . \tag{6.10}$$

In the FC and ZFC magnetization experiments, the depinning line can be defined when the irreversible part of the magnetic moment, i.e. δM, drops below the detecting threshold of the equipment. Since in the Bean model, the irreversible magnetization is proportional to both the current density and the size of the sample, i.e. $\delta M \propto j \cdot l$, where l is the lateral dimension of the sample, this criterion for the depinning line depends not only on the current density flowing in the sample but also on the size of the sample and on the sensitivity of the equipment. When the size of the samples and the sensitivity of the equipment are given, the

depinning line can be defined when the current density j drops to certain small value ε, i.e. j=ε≈0 (In our experiments, this criterion ε is about 10 A/cm^2). Since the irreversibility line of the high-T_c superconductors is well below $H_{c2}(T)$ (except at T close to zero K), $J_c(T,H)$ can be considered to be field independent. At the irreversibility line, i.e. when j=ε, we may assume that the temperature factor in the effective pinning potential of $U_{eff,0}[j/J_c(T)]$ can be separated, i.e.:

$$U_{eff,0}[\epsilon/J_c(T)]=U_{eff,0}[\epsilon/J_{c0}]\cdot a(T/T_c)\equiv U_c\cdot a(T/T_c) . \qquad (6.11)$$

Eq. (6.11) is justified by the result of the collective pinning theory. In this theory, we have $U_{eff}[j/J_c(T)]\propto[j/J_c(T)]^\mu$ for a vanishing j [39], in which the temperature factor can be separated.

Combining Eq.(6.11) and Eq. (6.9), and rearranging the terms, we have:

$$g(H/H_0) = \frac{kT_r\ln(E/E_0)}{U_c\, a(T_r/T_c)b(T_r/T_c)}, \qquad (6.12)$$

where T_r denotes the temperature at the irreversibility line for a magnetic field H. Since E_0 is contained in the logarithmic term, $\ln(E/E_0)$ could be considered to be temperature and field independent. For the field dependence of the pinning potential $U_0(H)$, the following empirical relation is introduced:

$$U_0(H) \equiv U_\alpha g(H/H_0) = U_\alpha(H/H_0)^{-\frac{1}{m}} , \qquad (6.13a)$$

or $$g(H/H_0) = (H/H_0)^{-\frac{1}{m}} , \qquad (6.13b)$$

where H_0 is a characteristic field depends on the types of samples. Eq. (6.13a) is justified by the fact that this kind of power-law field dependence has been obtained experimentally with m ranging from 1 to 4 [8, 41-47] and is also postulated theoretically for certain pinning regimes which gives m=1 [3,50] and m=2 [39]. Inserting (6.13b) into Eq. (6.12), and rearranging the terms, we obtain:

$$H(T_r,E) = H_0\left[\frac{U_c}{k\ln(E_0/E)}\right]^m \cdot \left[\frac{a(T_r/T_c)b(T_r/T_c)}{T_r}\right]^m . \qquad (6.14)$$

Here, the meaning of the electric-field dependence of the irreversibility filed $H(T_r,E)$ as expressed in Eq. (6.14) shall be discussed. During the heating in the ZFC or FC magnetization measurements, an electric field E will be generated in the sample due to the decrease of the magnetization, i.e.:

$$E \propto \frac{\Delta M}{\Delta t} = \frac{\Delta T}{\Delta t} \frac{\Delta M}{\Delta T} \equiv \nu_s \frac{\Delta M}{\Delta T}, \qquad (6.15)$$

where $\nu_s \equiv \Delta T/\Delta t$, which measures the speed of the temperature change. Therefore, the term $[\ln(E_0/E)]^{-m}$ in equation (6.14) describes the dependence of the irreversibility line on the heating rate. (Note: In magnetic hysteresis measurements, the electric field E is directly proportional to the sweep rate of the applied magnetic field.)

We will now focus on the temperature dependence of the irreversibility line. At low temperatures, $a(T/T_c) \approx 1$ and $b(T/T_c) \approx 1$, Eq. (6.14) is simplified to a power law of T, i.e.:

$$H(T_r, E) = H_a(E) \, T_r^{-m}, \qquad (6.16)$$

where $H_a(E) = H_0[U_c/k\ln(E_0/E)]^m$. Such a power law like Eq.(6.13) was used to fit the irreversibility line at low temperatures in Ref. [11,28], in which no modelling was given. The power law of T obtained in Eq. (6.16) is in contrast to the scaling law (6.1). Although the scaling law (6.1) attracted much attention in the earlier studies, from the point of view of the thermally activated depinning model, the irreversibility line at low temperatures has to deviate from the scaling law. This is because in the flux creep model, the critical factor is the thermal energy kT, which is not directly related to T_c. So, at low temperatures, the relevant physical quantities related to the thermally activated flux creep should be a function of T, and not a function of $(1-T/T_c)$. Only when T is approaching T_c, due to the temperature dependences of $H_c(T/T_c)$ and $\xi(T/T_c)$, $H(T_r)$ becomes a function of $(1-T_r/T_c)$ and the scaling law of Eq. (6.1) becomes valid.

When T_r is close to T_c, the temperature factor $b(T_r)$ of the pinning potential U_0 can be expressed as a power law of $(1-T_r/T_c)$ [41], i.e.:

$$b(T_r/T_c) = (1 - T_r/T_c)^\beta \equiv (\delta)^\beta, \qquad (6.17a)$$

where we define $\delta = 1 - T_r/T_c$ (For T close to T_c, $\delta \ll 1$). Since the temperature dependence of $J_c(T)$ and $U_0(T)$ have a similar form [40, 49], we assume that $a(T_r/T_c)$, which is defined by Eq. (6.11), can also be expressed as a power law of $(1-T_r/T_c)$ for T close to T_c, i.e.:

$$a(T_r/T_c) = (1 - T_r/T_c)^\gamma \equiv (\delta)^\gamma. \qquad (6.17b)$$

Inserting Eq. (6.17a) and (6.17b) into Eq. (6.14), and using $T_r = T_c(1-\delta)$, we obtain:

$$H(T_r) = H_c \frac{\delta^n}{(1-\delta)^m} \qquad [n \equiv (\beta+\gamma)m] \qquad (6.18a)$$

$$\approx H_c \frac{\delta^n}{(1-m\cdot\delta)} \qquad (\text{for } \delta \ll 1) \qquad (6.18b)$$

where $H_c = H_0 \cdot (U_c)^m / [kT_c \ln(E_0/E)]^m$. If $(m\cdot\delta) \ll 1$, from Eq. (6.18b), we obtain the scaling law identical to Eq. (6.1):

$$H(T_r) \approx H_c \, \delta^n = H_c \, (1-T_r/T_c)^n \; . \qquad (6.19)$$

Note that the condition $(m\cdot\delta) \ll 1$ was employed for obtaining the scaling law (6.19). This condition is not only related to the temperature T, but also related to the exponent m which originates from the field dependence of the pinning potential [Eq.(6.13)]. For a larger value of m, the value of δ must be smaller to meet the condition $(m\cdot\delta) \ll 1$. Since $\delta = 1 - T_r/T_c$, this means that the temperature range for the validity of the scaling law (6.19) will be narrower. For Bi-2212 single crystals, the value of m is usually larger than two [41,42,44,46,47], and for YBCO-123 single crystals, the value of m is typically one [3,7,45]. This explains why the scaling law (6.19) holds for a wider temperature range for some superconductors like YBCO-123, but holds for a very limited range for other superconductors like Bi-2212 single crystals. Furthermore, the exponent of the scaling law (6.19) is $n = (\beta+\gamma)m$, which is directly proportional to the exponent m originating from the field dependence of the pinning potential $U_0(H)$. For different types of samples, the field dependence of the pinning potential $U_0(H)$ expressed in Eq. (6.13) is not identical (i.e. m is different), therefore, a universal exponent n for the scaling law (6.19) should not be expected in this model. In fact, as we mentioned in the introduction (Section 6.1), the value of n has been found to vary from 1.2 to 2.3 [5,8,11].

In order to describe the irreversibility line over the whole superconducting temperature range, a combination of the results of Eqs. (6.16) and (6.19) is needed. We assume that $a(T_r/T_c)$ and $b(T_r/T_c)$ can also be described by Eqs.(6.17a) and (6.17b) over the whole temperature range. This leads to

$$H(T_r, E) = H_a(E) \frac{\left(1-T_r/T_c\right)^n}{T_r^m} \; . \qquad (6.20)$$

In order to fit the irreversibility line with Eq. (6.20), this equation is rewritten as:

$$H(T_r, E) = H_a(E) \left[\frac{(1-T_r/T_c)}{T_r^{m/n}} \right]^n \; . \qquad (6.21)$$

Eq. (6.21) indicates that in a double-logarithmic plot of H versus $(1-T_r/T_c)/T_r^{m/n}$, the data should show a straight line with a slope of n for an appropriate value of m/n. This appropriate value of m/n can be determined by a "trial and error" method as explained below.

6.4.2. Application of the theoretical results to the experimental data

In light of the result given in Eq. (6.21), we have analysed the irreversibility line of our samples by plotting $\log H(T_r)$ versus $\log[(1-T_r/T_c)/T_r^{m/n}]$ for different values of m/n. In Figs. 6.3 and 6.4, the results are shown for the Bi-2212 ceramic sample and the single crystal, respectively. For low values of m/n, the curves show a positive curvature; and for high values of m/n, the curves have a negative curvature. A straight line is observed only for a certain value of m/n. As shown in Fig. 6.3 for the ceramic sample, a straight line is observed at m/n≈0.75; and the slope of this line gives the value of n to be about 2.0 [This value of n is comparable with the value of 2.2 obtained in Section 6.3 by a directly fitting of the scaling law (6.1) near T_c]. The exponent m can be deduced to be 1.5, which means that for the ceramic samples, the field dependence of the pinning potential should be: $U_0(H) \propto H^{-1/1.5}$.
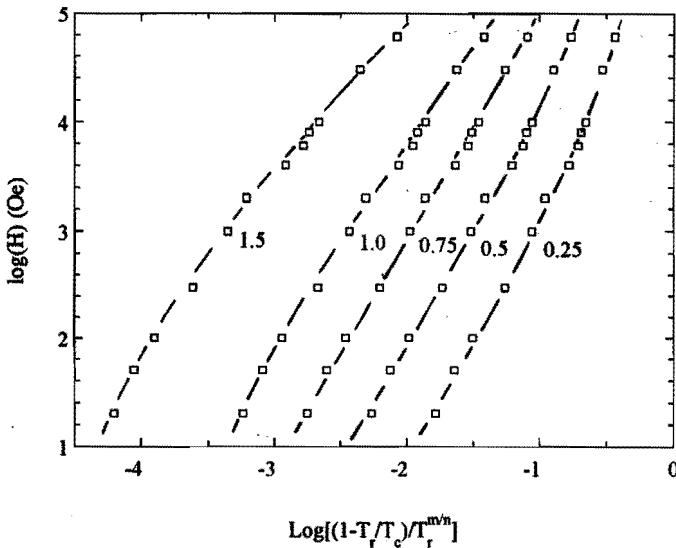

Fig. 6.3 Double logarithmic plot of $H(T_r)$ vs.$[(1-T_r/T_c)/T_r^{m/n}]$ (see the text) for the Bi-2212 polycrystalline sample. The different trial values of m/n are shown in the figure. Note the curvatures of the curves for different values of m/n.

For the Bi-2212 single crystals, there are two different regimes in the irreversibility line: one below 30 K and the other above 30 K. At T<30 K, $(1-T/T_c) \approx 1$, the data can be fitted with the power law of Eq. (6.16), and the exponent is found to be $m \approx 4.1$. This value ($m \approx 4.1$) is in good agreement with the direct experimental results reported in Ref. [8,42,44], where $U_0(H) \propto H^{-1/4}$ was found for Bi-2212 single crystals in high magnetic fields. For T>30 K, we plotted the data as $\log H(T_r)$ versus $\log[(1- T_r/T_c)/ T_r^{m/n}]$ for different values of m/n, as shown in Fig. 6.4. A straight line with a slope of $n \approx 1.26$ is found for $m/n \approx 1.75$ [A direct fitting of the scaling law (6.1) near T_c leads to n=1.2]. The exponent m is calculated to be 2.2, which
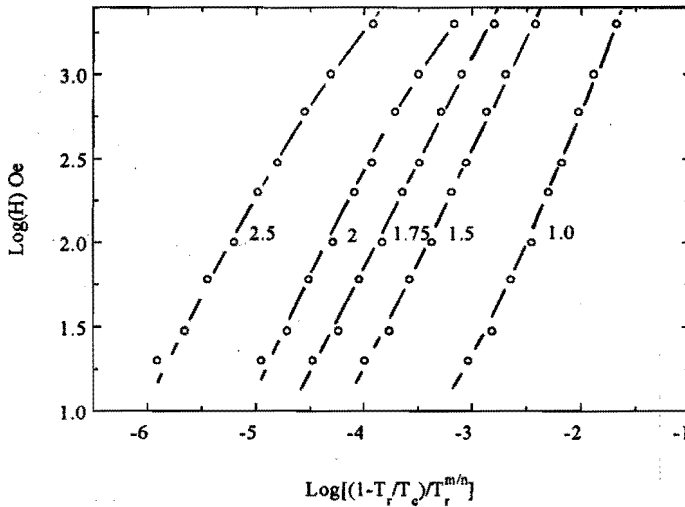
Fig. 6.4. Log (H) vs. log[(1-T_r/T_c)/T_r^{m/n}] for the Bi-2212 single crystal (T>30 K). The trial values of m/n are shown in the figure. Note the curvatures of the curves with different values of m/n.

means that for the single crystals in low magnetic fields, the field dependence of the pinning potential is: $U_0(H) \propto H^{-1/2.2}$. This result is also in good agreement with the direct experimental result of $U_0(H) \propto H^{-1/2}$ for low magnetic fields reported in Ref. [8]. Furthermore, at the irreversibility line near T_c (i.e. for low magnetic fields), this value of m=2.2 for the single crystal is larger than the value of 1.5 for the ceramic sample, therefore, as discussed in the above section, the irreversibility line of the Bi-2212 ceramic samples should obey the scaling law (6.1) over a wider temperature range near T_c than that of the Bi-2212 single crystals, which is what has been observed in our experiments (see Fig. 6.2).

6.4.3 A remark about the field dependence of the pinning potential

A final remark should be made about the field dependence of the pinning potential $U_0(H)$. When replacing Eq. (6.13b) by a logarithmic field dependence, i.e.

$$g(H/H_0)=\ln(H_0/H),\qquad\qquad\qquad(6.22)$$

from Eq. (6.12), the temperature dependence of the irreversibility line will become

$$H(T_r,E) = H_0 \exp\left[-\frac{kT_r\ln(E_0/E)}{U_c\,a(T_r/T_c)\cdot b(T_r/T_c)}\right].\qquad(6.23)$$

At low temperatures, $a(T_r/T_c)\approx1$ and $b(T_r/T_c)\approx1$, so the following is obtained:

$$H(T_r)=H_0\exp(-T_r/T_0),\qquad\qquad(6.24)$$

where $T_0=U_c/k\ln(E_0/E)$. This exponential law Eq. (6.24) was also used to fit the irreversibility line at low temperatures in literature [8,11,27]. For our data, Eq. (6.24) can also fit the irreversibility line of the single crystals for $T<30$ K, and of the ceramic samples for $T<60$ K. However, because of the relative narrow temperature range, it is difficult to distinguish a better fit between a power law of T_r^{-m} and an exponential law of $\exp(-T_r/T_0)$. Since the logarithmic field dependence of Eq.(6.22) lacks strong experimental and theoretical support, we prefer the power-law field dependence of Eq. (6.13), because it was obtained in various experiments [8, 41-47], and postulated in theories for $m=1$ [3,50] and $m=2$ [39].

6.5. Conclusion

In conclusion, the irreversibility line was determined down to 15 K for both Bi-2212 single crystals and ceramic samples. A "kink" was found at about 30 K in the irreversibility line of Bi-2212 single crystals, suggesting a transition between two different regimes. At low temperatures, the irreversibility line of both types of samples does not obey the scaling law: $H(T_r)\propto(1-T_r/T_c)^n$. In this Chapter, an approach for the irreversibility line within the framework of thermally activated flux creep is proposed, which is valid for any j dependence of the effective pinning potential $U_{eff}(j)$. Using an empirical power law field dependence of the pinning potential, i.e. $U_0(H)\propto H^{-1/m}$, this approach gives the temperature dependence of the irreversibility line to be $H(T_r)\propto(1-T_r/T_c)^n/T_r^m$. This result means that the irreversibility line $H(T_r)$ is a power law of T_r at low temperatures, and obeys the scaling law, i.e.

$H(T_r) \propto (1-T_r/T_c)^n$ at T_r close to T_c. The exponent n in the scaling law was found to be related to the field dependence of the pinning potential $U_0(H)$. Since the field dependence of the pinning potential $U_0(H)$ differs for different types of samples, no universality of the exponent n in the scaling law should be expected for different types of samples. Applying the theoretical results to the experimental data gave good agreement.

Finally, a comparison of this approach and the previous work of Yeshurun and Malozemoff [3] is shown in the following table.

Table 6.1 A comparison of this work and a previous work in Ref. [3].

	Previous work [3]	This work
T dependence of H(T$_r$)	$H(T_r) \propto (1-T_r/T_c)^n$	$H(T_r) \propto (1-T_r/T_c)^n/T_r^m$
j dependence of $U_{eff}(j)$	$U_{eff}(j)=U_0(1-j/J_c)$	any j dependence of $U_{eff}(j)$
Temperature range	for T near T$_c$	whole region (T<T$_c$)
H dependence of $U_0(H)$	$U_0(H) \propto H^{-1}$	$U_0(H) \propto H^{-1/m}$
The exponent n	n=1.5	no universality

References

[1] K. A. Müller, M. Takashige, and J. G. Bednorz, Phys. Rev. Lett. **58** (1987) 1143.

[2] E. H. Brandt, J. of Modern Phys. B, No. 5 (1991) 751.

[3] Y. Yeshurun, and A.P. Malozemoff, Phys. Rev. Lett. **60** (1988) 2202.

[4] A.P. Malozemoff, in "Physical Properties of High Temperature Superconductors" edited by D. Ginsberg, world Scientific, Singapore, Vol. I, p. 71.

[5] Y. Xu, M. Suenaga, Y. Gao, J.E. Crow, and N.D. Spencer, Phys. Rev. B 42 (1990) 8756; Youwen Xu and M. Suenaga, Phys. Rev. B **43** (1991) 5516

[6] A. Gupta, P. Esquinazi, H. F. Braun, and H. W. Neumüller, Phys. Rev. Lett. 63 (1989) 1869.

[7] T.T.M. Palstra, B. Batlogg, R. B. Van Dover, L. F. Schneemeyer and J. V. Waszczak, Appl. Phys. Lett. 54 (1989) 763.

[8] A. Gupta, P. Esquinazi, H.F. Braun, H.W. Neumüller, G. Ries, W. Schmidt, and W. Gerhäuser, Physica C 170 (1990) 95.

[9] L.W. Lombardo, D.B. Mitzi, A. Kapitulnik and A. Leone, Phys. Rev. B 46 (1992) 5615.

[10] J.R. Thompson, Y.R. Sun, H.R. Kerchner, D.K. Christen, B.C. Sales, B.C. Chakoumakos, A.D. Marwick, L. Civale and J.O. Thomson, Appl. Phys. Lett. 60 (1992) 2306.

[11] V. Hardy, J. Provost, D. Groult, M. Hervieu, B. Raveau, S. Durcok, E. Pollert, J. C. Frison, J. P. Chaminade and M. Pouchard, Physica C 191 (1992) 85.

[12] R.C. Budhani, M. Suenaga, and S.H. Liou, Phys. Rev. Lett. 69 (1992) 3816.

[13] L.T. Sagdahl, T. Lægreid, K. Fossheim, M. Murakami, H. Fujimoto, S. Gotoh, K. Yamaguchi, H. Yamauchi, N. Koshizuka, and S. Tanaka, Physica C 172 (1991) 495.

[14] F. Supple, A. M. Campbell, J. R. Cooper, Physica C 242 (1995) 233.

[15] M.P.A. Fisher, Phys. Rev. Lett. 62 (1989) 1415.

[16] G. Blatter, M.V. Feigel'man, V.B. Geshkenbein, A.I. Larkin, and V.M. Vinokur, Rev. Modern. Phys. 66 (1994) 1125.

[17] R.H. Koch, V. Foglietti, W.J. Gallagher, G. Koren, A. Gupta and M.P.A. Fisher, Phys. Rev. Lett. 63 (1989) 1151.

[18] P.L. Gammel, L.F. Schneemeyer, and D.J. Bishop, Phys. Rev. Lett. 66 (1991) 953.

[19] H. Safar, P.L. Gammel, D.J. Bishop, D.B. Mitzi, and A. Kapitulnik, Phys. Rev. Lett. 68 (1992) 2672.

[20] C . Dekker, W. Eidelloth, and R.H. Koch, Phys. Rev. Lett. 68 (1992) 3347.

[21] C.J. van der Beek, P.H. Kes, M.P. Maley, M.J.V. Menken, and A.A. Menovsky, Physica C 195 (1992) 307.

[22] D.R. Nelson and H.S. Seung, Phys. Rev. B **39** (1989) 9153.

[23] A. Houghton, R.A. Pelcovits, and A. Sudbo, Phys. Rev. B **40** (1989) 6763.

[24] P.L. Gammel, L.F. Schneemeyer, J.V. Wasczak, and D.J. Bishop, Phys. Rev. Lett. **61** (1988) 1666.

[25] R. Cubitt, E.M. Forgan, G. Yang, S.L. Lee, D. Mck. Paul, H.A. Mook, M. Yethiraj, P.H. Kes, T.W. Li, A.A. Menovsky, Z. Tarnawski, and K. Mortensen, Nature Vol 365, (1993) 407.

[26] D.R. Nelson, "Pinning, fluctuation and melting of superconducting vortex arrays", in « The vortex State », edited by N. Bontemps et al., NATO ASI Series, Kluwer Academic Publishers, p. 41 (1994).

[27] P. de Rango, B. Giordanengo, R. Tournier, A. Sulpice, J. Chaussy, G. Deutscher, J.L. Genicon, P. Lejay, R. Retoux and B. Raveau, J. Phys. (Paris) **50** (1989) 2857.

[28] W. Kritscha, F.M. Sauerzopf, H.W. Weber, G.W. Crabtree, Y.C. Chang, and P.Z. Jiang, Physica C 179 (1991) 59.

[29] T. Nojima and T. Fujita, Physica C **178** (1991) 140.

[30] K. Kadowaki and T. Mochiku, Physica C 195 (1992) 127.

[31] C.C. Almasan, M.C. de Andrade, Y. Dalichaouch, J.J. Neumeier, C.L. Seaman, M.B. Maple, R.P. Guertin, M.Y. Kuric, and J.C. Garland, Phys. Rev. Lett. 69 (1992) 3812.

[32] A. Schiling, R. Jin, J.D. Guo, and H.R. Ott, Phys. Rev. Lett. 71 (1993) 1899.

[33] C.C. Almasan, and M.B. Maple, Phys. Rev. 53 (1996) 2882.

[34] D. Hu, V.A.M. Brabers, J.H.P.M. Emmen, and W.J.M. de Jonge, Physica C 216 (1993) 315.

[35] E. Zeldov, D. Majer, M. Konczykowski, A.I. Larkin, V.M. Vinokur, V.B. Geshkenbein, N. Chikumoto, and H. Shtrikman, Euro. Phys. Lett. 30 (1995) 367.

[36] J.H.P.M. Emmen, S.K.J. Lenczowski, J.H.J. Dalderop, V.A.M. Brabers, J. Crystal Growth 118 (1992) 477.

[37] W. Paul and Th. Baumann, Physica C 175 (1991) 102.

[38] D. Dew-Hughes, Cryogenics 28 (1988) 674.

[39] V. Geshkenbein, A. Larkin, M. Feigel'man and V. Vinokur, Physica C 162-164 (1989) 239.

[40] D. Hu, W. Paul and J. Rhyner, Physica C 200 (1992) 359.

[41] T.T.M. Palstra, B. Batlogg, R.B. van Dover, L.F. Schneemeyer and J.V. Waszczak, Phys. Rev. B 41 (1990) 6621.

[42] C.J. van der Beek and P.H. Kes, Phys. Rev. B 43 (1991) 13032.

[43] P.J. Kung, M.P. Maley, M.E. McHenry, J.O. Willis, J.Y. Coulter, M. Murakami and S. Tanaka, Phys. Rev. B 46 (1992) 6427.

[44] J.H.P.M. Emmen, V.A.M. Brabers and W.J.M. de Jonge, Physica C 176 (1991) 137.

[45] S. Zhu, D. K. Christen, C. E. Klabunde, J. R. Thompson, E. C. Jones, R. Feenstra, D. H. Lowndes and D. P. Norton, Phys. Rev. B 46 (1992) 5576.

[46] J.T. Kucera, T.P. Orlando, G. Virshup and J.N. Eckstein, Phys. Rev. B 46 (1992) 11004.

[47] H. Yamasaki, K. Endo, S. Kosaka, M. Umeda, S. Yoshida and K. Kajimura, Phys. Rev. Lett. 70 (1993) 3331.

[48] P.W. Anderson, Phys. Rev. Lett. 9 (1962) 309; M.R. Beasley, R. Labusch and W.W. Webb, Phys. Rev. 181 (1969) 682.

[49] H.G. Schnack, R. Griessen, J.G. Lensink, and Wen Hai-Hu, Phys. Rev. B 48 (1993) 13178.

[50] M. Tinkham, Phys. Rev. Lett. 61 (1988) 1658.

Chapter VII. Substitution experiments on Bi$_2$Sr$_2$CaCu$_2$O$_{8+z}$ single crystals

In this chapter, our investigation on the substitution of Cu by Co or Ni, and the substitution of Ca by Y in the Bi$_2$Sr$_2$CaCu$_2$O$_{8+z}$ (Bi-2212) single crystals will be presented. Our object for the substitution in Bi-2212 single crystals is mainly related to the mechanism of the superconductivity and the influence on the flux pinning caused by the substitution.

7.1. Effects of partial Yttrium substitution in Bi$_2$Sr$_2$Ca$_{1-x}$Y$_x$Cu$_2$O$_{8+z}$ single crystals

[Part of this Section has been published in Physica C 235-240 (1994) 951.]

7.1.1 Introduction

Ever since the discovery of high-T$_c$ superconductivity in the Ba-La-Cu-O system, the substitution studies have led to the discoveries of various new high-T$_c$ compounds. In those substitution experiments, the object was to search new superconductors empirically. Meanwhile, many other researchers have used the substitution as a tool for investigating the mechanism of the superconductivity in the high-T$_c$ superconductors, since various relevant parameters, such as the ion size, carrier concentration, and valence state, can be changed by the substitution. For a review of earlier studies, see Ref. [1].

For Bi$_2$Sr$_2$CaCu$_2$O$_{8+z}$ superconductors, the substitution of Ca by Y has attracted considerable attention, mainly due to the following reasons: 1). the carrier concentration in this system could be changed continuously while retaining the crystal structure; 2).the compound with complete substitution, i.e. Bi$_2$Sr$_2$YCu$_2$O$_{8+z}$, was found to be an insulator, therefore, the metal-insulator transition occurring at Y$\approx$0.6 became interesting. Early work for this type of substitution, which was performed on polycrystalline Bi-2212 samples, was dealing with the effects on its influence on the structure, resistivity, Hall effect, transition temperature, oxygen concentration and magnetization of the material [2-9]. Later on, in

order to eliminate the problems of grain boundaries, oxygen inhomogeneity and secondary phases in the polycrystalline samples, Y-doped Bi-2212 single crystals grown by the self-flux crucible method were used for the investigation of their structure, oxygen concentration, transition temperature and resistivity [10-12].

In this work, $Bi_2Sr_2Ca_{1-x}Y_xCu_2O_{8+z}$ single crystals with the nominal composition of Y to be x=0, 0.01, 0.05, 0.1, 0.2 ,0.3 and 0.4 were grown by the travelling solvent floating zone (TSFZ) method. The composition, structure and c-axis length were characterized. The changes of the superconducting properties after doping, as well as the pinning properties at small substitution level were investigated.

7.1.2. Experimental

The TSFZ method for growing Bi-2212 single crystals has been described earlier (see Section 1.4 and Section 2.1). Since the melting point of Y-substituted Bi-2212 was enhanced compared with the pure Bi-2212 material, the final sintering temperature of the precursor bars was increased by about 2 ^0C for each atomic percentage of Yttrium. The Bi-2212 crystals with partial substitution of Yttrium have a typical size of $1x1x0.05$ mm^3, which are smaller than the pure Bi-2212 crystals .

The θ-2θ X-ray diffraction scans and Laue X-ray diffraction were used to detect the structure of the crystals. The chemical composition was determined with electron probe micro analysis (EPMA). The T_c of single crystals was derived from AC susceptibility measurements and $j_c(T)$ was obtained from the remanent magnetisation measured with a Flux-gate magnetometer.

7.1.3. Experimental results

The chemical compositions of the crystals measured with the electron microprobe is given in Fig. 7.1. The total composition of Bi, Sr, (Ca+Y) and Cu elements is normalized to 7. The results showed some deviation from the nominal composition. Nevertheless, the actual Y content increased and the Ca content decreased with the nominal Y content, while the other

concentrations remained steady. Later on, the actual Y concentration will be used for analysis.
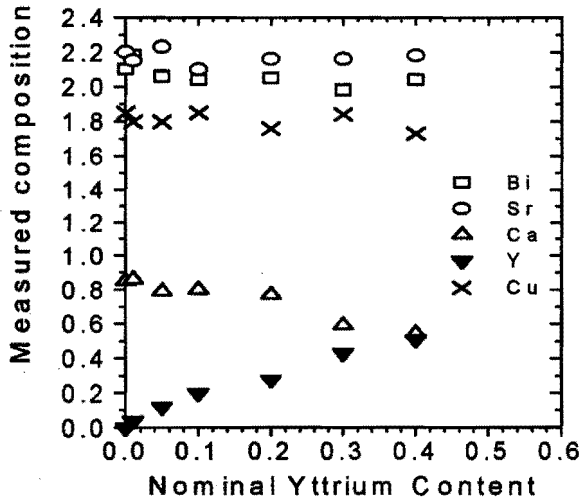

Fig. 7.1. *Measured Composition of Y-substituted Bi-2212 single crystals against the nominal Y concentration.*
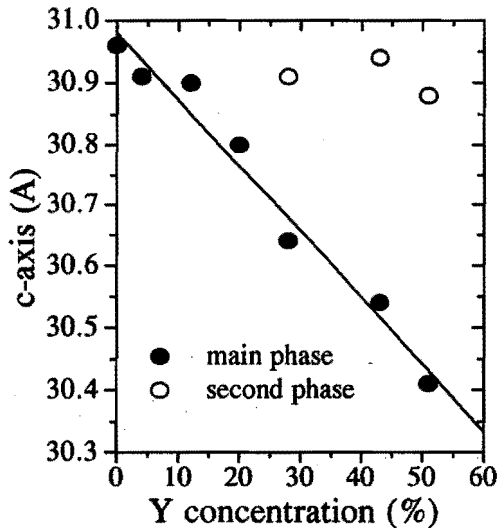

Fig. 7.2. *The c-axis length versus the Y concentration of Y-substituted Bi-2212 single crystals.*

With X-ray diffraction, it was found that the Y-doped Bi-2212 single crystals retained the basic structure of pure Bi-2212 single crystals. However, for x>0.2, an intergrowth of a secondary phase appeared too, probably it was related to the substitution of Y in the Sr sites [13]. The c-axis of the main phase decreased almost linearly with the Y concentration, as shown in Fig.7.2, which is in good agreement with the results reported in Ref. [11]. The c-axis of the second phase, however, changed little.
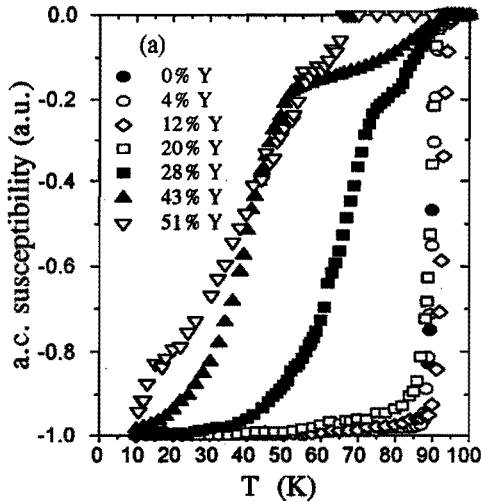
Fig. 7.3 AC. susceptibility of Yttrium-substituted Bi-2212 single crystals

The normalised AC susceptibility of Y doped Bi-2212 single crystals are given in Fig.7.3. For the crystals with x<0.2, the transition width (defined as the temperatrue interval between 10% and 90% of the full susceptibility) was only 2-4 K, indicating the homogeneity of the crystals. For x=0.28 and 0.43, a two-step transition was observed due to the intergrowth of two phases [13]. For x=0.51, the transition became very broad. The transition temperature T_c can be determined from the onset of the AC susceptibility curves shown in Fig. 7.3. The results are plotted in Fig. 7.4. The T_c initially increases from 91.5 K to 95.3 K when the Y content increased from 0 to 0.2, but it is followed by a steep decrease with larger Yttrium concentration.

A flux-gate magnetometer was used to measure the remanent magnetization at various temperatures. The critical current density $j_c(T)$ was deduced from the remanent magnetization using the Bean model. The results are shown in Fig. 7.5 for several samples.

Fig. 7.4 The transition temperature versus the Y concentration of Y-substituted Bi-2212 single crystals

Fig. 7.5 The critical current density $j_c(T)$ of Y-doped Bi-2212 single crystals in a semi-logarithmic plot. The insert shows the changes of j_c at T=5 K with the doping level.

As shown in Fig. 7.5, the "kink" at a temperature between 24-28 K is always present in the $j_c(T)$ curves. This kink marks a boundary between two different pinning regimes [14], as has al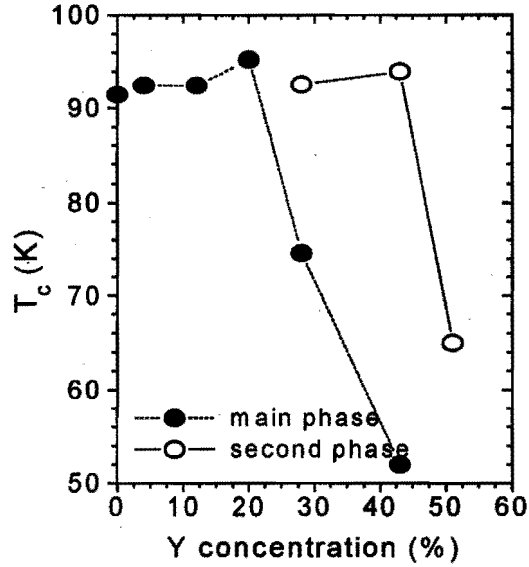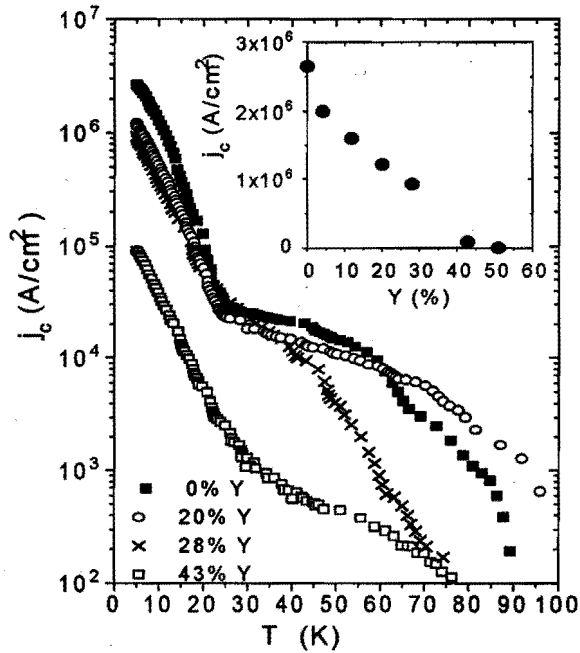ready been discussed in Section 3.5 and Section 5.5 for the pure Bi-2212 single crystals. The value of j_c at T=5 K decreases approximately linearly, as shown in the inset of Fig. 7.5, which indicates that the defects introduced by the Yttrium ions does not act as pinning centres. This is probably because that the Bi-2212 system is quasi-2D, only the defects in the superconducting Cu-O planes can be major pinning centers. Furthermore, when Y^{3+} replaces Ca^{2+}, more oxygen might be located in the Cu-O planes in order to compensate the valence change, which means a decreased number of the oxygen vacancies in the Cu-O planes. Since oxygen vacancies are the major pinning centres in Bi-2212 single crystals [15,16], the substitution of Yttrium will lead to a decrease of j_c. However, although the value of j_c at 5 K decreased with Y doping, for Y<0.3, the "kink" occurred always when j_c drops to about 3×10^4 A/cm^2, as can be seen from Fig. 7.5. For Y>0.3, the "kink" appeared at a lower value of j_c, which was likely to be due to the influence of the secondary phase and inhomogeneity of the single crystals for a high level of Yttrium doping.

7.2. Substitution effects of $Bi_2Sr_2Ca(Cu_{1-x}M_x)_2O_{8+z}$ (M=Co, Ni) single crystals

[Part of this Section has been published in Chinese J. of Phys. 34 (1996) 597.]

7.2.1   Introduction

Substitution of Cu by 3d-elements in high-T_c cuperate oxides will directly affect the superconducting Cu-O layers and, therefore, it is an effective way of studying the superconductivity mechanism. Most of the earlier substitution studies on Bi-2212 system used polycrystalline samples [17-20], which showed that 3d-elements could sharply depress the transition temperature T_c. The decrease of T_c was attributed to the impurity-induced pair breaking [18,20], or to the influence of excess oxygen concentration caused by the substitution [19,21]. Because of the sensitivity of T_c to the doping level, it is important to grow single crystals that are uniformly substituted with 3d-elements. Single crystals of Bi-2212 substituted with Co, Fe, Ni and Zn were grown by the self-flux crucible method and

studied the effects in Ref. [21-23]. Investigations on Bi-2212 single crystals grown by the TSFZ method with a partial substitution of up to 3% Fe [24] and up to 2% Ni [25] were also reported.

Another interesting issue is the pinning mechanisms in high-T_c superconductors. There has been strong evidence that oxygen deficiencies in the Cu-O planes are the major pinning centers for Bi-2212 single crystals [15,16]. Since substitution of Cu by 3d-elements introduces point defects in the Cu-O planes, an investigation of its influence on the critical current density j_c could give some insight into the pinning mechanism in Bi-2212. In a study of Fe, Ni and Zn doped Bi-2212 single crystals, in a magnetic field of H≈0 T, a decrease of j_c was reported [22]. However, in a later publication [23], it was observed that for H=0.2 T, the critical current density j_c at T>10 K was increased for low doping level of 3d-elements (x<1%).

In our substitution experiments, the TSFZ technique was used to grow single crystals of Bi-2212 with a substitution of Cu by Co or Ni. The nominal concentration of Co is 1%, 2% and 5%; and that of Ni is 2% and 4%. The effects of the substitution on the structure, transition temperature T_c, as well as the critical current density j_c, were investigated.

7.2.2. Experimental

The single crystals of $Bi_2Sr_2Ca(Cu_{1-x}M_x)_2O_{8+z}$ with M=Co or Ni were grown by the TSFZ method, which has been described in Section 1.4 and Section 2.1. The size of the single crystals after doping with the 3d-elements is typically $3\times1.5\times0.15$ mm^3, which is smaller than the pure Bi-2212 single crystals ($10\times3\times0.3$ mm^3). The c-axis of the crystals is along the smallest dimension.

The θ-2θ X-ray diffraction scans and Laue X-ray diffraction were used to detect the structure of the crystals. The chemical composition was determined with electron probe micro analysis (EPMA). The T_c of the single crystals was derived from AC susceptibility measurements and $j_c(T)$ was obtained from the remanent magnetisation measured with a SQUID magnetometer.

7.2.3. Experimental results and discussion

The chemical composition of the Bi-2212 single crystals doped with 3d-elements was slightly different from the nominal one. The results are presented in Table 7.1, in which the total composition of Bi, Sr, Ca and (Cu+M) elements (M=Ni or Co) is normalized to 7. Although a deviation from the nominal concentration was observed, the substituent (Co or Ni) in the Bi-2212 single crystals increased with the nominal concentration. The X-ray diffraction patterns of all the substituted single crystals did not reveal any secondary phase.

Table 7.1 The chemical composition of Co or Ni substituted Bi-2212 single crystals measured by EPMA

nominal	Bi	Sr	Ca	Cu	M(Co/Ni)	M/Cu ratio
Ni2%	2.00	1.91	1.00	2.02	0.04	2.0%
Ni4%	2.00	1.96	0.93	2.01	0.10	5.0%
Co1%	2.13	2.26	0.81	1.76	0.04	2.3%
Co2%	2.10	2.18	0.90	1.76	0.07	4.0%
Co5%	2.12	2.17	0.98	1.64	0.09	5.5%

As shown in Fig.7.6(a), the c-axis length of the crystals decreased with both Ni and Co concentration. The decrease is more or less linear for the Co-doped samples, although it seems not to be the case for the Ni-doped single crystals up to 5% Ni concentration. The shrinking of the c-axis length can be related to the smaller ion size of the substituents ($r=0.79$ Å for Cu^{+2}, 0.74 Å for Co^{2+} and 0.72 Å for Ni^{2+}).

The AC susceptibility data given in Fig. 7.7 show also no sign of any second superconducting phase, which is in agreement with the X-ray diffraction data. The transition width, defined by the temperature difference between 10% and 90% of the full AC field expulsion, is nearly the same (5-7 K) for all the samples. The transition temperature T_c, defined as the onset temperature, decreases with the Co or Ni concentration, as given in Fig.

7.6(b). The initial changing rate of T_c is about 5 K per atomic percentage of the 3d-element concentration, which is in good agreement with the existing published data [18,20-21].
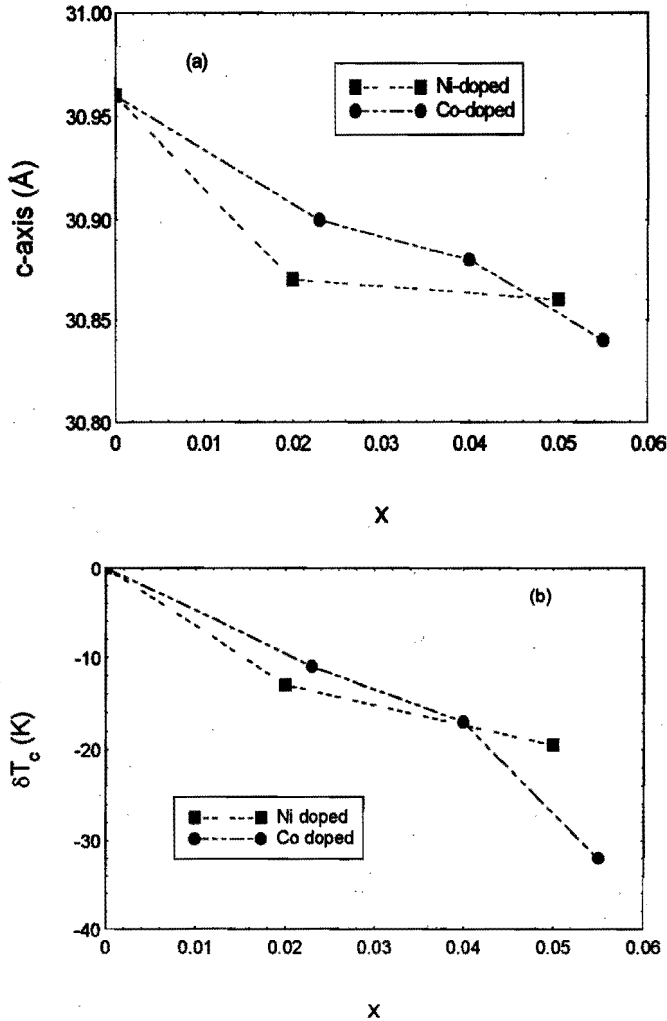
FIG. 7.6 (a)The c-axis length and (b) the change of the critical temperature for the Co and Ni substituted Bi-2212 single crystals versus the substituent concentration.

The critical current density $j_c(T)$ of the single crystals is shown in Fig. 7.8 with a semi-log plot. The critical current density at 5 K, i.e. $j_c(T=5K)$, decreased with increasing substitution. A "kink" in the $j_c(T)$ curves was found for all the samples, which is typical for Bi-2212 single crystals (See Section 3.5 and Section 5.5). As can be seen in Fig. 7.8, for low level of

doping, i.e. for x=0 and x=2% of Co, as well as for x=2% of Ni, the kink occurs at $j_c \approx 3 \times 10^4$ A/cm^2. However, for x=3.5% and 4.5% of Co, and x=5% of Ni, the position of the kink shifts to a lower j value at about 7×10^3 A/cm^2. The implication of these results will be discussed in more details in Section 7.3.

FIG. 7.7 *AC susceptibility (H_{ac}=8 Gauss, f=920 Hz) of Co and Ni substituted Bi-2212 single crystals.*

FIG. 7.8 *Temperature dependence of j_c (T) for Co or Ni substituted Bi-2212 single crystals. Note the position of the "kink" in the curves for different doping levels, as indicated by the dashed horizontal lines.*

7.3. The influence of the substitution on the transition between the two different pinning regimes
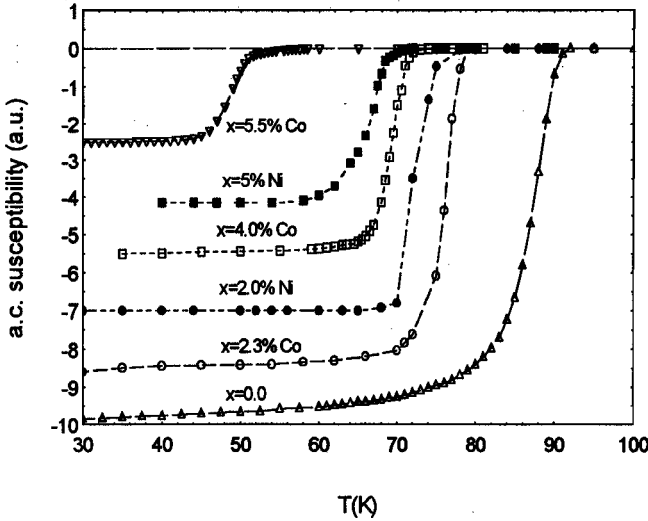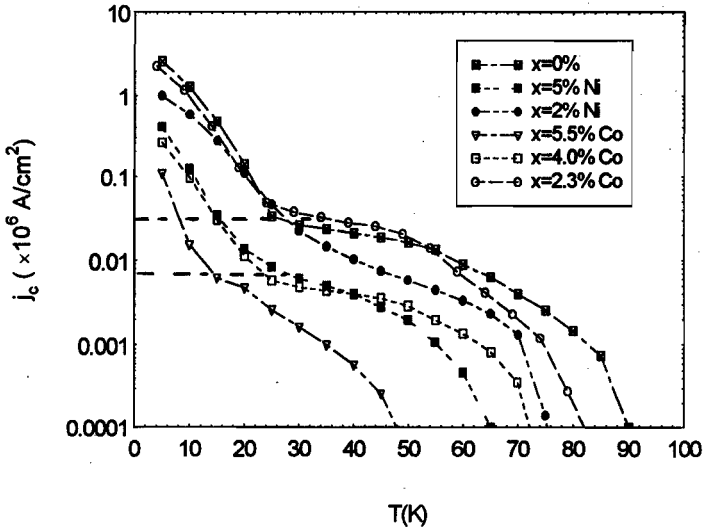
In this section, we will pay more attention to the influence of substitution on the two different pinning regimes found in Bi-2212 single crystals, as marked by the "kink" in $\ln[j_c(T)]$. As has been discussed in Section 3.5 of Chap. III, Metlushko et al. [26] proposed that this "kink" is caused by a transition from a individual/small-bundle flux pinning regime to a large-flux-bundle collective pinning regime. They postulated that the "kink" should occur when j_c drops to a certain value J_{cr}:

$$J_{cr} = j_0/\kappa^2 , \qquad\qquad (7.1)$$

where j_0 is the depairing current, i.e. $j_0 = \phi_0 c/(12\pi^2\sqrt{3}\lambda_{ab}^2\xi_{ab})$, and κ the Ginzburg-Landau (G-L) parameter, i.e. $\kappa = \lambda/\xi$. By using the available parameters for Bi-2212 ($\kappa = 80-200$), the value of J_{cr} was found to be in the range of 10^4-10^5 A/cm^2. In our experiments on $Bi_2Sr_2Ca(Cu_{1-x}M_x)_2O_{8+z}$ (M=Co or Ni) single crystals (Fig. 7.8), for x=0, x=2% of Co and x=2% of Ni, the value of J_{cr} is always about 3×10^4 A/cm^2, which is indeed within the range of the theoretical value. However, for x=3.5%, 4.5% of Co, and x=5% of Ni, the kink appears at a smaller value of J_c, i.e. $J_{cr} \approx 7\times10^3$ A/cm^2. This indicates that a relative small concentration of 3d-elements (x~5%) in the Bi-2212 single crystals can effectively reduce the value of J_{cr}. This is in contrast with the results obtained on the Y-substituted Bi-2212 single crystals, for which J_{cr} is almost the same for up to 28% of Y (x≤0.28), as can be seen in Fig. 7.5. An explanation for such different effects might be that Yttrium substitution affects the pinning mainly by decreasing the number of oxygen vacancies in the Cu-O planes, but doping with 3d elements for Cu mainly introduces cation impurities into the Cu-O planes, which leads to a decrease in the coherent length ξ and an increase in the G-L parameter κ [22]. So, according to Eq. (7.1), the latter (3d-element substitution) will more effectively reduce the value of J_{cr}. It is noted that neither the impurities of Y nor the defects of 3d-elements can increase the value of j_c at T=5 K, which is due to the fact that only the oxygen deficiencies in the Cu-O planes are the main pinning centres in the Bi-2212 single crystals [15,16].

References

[1] A. V. Narlikar, C. V. Narasimha Rao and S. K. Agarwal, "Substitutional Studies on High Temperature Superconductors" in 《Studies of High Temperature Superconductors》 edited by A. Narlikar, vol.1, p 341, 1989.

[2] R. Yoshizaki, Y. Saito, Y. Abe, and H. Ikeda, Physica C 152, 408 (1988).

[3] Noburu Fukushima, Hiromi Niu, and Ken Ando, Jpn. J. Appl. Phys. 27, L1432 (1988).

[4] Ando, K. Fukuda, S. Kondoh, M. Sera, M. Onoda, and M. Sato, Solid State Commun. 67, 815 (1988).

[5] A. Manthiriam and J. B. Goodenough, Appl. Phys. Lett. 53, 420 (1988).

[6] T. Tamegai, K. Koga, K. Suzuki, M. Ichihara, F. Sakai, and Y. Iye, Jpn. J. Appl. Phys. 28, L112 (1989).

[7] A. Maeda, M. Hase, I. Tsykada, K. Noda, S. Takebayashi, and K. Uchinokura, Phys. Rev. B 41, 6148 (1990).

[8] W. A. Groen, D. M. DeLeeuw, and L. F. Feiner, Physica C 165, 55 (1990).

[9] P.Mandal, A. Poddar, B. Ghosh, and P. Choudhury, Phys. Rev. B 43, 13102 (1991).

[10] D. B. Mitzi, L. W. Lombardo, A. Kapitulnik, S. S. Laderman, and R. D. Jacowitz, Phys. Rev. B 41, 6564 (1990).

[11] C. Kondziora, L. Forro, D. Mandrus, J. Hartge, P. Stephens, L. Mihaly, R. Reeder, D. Moecher, M. Rivers, and S. Sutton, Phys. Rev. 45 (1992) 13025.

[12] R. Jayavel, A. Thamizhavel, P. Murugakoothan, C. Subramanian and P. Ramasamy, Physica C 215, 429 (1993).

[13] X. F. Zhang, G. Van Tendeloo, S. L. Ge, J. H. P. M. Emmen and V. A. M. Brabers, Physica C 215, (1993) 39.

[14] D. Hu, W. Paul and J. Rhyner, Physica C **200**, 359 (1992).

[15] C. J. van der Beek and P. H. Kes, Phys. Rev. B 43 (1991) 13032.

[16] T.W. Li, A.A. Menovsky, J.J.M. Franse, and P.H. Kes, Physica C 257 (1996) 179.

[17] T. E. Jones, P.M. Thibado, W.C. McGinnis, R.D. Boss, J.W. Schindler, and S. Oseroff, Physica C **162-164**, 25 (1989).

[18] A. Maeda, T. Yabe, S. Takebayashi, M. Hase, and K. Uchinokura, Phys. Rev. B **41**, 4112 (1990).

[19] S. T. Lin, W.S. Chung, C. Y. Chou and C. M. Lin, J. Phys. Condens. Matter **2**, 8763 (1990).

[20] P. Sumana Prabhu, M.S. Ramachandra Rao and G. V. Subba Rao, Physica C **211**, 279 (1993).

[21] M. Boekholt, Th. Bollmeier, L. Buschmann, M. Fleuster and G. Güntherodt, Physica C **198**, 33 (1992).

[22] B. vom Hedt, W. Lisseck, K. Westerholt and H. Bach, Phys. Rev. B **49**, 9898 (1994).

[23] R. Noetzel, B. vom Hedt, W. Lisseck, K. Westerholt, Physica C 260 (1996) 290.

[24] G.D. Gu, K. Takamuku, N. Koshizuka, S. Tanaka, J. Crystal Growth **137**, 472 (1994).

[25] M.J.V. Menken, A.J.M. Winkelman and A.A. Menosky, J. Crystal Growth **113**, 9 (1991).

[26] V.V. Metlushko, G. Güntherodt, V.V. Moshchalkov and Y. Bruynseraede, Europhys. Lett. **26**, 371 (1994).

Chapter VIII   Resistivity measurements by means of flux-transformer geometry on Bi₂Sr₂CaCu₂O₈₊z single crystals with or without long-term annealing

In this chapter, our electric transport measurements using the so called flux-transformer geometry are presented. The emphasis will be on the temperature and field dependence of the bottom voltage $V_{bot}(T,H)$.

8.1. Introduction

Resistivity measurements have played an important role in the understanding of flux flow, thermal fluctuation of the vortices, vortex pinning and vortex phase transitions in high-T_c superconductors. A powerful technique for the resistivity measurements is based on the so called flux-transformer geometry, as shown schematically in Fig. 8.1 and introduced in Section 1.10 of Chapter I. With this technique, the voltages at the top and bottom surfaces of the sample, i.e. $V_{top}(T,H)$ and $V_{bot}(T,H)$ (see Fig. 8.1) can be measured and analysed. This type of measurements have been used [1-8] to study the vortex correlation, the coupling strength of the layers and the dimensionality of the vortices in the vortex-liquid regime, as well as anisotropic resistivity in the normal state.

Using the this technique with the flux transformer geometry, a field-dependent characteristic temperature, denoted as $T_{th}(H)$, was observed for YBa₂Cu₃O₇₋δ (YBCO-123) single crystals in the vortex-liquid regime [4-8]. Below this boundary line of $T_{th}(H)$, the vortices are of three dimensional (3 D), but above $T_{th}(H)$ the vortex correlation in the c-direction is not maintained across the sample. In contrast, for more anisotropic Bi-2212 single crystals, it was found [1-3] that vortices in the whole vortex-liquid regime are of 2D character. However, for the Bi-2212 single crystals, the temperature and magnetic field dependence of the bottom voltage $V_{bot}(T,H)$ (which is called "the secondary voltage" in Ref. [2]) differs in the three studies published. Safar

et al. [3] reported a behaviour of $V_{bot}(H,T)$ very similar to $V_{top}(H,T)$, i.e. it exhibited thermally activated flux-flow (TAFF) behaviour. In the experiments of Busch et al [1], the temperature dependence of $V_{bot}(H,T)$ in magnetic fields showed a broad peak (over a temperature interval of more than 20 K below T_c) which did not appear at zero applied magnetic field. In contrast, Wan et al. [2] observed a very narrow peak (over a temperature interval of about 2 K) in the curve of $V_{bot}(T,H)$ at T near T_c in zero applied magnetic field, which was suppressed by applying a magnetic field parallel to the a-b plane. This anomalous behaviour could not be simply explained by the local anisotropic resistivity model developed by Busch et al. [1], and was postulated [2] to be caused by the combined effects of the free vortex excitation and the Josephson coupling between the superconducting layers. Although these results on $V_{bot}(T,H)$ are apparently not in agreement with each other, it is not clear whether these different results were caused by material difference or different physical regimes.

In this chapter, we will focus our attention on measurements of the temperature and magnetic field dependence of the bottom voltage $V_{bot}(H,T)$ for Bi-2212 single crystals. Four Bi-2212 single crystals grown by the travelling solvent floating zone (TSFZ)
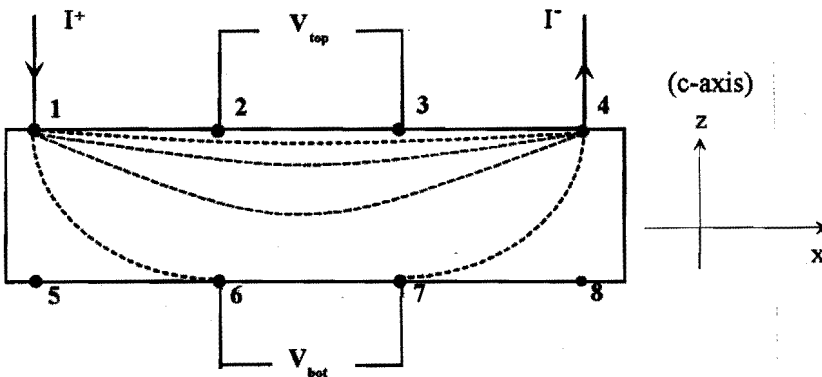

Fig. 8.1 *The configuration for eight-contact transport measurements as used in the experiments. The dashed line represents schematically the inhomogeneous distribution of the current density in the sample.*

method [9] were used for the transport measurements using the flux-transformer geometry. Furthermore, crystals after annealing were also used for the transport measurements, since the resistivity of the high-T_c superconductors, especially the c-axis resistivity, depends strongly on the oxygen concentration [10-11,13]. For this purpose, two as-grown single crystals were used and two other crystals were long-term annealed.

8.2. Experimental

Single crystals of $Bi_2Sr_2CaCu_2O_{8+z}$ were grown by the TSFZ method [9], which has been described in Section 1.4 and Section 2.1.

Samples I (6.5x1.5x0.074 mm^3) and II (10.0x2.0x0.045 mm^3) were as-grown single crystals; the single crystals III (8.7x2.0x0.020 mm^3) and IV (5x1.75x0.045 mm^3) were post-grown annealed at 600 ^{0}C for about 60 hours in oxygen (1 atm.) before quenching into liquid nitrogen.

The contacts were made as follows. First, dots of silver with a diameter of 0.5 mm were sputtered on the two surfaces of the Bi-2212 single crystals. In order to improve the contact between the silver dots and the crystal, the sample with the dots of silver was annealed at 600 ^{0}C for about 2 hours in oxygen (1 atm.), and subsequently quenched to liquid nitrogen temperature. Finally, silver paste was used to connect silver wires to the silver dots. For samples I, II and III, the distance between the current contacts was 5 mm, and between the voltage contacts 2 mm. For sample IV the distance between the current contacts was 3 mm and between the voltage contacts 1 mm. It is noted that during the contact-making process, all the samples were annealed at 600 ^{0}C for about 2 hours, so, the "as-grown" samples referred in this paper are actually different from the real as-grown samples. However, in order to distinguish the long-term annealed samples, the samples I and II are referred to "as-grown" samples. After making the contacts (i.e. after the 2 hours annealing), the transition temperature T_c of samples I and II changed from 88 K to 80-84 K, from which the

samples are believed to be in the slightly over-doped regime. The long-term annealed samples III and IV have a T_c of about 84 K, so they are aslo believed to be in the slightly over-doped regime. After the long-term annealing, the oxygen distribution in samples III and IV is expected to be more homogenous than samples I and II.

The contact resistance of all the contacts was typically a few Ohms at room temperature. The resistivity measurements were performed in a home-built cryostat with a superconducting magnet. Magnetic fields ranging from 0 T to 5 T were applied parallel to the c-axis of the sample, before the sample was cooled below T_c (FC). The voltage was detected by a Keithley-182 nano-voltmeter. The DC current was typically 10 mA, and for each measurement point, the direction of the current was reversed in order to eliminate the thermo-electric effect. The temperature accuracy is about 0.25 K or less.

8.3. Experimental results and discussion

Before presenting the results, the notation has to be discussed. As shown in Fig. 8.1, when a current passes from contact 1 to contact 4 (denoted as I_{14}), the voltage on the top surface over contacts 2 and 3 (denoted as V_{23}) is called V_{top}; and the voltage on the bottom surface over contacts 6 and 7 (denoted as V_{67}) is called V_{bot}. The "apparent" resistance on the top, i.e. $R_{top}(T,H)$, is defined as V_{top}/I (i.e. V_{23}/I_{14} in this case); and the apparent resistance on the bottom, i.e. $R_{bot}(T,H)$, is defined as V_{bot}/I (i.e. V_{67}/I_{14} in this case). Note that these resistance, i.e. $R_{top}(T,H)$ and $R_{bot}(T,H)$, actually reflect only the distribution of the voltage on the top and bottom surfaces, i.e. $V_{top}(T,H)$ and $V_{bot}(T,H)$, and are not simply the measurements of the resistivity of the sample. When the current is injected on the other surface, i.e. through contacts 5 and 8 (I_{58}), then V_{67} will be V_{top} and V_{23} will be V_{bot}.

First, we will check the homogeneity of the crystals and the effect of the long-term annealing by comparing V_{23}/I_{14} (i.e. R_{top} for I_{14}) with V_{67}/I_{58} (i.e. R_{top} for I_{58}). Such a comparison could give some indication about the homogeneity of the single crystals,

because for a more homogenous single crystal, a smaller difference between these two values is expected. The results are shown in Fig. 8.2 for the as-grown samples I and II. The normal-state resistance of the two surfaces, i.e. V_{23}/I_{14} and V_{67}/I_{58}, differs by a factor of about 2.5: $V_{67}/I_{58} \approx 2.5 \times (V_{23}/I_{14})$. The superconducting transition width of the two samples is about 5 K [For sample II, a relatively large difference (~4 K) between the T_c of the two surfaces was observed, probably due to an inhomogeneous oxygen distribution]. For the long-term annealed single crystals III and IV, as shown in Fig. 8.3, the difference between the normal-state resistance of the two surfaces is somewhat reduced (for T>110 K): $V_{67}/I_{58} \leq 1.5 \times V_{23}/I_{14}$. The superconducting transition width is about 2 K, which is smaller than samples I and II. This confirms our expectation that the oxygen is more homogeneously distributed in the samples after long-term annealing (For the sample III, the resistance curve has a step near 108 K, representing the Bi-2223 phase, which is probably caused by some stacking faults). It is noted that a factor of 2.5 difference between the apparent resistance of the two surfaces was also reported by Busch et al. [1] for their samples.

The resistivity anisotropy ρ_c/ρ_{ab} can be obtained using the anisotropic resistivity model [1], as described in details in Section 1.10. For the four Bi-2212 single crystals, the value of ρ_c/ρ_{ab} at 300 K is calculated to be in the range of 0.5×10^4 to 1.1×10^4. It is in contrast to the scattering data of ρ_c/ρ_{ab} ranging from 6×10^2 to 6×10^4 in the literature [10-11, 14-18], which might be due to different crystal growth methods.

The resistance $R_{top}(T,H)$ (which is either V_{23}/I_{14} or V_{67}/I_{58}) showed a field-induced broadening in the presence of magnetic fields. Such a behaviour has been widely observed in the literature and can be explained by the TAFF model, so we will not discuss it in detail here, instead, we will focus on the behaviour of the bottom resistance $R_{bot}(T,H)$ (which is either V_{67}/I_{14} or V_{23}/I_{58}).

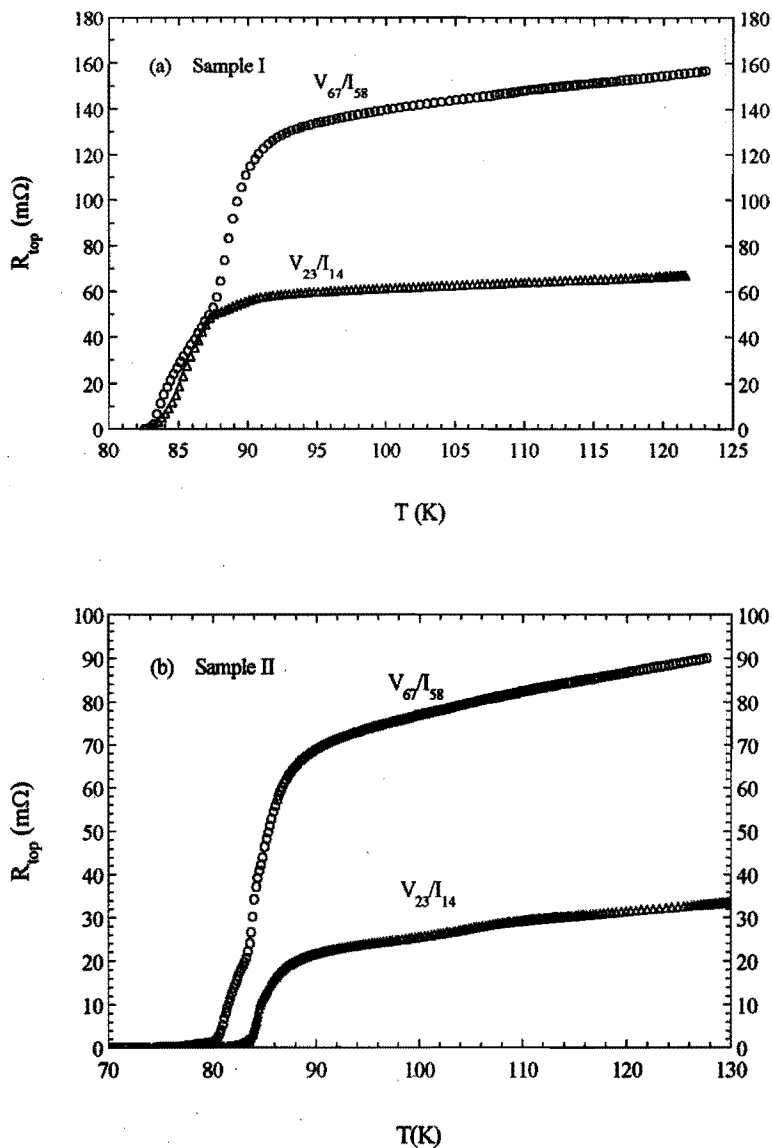**Fig. 8.2** *The resistance R_{top} of the two surfaces of the as-grown Bi-2212 single crystals I and II in zero applied magnetic field. The current and voltage configuration is indicated for each curve.*
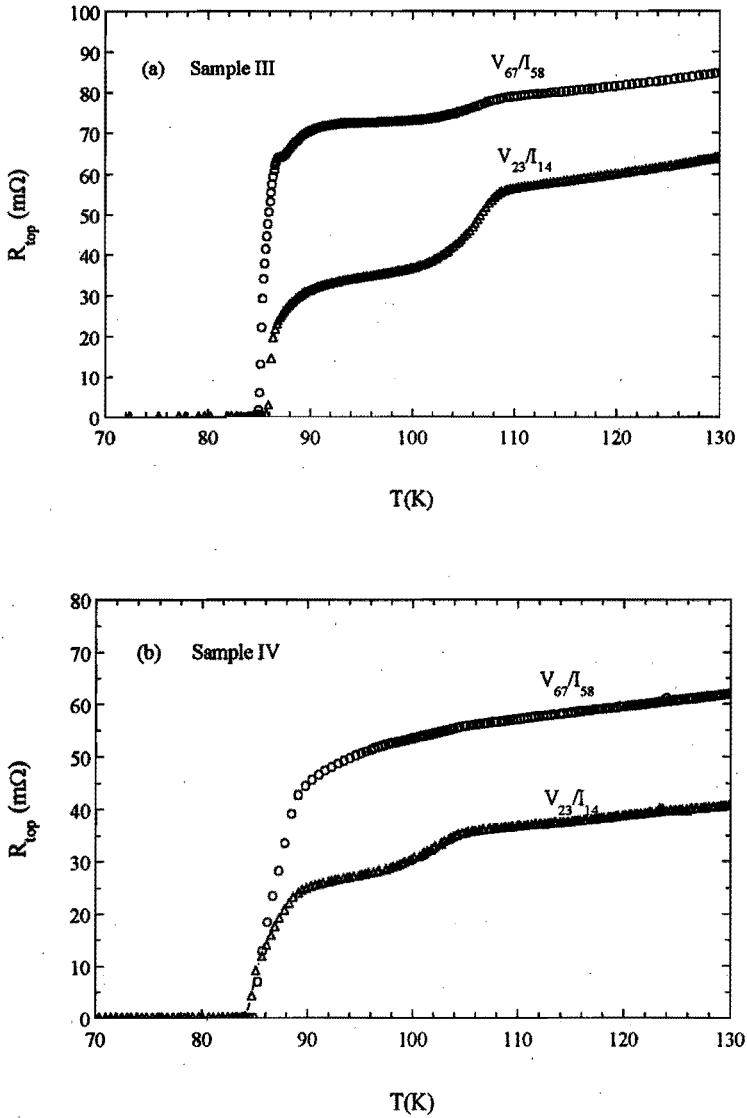
Fig.8.3. The resistance R_{top} of the two surfaces of the annealed Bi-2212 single crystals III and IV in zero applied magnetic field. The current and voltage configuration is indicated for each curve.

For the samples II and III, the bottom voltage $R_{bot}(T,H)$ in magnetic fields of 0 T and 1 T are shown in Figs. 8.4, in which the top voltage $R_{top}(T,H)$ is also given for comparison. As can be seen in the figure, a field-induced broadening of $R_{bot}(T, H)$, as well as $R_{top}(T,H)$, was observed. Such a behaviour in $R_{bot}(T,H)$ can be explained also by the TAFF mechanism.

However, for samples I and IV, as shown in Figs. 8.5, the field dependence of $R_{bot}(T,H)$ is quite different from that of $V_{top}(T,H)$. For sample I, in zero applied field, $R_{bot}(T,H)$ has a peak near T_c, which occurs between 83 K and 89 K. When the applied current is reduced from 10 mA to 5 mA, the height of the peak in $R_{bot}(T,H)$ became smaller. When a magnetic field of $H \geq 0.1$ T was applied, the peak was suppressed. For sample IV, $R_{bot}(T,H)$ reaches a zero-resistance at about 98 K in zero applied magnetic field, which is considerably higher than the real T_c measured by the normal four-contact method [see Fig. 8.3(b)]. In the presence of magnetic fields, the temperature of the zero-resistance in $R_{bot}(T,H)$ was gradually reduced, which reached a minimum value of 86 K for $H \geq 1$ T. Although the anomalous $R_{bot}(T,H)$ at H=0 T is quite different for samples I and IV [Fig. (8.5a) and Fig. (8.5b)], it shows a similar behaviour in high magnetic fields of $H \geq 1$ T, namely, $R_{bot}(T,H)$ is a linear extension of the temperature dependence of the resistance, which starts at T>108 K and extrapolates to zero at about 86 K. The anomalous behaviour of $V_{bot}(T,H)$ found in samples I and IV dramatically differs from $V_{top}(T,H)$ and could not be explained by the TAFF mechanism. It has to be emphasised that such an anomaly is not due to any contact problem, because other current and voltage configurations, like $V_{23}(T,H)/I_{14}$, $V_{67}(T,H)/I_{58}$ and $V_c(T,H)/I_c$ (i.e. current and voltage along the c-axis) showed TAFF behaviour without any trace of poor contact. We have to mention that exchanging both the current and voltage configuration to the other surface gave similar results. Since samples I and II are as-grown samples and sample III and IV are long-term annealed samples, the long-term annealing does not seem to have a pronounced effect on the occurrence of such an anomaly.
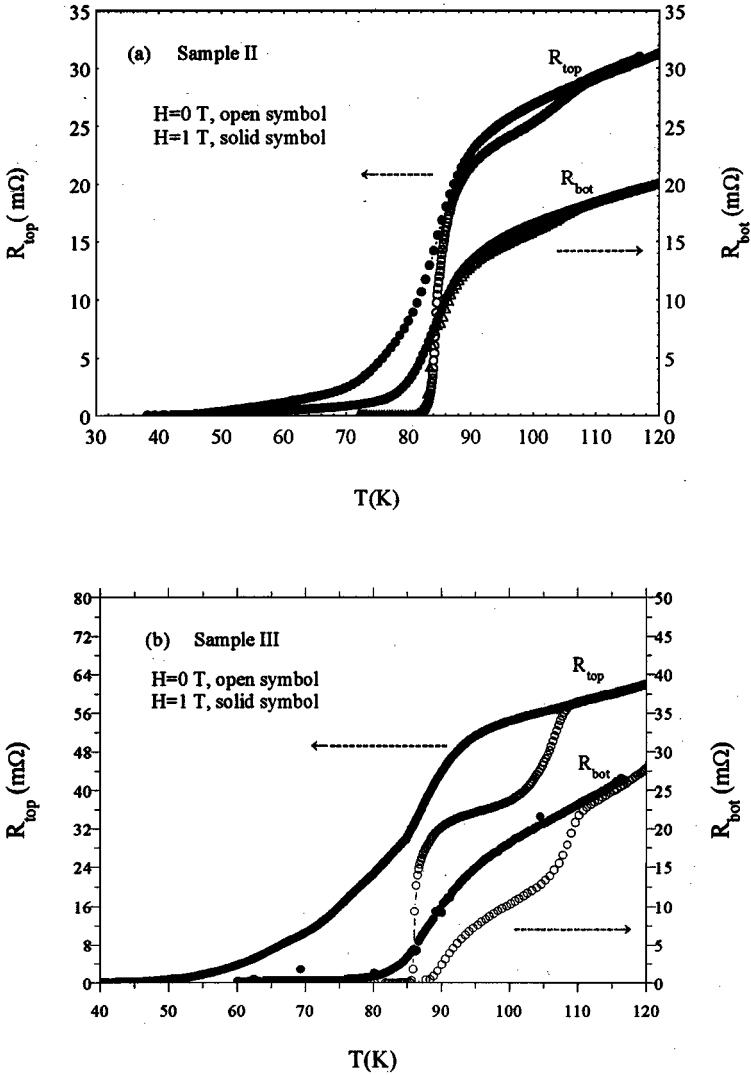
Fig. 8.4 *The field dependence of R_{top} (=V_{top}/I) and R_{bot} (=V_{bot}/I) for samples II and III, in which $R_{bot}(H, T)$ shows a field broadening similar to $R_{top}(T, H)$ [The left-hand scale is for $R_{top}(T,H)$; right-hand scale is for $R_{bot}(T,H)$].*

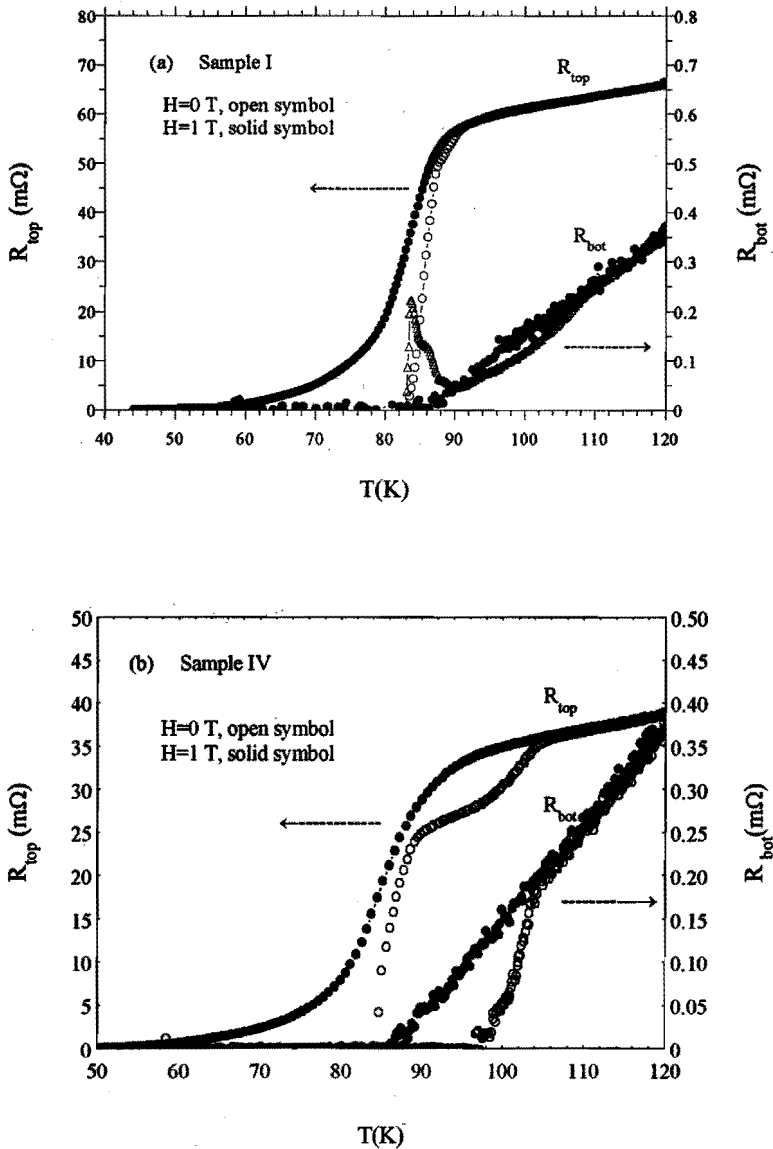**Fig. 8.5** *The field dependence of R_{top} and R_{bot} for samples I and IV. Note that $R_{bot}(H,T)$ differs from R_{top} (T,H) and exhibits no TAFF behaviour. [The left-hand scale is for $R_{top}(T,H)$; right-hand scale is for $R_{bot}(T,H)$]. Note also the large difference between the scales for R_{top} and R_{bot}.*

It is of interest to see whether the explanations proposed by Busch et al [1] and Wan et al [2] for their observed peaks in the bottom voltage $V_{bot}(T,H)$ are applicable to our experimental results observed in samples I and IV. In the experiments of Busch et al [2], the peak in $V_{bot}(T,H)$ was observed only when a magnetic field was applied. Using the local resistivity model [2] (see also Section 1.10), they evaluated the ab-plane resistivity $\rho_{ab}(T,H)$ and c-axis resistivity $\rho_c(T,H)$ from $V_{top}(T,H)$ and $V_{bot}(H)$, in which $\rho_c(T,H)$ showed a "knee" near T_c. This "knee" in $\rho_c(T,H)$ was then used for the explanation for the appearance of the broad peak. Such an explanation does not apply to the anomalous effects observed in our experiments, because first the anomaly for the samples I and IV was observed already in zero magnetic field; also, since for sample I and IV, $R_{top}(T,H)=0$ for T<86 K, it is obvious that the local resistivity model used in Ref. [2] cannot be applied for these two samples below T_c. Wan et al. proposed [2] that the anomalous peak observed in their experiments results from the competition between the temperature dependences of the free vortex density and the Josephson coupling energy. The anomalous $V_{bot}(T,H)$ observed in sample I is similar to that observed by Wan et al. [2], especially the height of the peak is strongly affected by the magnetic field and the value of the applied current. However, their explanation was based on the following two facts observed in their experiments: 1). the transition temperature of the c-axis resistivity ρ_c is about 2 K higher than that of the ab-plane resistivity ρ_{ab}, i.e. $T_c^c - T_{ab}^c \approx 2$ K; 2). the peak occurs exactly in the temperature interval between T_{ab}^c and T_c^c. However, in our experiments, for sample I, no difference between T_{ab}^c and T_c^c was observed in $\rho_c(T)$ and $\rho_{ab}(T)$ measurements, and the peak in V_{bot} has a temperature interval of 4-6 K. For sample IV, $V_{bot}(H,T)$ showed a different anomaly, where no peak appears. Therefore, the explanation proposed by Wan et al. seems not be applicable for our samples.

Although no definite explanation is available for our experimental results on samples I and IV, a common feature for samples I and IV, which is in contrast to samples II and III, is observed. Comparing Fig. 8.4 with Fig. 8.5, we note that for samples II and III, the ratio between the bottom and top voltage is large, namely V_{bot}/V_{top} (T≈110 K)>1/10; but for both samples I and IV, in which anomalous behaviour of $V_{bot}(H,T)$ appeared, V_{bot}/V_{top} (at T≈110 K) is smaller than 1/100 (about 1/250 for sample I and

1/140 for sample IV). This means that for these two samples, the current flowing at the bottom surface was much smaller than that at the top surface. Examining the published data, we noticed that, in the experiments of Busch et al [1] and Safar et al [3], the ratio of V_{bot}/V_{top} ($T \approx 110$ K) is larger than 1/10; but in the experiments of Wan et al [2], this ratio is much smaller, i.e. V_{bot}/V_{top} ($T \approx 110$ K)<1/100, as can be estimated from their data of ρ_c and ρ_{ab}. Since for the broad peak of $V_{bot}(T,H)$ observed by Busch et al. for H> 0 T [1], only a trivial explanation (the "knee" in ρ_c) was given, which did not suggest any new physical mechanism, it might be concluded that, based on the experimental data obtained up to now, the anomalous effect in V_{bot} (T,H) is related to the small value of V_{bot}/V_{top}, i.e $V_{bot}/V_{top}(T \approx 110$ K)<1/100. Such a small value of V_{bot}/V_{top} indicates a strong gradient of the current density across the sample, which also means a strong gradient of the Lorentz force acting on the vortices along the c-axis.

Finally, it has to be mentioned that for all the samples, it was found that $V_{top}(T,H)>V_{bot}(T,H)$. This is in agreement with the published results [1-3], indicating that vortices in Bi-2212 single crystals are of 2D character in the vortex-liquid regime.

8.4 Conclusion

In conclusion, from the resistance measurements of the two surfaces, it is indicative that the long-term annealing of Bi-2212 single crystals resulted in a more homogenous oxygen distribution in the crystals. In the vortex-liquid regime, the bottom resistance $R_{bot}(T,H)$ in the flux-transformer configuration showed both normal and anomalous behaviour for different single crystals. While normal behaviour showed a TAFF behaviour in magnetic fields, anomalous behaviour observed in $R_{bot}(T,H)$ exhibited either a peak near T_c or a higher zero-resistance temperature ($T>T_c$). In high magnetic fields (H≥1 T), a same behaviour of $R_{bot}(T,H)$ was observed , i.e $R_{bot}(T,H)$ was simply a linear extrapolation of resistance which starts from T>108 K and extrapolates to zero at about 86 K. It is noted that when normal behaviour was observed, the ratio between the bottom and top voltage, i.e. $V_{bot}/V_{top}(110K)$, was larger than 1/10, but when

anomalous behaviour was found, this ratio was much smaller, i.e. $V_{bot}/V_{top}(110K) < 1/100$. This suggests that the anomalous $R_{bot}(T,H)$ could be related to the strong gradient of the Lorentz force acting on the vortices at different layers along the c-axis, although the details of the mechanism are not yet known.

References

[1] R. Busch, G. Ries, H. Werthner, G. Kreiselmeyer, and G. Saemann-Ischenko, Phys. Rev. Lett. **69**, 522 (1992).

[2] Y.M. Wan, S.E. Hebboul, D.C. Harris, and J.C. Garland, Phys. Rev. Lett. **71** 157 (1993); Y.M. Wan, S.E. Hebboul, and J.C. Garland, Phys. Rev. Lett. **72**, 3867 (1994).

[3] H. Safar, P.L. Gammel, D.A. Huse, S.N. Majumdar, L.F. Schneemeyer, D.J. Bishop, D. Lopez, G. Nieva, and F. de la Cruz, Phys. Rev. Lett. **72**, 1272 (1994).

[4] H. Safar, E. Rodriguez, F. de la Cruz, P.L. Gammel, L.F. Schneemeyer, and D.J. Bishop, Phys. Rev. **46**, 14238 (1992).

[5] David A. Huse and Satya N. Majumdar, Phys. Rev. Lett. **71**, 2473 (1993).

[6] F. de la Cruz, H. Pastoriza, D. Lopez, M.F. Goffman, A. Arribere, and G. Nieva, Physica C **235-240**, 83 (1994).

[7] Yu. Eltsev, W. Holm, and O. Rapp, Phys. Rev. B **49**, 12333 (1994).

[8] F. de la Cruz, D. Lopez, and G. Nieva, Philos. Magz. B **70**, 773 (1994).

[9] J.H.P.M. Emmen, S.K.J. Lenczowski, J.H.J. Dalderop and V.A.M. Brabers, J. Crystal Growth **118**, 477 (1992).

[10] T. Ito, H. Takagi, S. Ishibashi, T. Ido and S. Uchida, Nature **350**, 596 (1991).

[11] L. Forro, Phys. Lett. A **179**, 140 (1993).

[12] N. Kumar, and A.M. Jayannavar, Phys. Rev. B **45**, 5001 (1992).

[13] K.H. Yoo, D.H. Ha, Y.K. Park and J.C. Park, Phys. Rev. B **49**, 4399 (1994).

[14] K. Kadowaki, A.A. Menovsky and J. J. M. Franse, Physica B **165& 166**, 1159 (1990).

[15] M.F. Crommie and A. Zettl, Phys. Rev. B **43**, 408 (1991).

[16] M. Brinkmaan, H. Somnitz, H. Bach and K. Westerholt, Physica C **217**, 418 (1993).

[17] J. B. Mandal, S. Keshri and B. Ghosh, Physica C **216**, 195 (1993).

[18] Dong-Seong Jeon, Masahiro Akamatsu, Hiroshi Ikeda, and Ryozo Yoshizaki, Physica C **253**, 102 (1995).

Summary

This thesis describes experimental studies and modelling of the physical properties of $Bi_2Sr_2CaCu_2O_{8+z}$ (Bi-2212) high-temperature superconductors with the emphasis on vortex dynamics. The topics cover the critical current density, vortex pinning, thermally activated flux motion, the current dependence of the pinning potential, the distribution of pinning energies, the irreversibility line, the substitution effects, and transport measurements with the flux-transformer geometry. Various experimental techniques have been used, including crystal growth by travelling solvent floating zone (TSFZ) method, materials characterisation techniques, magnetometry, AC susceptibility and electrical transport measurement techniques.

After a general introduction in Chapter I and a brief description of the experimental techniques in Chapter II, a detailed experimental studies on the magnetic relaxation and the critical current density in Bi-2212 single crystals and polycrystalline samples are presented in Chapter III. With a time window of more than 3 decades, the nonlogarithmic decay of magnetization at temperatures down to 10 K was observed in Bi-2212 superconductors, which is in contradiction to the traditional Anderson-Kim model. The behaviour of magnetic relaxation was found to be different for Bi-2212 single crystalline and polycrystalline samples. The temperature dependence of the normalized initial decay rate $S(t_b, T)$ showed a strong peak at about 25 K for single crystals, while $S(t_b, T)$ increased monotonically with temperature for Bi-2212 bulk ceramic samples. By crushing the bulk ceramic samples into powders, a small peak was found at about 20 K in the $S(t_b, T)$ curve. The peak in the temperature dependence of $S(t_b, T)$ and the kink in the temperature dependence of $j_c(T)$ at about 25 K observed in the Bi-2212 single crystals indicates two different pinning mechanisms below and above 25 K.

In Chapter IV and V, those experimental results, especially the nonlogarithmic decay of the magnetization, will be analysed and discussed. In Chapter IV, it is demonstrated

that all the relaxation curves measured at different temperatures can be directly combined by expressing them in terms of the common variable $kT\ln(t/\tau_0)/b(T)$, i.e. $j(t,T)/c(T)$ vs. $kT\ln(t/\tau_0)/b(T)$. With this method, the current dependence of $U_{eff}(j)$ can be obtained from the experimental relaxation data, rather than from theoretical considerations. In contrast to the Maley's method, the temperature dependences of the pinning potential $U_0(T)$ and the critical current density $J_c(T)$ are included in our method.

In Chapter V, the decay of magnetization is analysed within the Hagen-Griessen model, which assumes a broad distribution of pinning energies. Using a particular class of distribution functions, an analytical solution has been obtained for the decay of the magnetization. The parameters of the distribution can be obtained by fitting the relaxation curves. The magnetic relaxation curves of Bi-2212 single crystals, bulk ceramic samples and powdered samples are well fitted in terms of a distribution of pinning energies. It is found that it is important to include the high-pinning-energy tail in the distribution in order to fit the magnetic relaxation data. Without the high-energy tail, no kink in $j_c(T)$ and no peak in $S(t_b, T)$ could be reproduced in the model for the Bi-2212 single crystals. However, defects with such high pinning energy (~ 140 meV) can hardly exist in the highly anisotropic Bi-2212 single crystals, in which the maximum pinning energy is expected to be about 90 meV. It was argued that those high pinning energies in the distribution $N(u)$ could be explained by reinterpreting $N(u)$ in the framework of collective pinning theory, namely, the high pinning energies are produced dynamically by the interaction between the vortices.

The irreversibility line of Bi-2212 superconductors is the topic in Chapter VI. After a presentation of the experimental results, an approach for the irreversibility line within the framework of thermally activated flux creep is proposed. Compared with the previous work of Yeshurun and Malozemoff, this approach is valid for any current dependence of the pinning potential, and is applicable to the whole superconducting temperature range.

In Chapter VII, the experimental results of the Y-substitution of Ca, and Co or Ni substitution of Cu in the $Bi_2Sr_2CaCu_2O_{8+z}$ single crystals are described. The effects of the substitutions on the structure, superconductivity and critical current density of the superconductors are investigated. The influence of the substitutions on the transition between the two different pinning regimes below and above 25 K in the single crystals is discussed.

Finally, Chapter VIII describes the transport measurements by means of the flux-transformer geometry on Bi-2212 single crystals. It is found that in the vortex liquid state, the voltage at the bottom surface $V_{bot}(T,H)$ shows both normal and anomalous behaviour for different single crystals. While normal behaviour showed a TAFF behaviour in the presence of magnetic fields, anomalous behaviour observed on the bottom voltage $V_{bot}(T,H)$ exhibited either a peak near T_c or a zero voltage at a temperature higher than the T_c in zero magnetic field and no TAFF behaviour in magnetic fields. It is noted that when normal behaviour is observed, the ratio of the bottom and top voltages, i.e. $V_{bot}/V_{top}(110K)$, is larger than 1/10, but when anomalous behaviour occurs, this ratio is much smaller: $V_{bot}/V_{top}(110 K)<1/100$. This suggests that the anomalous $V_{bot}(T,H)$ could be possibly related to a strong gradient of the Lorentz force acting on the vortices at the different layers along the c-axis of the crystals.

Samenvatting

In dit proefschrift wordt een experimenteel onderzoek naar de fysische eigenschappen van $Bi_2Sr_2CaCu_2O_{8+x}$ (Bi-2212) hoge-temperatuur supergeleiders beschreven, evenals de daarbij behorende modelvorming met als hoofdthema vortex dynamica. De onderwerpen die hierbij aan de orde komen zijn: kritische stroomdichtheid, vortex pinning, thermisch geactiveerd flux transport, de stroom afhankelijke pinning energie, de verdelingsfunctie van de pinning energie, de irreversibiliteits-lijn, chemische substituties en elektrisch geleidingsmetingen met behulp van de "flux-transformer" configuratie. Bij het onderzoek zijn verschillende experimentele technieken gebruikt; voor de vervaardiging van de preparaten is gebruik gemaakt van keramisch methoden evenals van de travelling solvent floating zone techniek (TSFZ) voor de bereiding van eenkristallen. Karakterizatie van de preparaten geschiedde d.m.v. röntgendiffractie en elektron micro probe analyse (EPMA). De fysische eigenschappen worden bestudeerd d.m.v. magnetometrie (VSM en SQUID), a.c.-susceptibiliteit en elektrische transport metingen.

Na een algemene inleiding in hoofdstuk I en een korte beschrijving van de experimentele technieken in hoofdstuk 2 volgt in hoofdstuk 3 een meer gedetailleerde beschrijving van het experimentele onderzoek naar de magnetische relaxatie en de kritische stroomdichtheid in Bi-2212 één en polykristallijne preparaten. De tijdsafhankelijkheid van de magnetizatie bleek in het bestudeerde temperatuurgebied, 10-90 K, over een tijdsinterval van meer dan drie decaden niet te voldoen aan een logarithmische relaxatie, hetgeen in tegenspraak is met het gebruikelijke Anderson-Kim model. Tussen één en polykristallijne samples worden verschillen in magnetisch relaxatie-gedrag gevonden. De temperatuur afhankelijkheid van de genormaliseerde relaxatie-snelheid $S(t_b, T)$ vertoonde een sterke piek rond 25 K voor éénkristallijn materiaal, terwijl een monotone toename voor gesinterd keramisch materiaal werd gevonden. Voor verpoederd keramisch polykristallijn materiaal werd echter een kleine piek rond 20 K gevonden in de temperatuur afhankelijkheid van $S(t_b,T)$. De piek in de temperatuurafhankelijkheid van $S(t_b,T)$ en de knik in de temperatuurafhankelijkheid

van $j_c(T)$, rond 25 K gevonden bij de Bi-2212 éénkristallen, suggereert twee verschillende pinning mechanismen, boven en onder 25 K.

In de volgende hoofdstukken IV en V wordt een gedetailleerde analyse gegeven van de experimentele resultaten en speciaal de niet-logarithmische relaxatie van de magnetizatie wordt besproken. In hoofdstuk IV wordt aangetoond dat alle isotherme relaxatie-curven voor alle gebruikte temperaturen genormaliseerd kunnen worden als functie van één variabele $A=kTln(t/\tau_0)/b(T)$, d.w.z. $j(t,T)/c(T)$ als functie van A. Met behulp van deze rekenmethode kan een effectieve pinning energie $U_{eff}(j)$ rechtstreeks verkregen worden uit de experimentele relaxatiegegevens, zonden gebruik te maken van specifieke theoretische modellen. In tegenstelling tot b.v. de analyse voorgesteld door Maley et al. wordt in onze analyse-methode rekening gehouden met een temperatuur afhankelijkheid van de pinning potentiaal $U_0(T)$ en de kritische stroomdichtheid $j_c(T)$.

In hoofdstuk V wordt de relaxatie van de magnetizatie geanalyseerd m.b.v. het Hagen-Griessen model, waarbij een grote verdeling van pinning energien wordt verondersteld. Door gebruik te maken van een specifieke klasse van distributie-functies kan een analytische uitdrukking gevonden worden voor de afname voor de magnetizatie. De parameters van deze distributie-functies kunnen door middel van een fit-procedure uit de relaxatie curven worden afgeleid. Voor zowel Bi-2212 éénkristallen als keramische bulk en poeder preparaten werd een goede overeenstemming tussen berekende en gemeten curven gevonden door gebruik te maken van een verdeling in de pinning-energie. Voor het optreden van de waargenomen knik in de temperatuurafhankelijkheid van $j_c(T)$ bij de Bi-2212 éénkristallen bleek het noodzakelijk om een staart in de verdelingsfunctie bij hoge waarden van de pinning-energie in te voeren om tot een redelijke aanpassing te komen tussen de berekende en experimentele data. Echter, defecten met een dergelijk hoge pinning-energie (~140 meV) kunnen waarschijnlijk niet voorkomen in de zeer anisotrope Bi-2212 kristallen; de maximaal te verwachte pinning-energie is ongeveer 90 meV. Een verklaring voor de bijdrage van de hoge pinning-energie in de distributie $N(u)$ kan gevonden worden indien men de verdelingsfunctie herwaardeert in het kader van collectieve pinning,

namelijk hoge pinning-energien kunnen worden gerealiseerd door de dynamische interactie tussen de vortices onderling en tussen de vortices en de pinning-centra.

De irreversibiliteits-lijn van de Bi-2212 superconductors is het onderwerp van hoofdstuk VI. Na de presentatie van de experimentele resultaten wordt een model, gebaseerd op het concept van de flux-depinning lijn besproken. Het voordeel van dit model in vergelijking met bijvoorbeeld eerder werk van Yeshurun en Malozemoff is dat deze beschrijving geldig is voor elke stroomafhankelijkheid van de pinning-potentiaal en voor het gehele supergeleidende temperatuur traject.

Via een variabele chemische substitutie in éénkristallen van Bi-2212, namelijk Y-substitutie voor Ca en Co/Ni voor Cu, wordt de invloed van de substitutie op structuren, kritische temperatuur en kritische stroomdichtheid onderzocht. De resultaten zijn vermeld in hoofdstuk VII. De invloed van de substitutie op de overgang tussen de twee verschillende pinnings gebieden, boven en onder 25 K, wordt besproken.

Tot slot wordt in hoofdstuk VIII de transport metingen beschreven die uitgevoerd zijn met behulp van een flux-transformer geometrie aan Bi-2212 kristallen. Als resultaat werd gevonden dat in de vortex-vloeistof toestand, de spanning aan het bodem oppervlak $V_{bot}(T,H)$ zowel normaal as abnormaal gedrag kan vertonen, afhankelijk van het gebruikte kristal. Bij normal gedrag, werd thermisch geactiveerd flux vloeien (TAFF) in het magnetische veld waargenomen. Bij afwijkend gedrag van $V_{bot}(T,H)$ werd ofwel een piek in de buurt van T_c waargenomen, ofwel een nul spanning bij een temperatuur hoger dan de T_c in nul magneetveld en geen typisch TAFF gedrag in het magneetveld optrad. Opmerkelijk is dat wanneer het normale gedrag waargenomen wordt, de verhouding tussen de bodem en top spanning, V_{bot}/V_{top} (bij 110K) groter is dan 1/10, maar dat bij anomaal gedrag deze verhouding kleiner is dan 10^{-2}. Dit suggereert dat het abnormale gedrag van $V_{bot}(T,H)$ gerelateerd zou kunnen zijn aan een sterke gradient van de Lorentz kracht werkend op de vortices in de successieve lagen in de c-richting van de kristallen.

List of Publications

1. W. Paul, D. Hu and Th. Baumann,
"Voltage-current characteristic between 10^{-13} V/cm and 10^{-3} V/cm of BSCCO (2212) and the time decay of magnetization", Physica C 185-189 (1991) 2373.

2. D. Hu, W. Paul and J. Rhyner,
"Critical current density, magnetic relaxation and pinning distribution in $Bi_2Sr_2CaCu_2O_x$ superconductors", Physica C 200 (1992) 359.

3. D. Hu,
"The current dependence of the effective pinning potential in high-T_c superconductors", Physica C 205 (1993) 123.

4. D. Hu, V. A. M. Brabers, J. H. P. M. Emmen and W. J. M. de Jong,
"The temperature dependence of the irreversibility line of $Bi_2Sr_2CaCu_2O_{8+z}$ superconductors", Physica C 216 (1993) 315.

5. M. Mittag, M. Rosenberg, D. Pelligrad, R. Wernhardt, V.A.M. Brabers, J.H.P.M. Emmen and D. Hu,
"A study of the reversible and irreversible magnetic properties of a Bi-2212 single crystal in high magnetic fields", Supercond. Sci. Technol. 7 (1994) 214.

6. D. Hu, V. Brabers and W. J. M. de Jonge,
"Effects of partial Yttrium substitution in $Bi_2Sr_2Ca_{1-x}Y_xCu_2O_{8+z}$ single crystals", Physica C 235-240 (1994) 951.

7. M. Pakala, E. Maka, D. Hu, V. Brabers and M. Ausloos,
"Mixed-state thermoelectric and thermomagnetic effects of a $Bi_2Sr_2CaCu_2O_{8+z}$ single crystal", Phys. Rev. B 52 (1995) 7647.

8. D. Hu, V. A. M. Brabers and W. J. M. de Jonge,
"Substitution effects of $Bi_2Sr_2Ca(Cu_{1-x}M_x)_2O_{8+z}$ (M=Co, Ni) single crystals", Chinese Journal of Physics, vol. 34, No. 2-II, (1996) 597 (Proc. of 1995 Taiwan International Conf. on Superconductivity).

9. D. Hu, V. A. M. Brabers and W. J. M. de Jonge,
"Resistivity measurements by means of flux-transform geometry on $Bi_2Sr_2CaCu_2O_{8+z}$ single crystals with or without long-term annealing", to be published.

Curriculum Vitae

The author was born in Gan-Xian County of Jiangxi Province, China on May 12, 1965.

In 1981, he took the nation-wide examination for high education and was enrolled in the Department of Physics of Wuhan University, which is about a thousand kilometers away from his home town. After receiving his Bachelor of Science in 1985, he went to Beijing for his Master's Degree at the Institute of Physics, Chinese Academy of Sciences, which took him three years to accomplish.

In 1989, he decided to go abroad. In the Spring of that year, he went to work at Asea Brown Boveri (ABB) Research Centre, Baden, Switzerland. After taking some courses at ETH-Zürich, he did some research on high-T_c superconductors in ABB research center. In 1992, he went to the Department of Physics, Eindhoven University of Technology, the Netherlands for continuing his research on superconductors. In the group of Prof. de Jonge, he finished his Ph. D thesis in 1996.

Acknowledgements

I am very grateful to all the colleges who helped me in one way or another during the period of my research on superconductors, which includes my former colleges in Switzerland and the present colleges in Eindhoven.

I am indebted to Prof. de Waele, Prof. Kopinga and Prof. van Poucke for their comments on the thesis. Here, in particular, I would like to thank Prof. W. de Jonge and Dr. V. Brabers, because without their supports and help, this thesis would not have been realised.

Stellingen

Investigations on $Bi_2Sr_2CaCu_2O_{8+z}$ Superconductors:

Magnetic relaxation, vortex pinning,

substitution effects and transport measurements

Dian-wen Hu

胡典文

4 December 1996

1. In the literature, the nonlogarithmic decay of the magnetization is explained to be either due to a non-linear current dependence of the effective pinning potential or due to a distribution of pinning energies. In reality, both factors can simultaneously exist during the magnetic relaxation.

This thesis, Chapter V.

2. Malozemoff proposed that the irreversibility line is defined when the distance between the vortices, denoted as a_0, scales with the coherence length ξ, i.e. $a_0 = f \cdot \xi$, where f was assumed to be a constant. However, a simple calculation of the values of a_0 and ξ at the measured irreversibility line at low temperatures reveals that f is not a constant but strongly field dependent.

A. P. Malozemoff, in <<Physical Properties of High Temperature Superconductors>>, Vol. 1, Editor: D. M. Ginsberg. World Scientific, 1989.

3. At low temperatures, the time and temperature dependence of the current density $j(t,T)$ in the high-T_c superconductors is simply a function of $[kT\ln(t/\tau_0)]$.

This thesis, Chapter IV.

4. Because of the thermal activation of the vortices, the temperature dependence of the irreversibility line at low temperatures cannot be scaled as a function of $(1-T/T_c)$.

This thesis, Chapter VI.

5. The scientific researchers usually think that what they are doing will change the society. On the other hand, what the other people in the society are doing can also change the activities of the scientific research.

6. During the first period of the industrialisation in the developing countries, less-advanced technologies are widely used due to a lack of capital, which causes serious pollution. In order to protect the environment, more advance technologies should be sold at a lower price in the developing countries than in the developed countries; also, within a developing country, the government should encourage the poorer regions to use more advanced technologies by providing some subsidies.

7. Humour perceived in one culture may not be understood or even perceived as offensive in another culture. In order to avoid such or other misunderstandings, to talk in a simple and straight way might be the best in the communication involved with people from different cultures, although sometimes this could result in a dull talk.

8. To have a better structure of the society is more important than to have a wiser leader.

9. In the Internet, it takes a lot more time to load a picture than the text. Our brain must be much superior to the present technologies, since we can remember a picture as quickly as words or text.

10. A small improvement can lead to a quite different result.

（ 弱 者 道 之 用．）

"Lao Tze", Chapter 40.